

# The QCD phase diagram

Szabolcs Borsányi<sup>a</sup> and Paolo Parotto<sup>b</sup>

<sup>a</sup>University of Wuppertal, Theoretical physics, 42119 Gausstr 20, Wuppertal, Germany

<sup>b</sup>Università di Torino, Dipartimento di Fisica and INFN Torino, via P. Giuria 1, I-10125 Torino, Italy

© 20xx Elsevier Ltd. All rights reserved.

Chapter Article tagline: update of previous edition, reprint.

## Contents

Nomenclature	1
Objectives	1
1 Introduction	2
2 Phenomenology of the phase diagram	4
2.1 Evidence based on collision experiments	4
2.2 Evidence based on lattice QCD	6
2.3 Diagrammatic approaches to QCD	10
2.4 Models that approximate QCD	13
3 Theory of the phase diagram	14
3.1 Quark masses and symmetries: the Columbia plot	14
3.2 Imaginary valued chemical potentials	18
3.3 Yang-Lee edge singularities	20
4 The multidimensional phase diagram	21
4.1 External magnetic fields	21
4.2 Isospin chemical potential	22
5 Phase diagram of dense matter	24
5.1 Dense matter equation of state	24
5.2 Color superconductivity	25
6 Conclusions	26
Acknowledgments	26
References	26

## Abstract

Strongly interacting matter exhibits new phases under extreme conditions. Matter was exposed to such extremes not only in the Early Universe, but also today in the cores of neutron stars, as well as in laboratory experiments at a much smaller scale. We study the underlying theory, Quantum Chromodynamics (QCD) with the methods of statistical physics and explore the various phases we may encounter in experiment, such as the Quark Gluon Plasma. We briefly summarize the experimental evidence for the new forms of matter and review the theoretical efforts to embed these findings in the broader context of quantum field theory, with special attention to exact and broken symmetries and critical behaviour.

**Keywords:** Quark gluon plasma, Quark matter, Color superconductivity, Chiral symmetry, Lattice QCD, Heavy ion experiments

## Nomenclature

QCD	Quantum Chromodynamics, the theory of strongly interacting matter based on quarks and gluons
Lattice QCD	The discipline where theorists use large computers as experimental devices to solve the QCD with stochastic methods.
RHIC	Relativistic Heavy Ion Collider, a leading facility at Brookhaven National Lab to study the phase diagram
HRG	Hadron Resonance Gas, a successful model that approximates QCD thermodynamics at low temperature
QGP	Quark Gluon Plasma, a phase of QCD at large energy density where quarks are liberated from hadrons
CFL	Color Flavor Locking, a phase of QCD at large baryon density
physical mass	Theorists can study QCD with whatever quark masses. 'Physical mass' means that Nature's choice is taken
chiral limit	The up and down quarks are very light. It is instructive to study what would happen if they were massless.

## Objectives

- The reader is first introduced to the most studied representation of the phase diagram in the temperature – chemical potential plane with an emphasis on existing evidence. Our focus will be what we have learned on the phase diagram from heavy ion experiments, lattice QCD and other theoretical approaches.

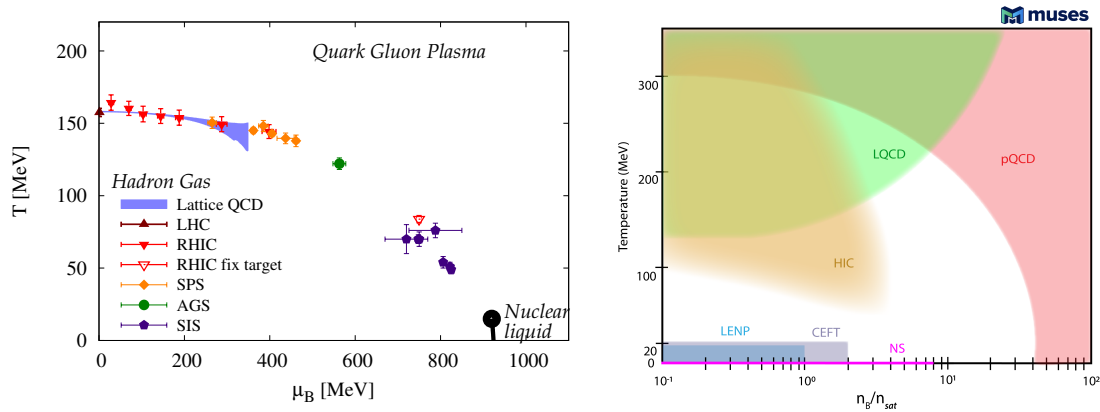


**Fig. 1** Data on the QCD phase diagram. The left panel shows the diagram in the temperature ( $T$ ) – baryon chemical potential ( $\mu_B$ ) plane. We know from lattice simulations [3] that on the temperature axis the transition is a cross-over. A cross-over line starts at  $T \approx 157$  MeV [4, 5] and stretches into the bulk of the phase diagram [6]. The width of the band refers to the theoretical uncertainties not to the width of the transition. The data points on and beyond the cross-over line show the thermodynamic parameters of the chemical freeze-out [7–13]. The small feature at  $T \approx 18$  MeV is the liquid gas transition and the corresponding end-point, measured in low energy heavy ion collision experiments [14]. The right panel uses the density, normalized to the nuclear saturation density  $n_0 = 0.17 \text{ fm}^{-3}$  as the first axis. It shows not the data, but where we can expect information from. (Picture presented by the Muses collaboration [15])

- The subsequent section is more theoretical: we review the predictions based on the symmetry breaking pattern of QCD and study indirect evidences from lattice QCD. We discuss the famous Columbia plot and the role of imaginary chemical potentials in the uncovering of finite density QCD.
- We then extend the scope to include the effects of an external magnetic field, isospin density or a theta parameter that couples to topology.
- The final section looks into the more elusive phases, with a special emphasis of large density QCD. We relate the theoretical expectation to future astrophysical observations.

## 1 Introduction

The strong force is manifest in our Universe as the short-range interaction that holds together the massive hadrons, most importantly protons and neutrons. We are fortunate to possess a powerful theory, Quantum Chromodynamics (QCD), which is able to explain and to predict the masses, decay properties and internal structure of the hundreds of hadrons and resonance states Nature presents us with. QCD is a quantum field theory with six quark species, playing the role of matter, and an eight-component gauge field, the gluons, responsible for interactions. As opposed to other gauge theories, like quantum electrodynamics (QED), self interactions between gluons play a crucial role. Their most important consequence is asymptotic freedom: the theory is weakly coupled at very short distances or at high energy scales. Thus, at sufficiently high temperatures, gluon fields lose the strength to bind hadrons together.

The extreme energy density required to unbind hadrons was indeed realized in nature immediately after the Big Bang. The hot early Universe cooled below this threshold when it was approximately  $10 \mu\text{s}$  old, and the temperature was around  $2 \cdot 10^{12}$  K. Whether still today the extreme densities inside the cold cores of neutron stars could induce a similar transition from hadronic matter to quarks is the subject of intensive research. Thanks to recent and future gravitational wave observatories, we can observe simultaneously hot and dense matter in the mergers of binary neutron stars. The first observation of such an event, GW170817, showed the potential of multi-messenger astronomy, where gravitational and neutrino measurements complement the photon-based observations [1, 2].

The transition between the quark and hadronic phases is, however, best studied in the laboratory with heavy ion collisions. After compelling hints from the SPS at CERN, the Relativistic Heavy Ion Collider (RHIC) facility at BNL has uncovered the features of a hot new phase, the quark gluon plasma. Extreme energy collisions at the LHC at CERN have subsequently pushed the experimental study of the formation, flow and freeze-out of the plasma into the realm of precision science. The precious synergy between theory and experiment has allowed a new field to emerge, focused on the mapping of the phase diagram of strongly interacting matter through the prediction of new phases and the identification of observable signatures. This chapter seeks to summarize what has been learned in the process.

Although there are numerous different sketches of possible structures for the QCD phase diagram, our actual knowledge is rather limited. This is summarized in the left panel of Fig. 1 in the most common picture of temperature vs baryo-chemical potential. Since in QCD the baryon number is integer valued and conserved, a grand canonical description with a well defined chemical potential can be employed. The baryo-chemical potential expresses the thermodynamic force associated with the creation of a single baryon.

We have good reason to believe that nature is described in the energy range of 0.1...10 GeV by quantum chromodynamics [16]. Simulations of QCD on the lattice have calculated the masses of most low lying hadrons [17, 18], and nuclear lattice simulations have reproduced the radii and binding energies of the lightest nuclei [19].

Also at finite temperature – and, though with severe limitations, finite density – lattice QCD simulations can provide rigorous evidence, and thus constrain the structure of the phase diagram. Continuum extrapolated simulations have shown that a broad transition around 155 – 160 MeV [4, 5] separates a low temperature phase where the hadronic description is successful from a high temperature one, where observables are still non-perturbative but dominated by light degrees of freedom. The transition for vanishing chemical potential is a crossover [3] marked by the spontaneous breaking of the chiral symmetry. By reducing the quark masses below their physical value, the crossover was connected to a second-order chiral transition at  $T_c = 132^{+3}_{-6}$  MeV in the chiral limit [20]. At finite chemical potential, the crossover is believed [21] to become stronger and eventually turn into a first-order transition, thus implying the existence of a critical point. The transition temperature in the chiral limit is expected to be an upper bound for the temperature at this critical end-point.

Lattice simulations are severely limited by a sign problem at finite density, which originates from the gluon-based approach of lattice QCD. In order to avoid the impossible task of representing Grassmann variables, the quark fields are integrated out and the resulting bosonic effective action is simulated. The resulting euclidean path integrals are computed via importance sampling, which is possible if the effective action is real and positive, but for a generic chemical potential it is not. Only in a few special cases is the effective action strictly positive, i.e. if i) the chemical potential is purely imaginary; ii) the chemical potential is real but has opposite sign for two degenerate quarks (e.g. with finite isospin chemical potential). Additionally, non-vanishing electric fields introduce a sign problem, while magnetic fields don't. We will discuss these extra directions in a separate section below.

The phase boundary at finite density has thus been explored by determining the curvature of the crossover line, which has been computed in the continuum limit by several lattice groups [22–24]. The band in the left panel of Fig. 1 shows the result from Ref. [6]. In the same work the broadness of the transition  $\Delta T \approx 15$  MeV was also determined, defined as the width of the chiral susceptibility peak. While the transition line unambiguously shows a negative curvature, the width does not significantly change for  $\mu_B < 300$  MeV. We deliberately omitted from the left panel of Fig. 1 possible locations of the chiral end-point, as no reliable extrapolations exist, let alone continuum extrapolated results. Still, exclusion regions can be set up: a recent continuum extrapolated result claims  $\mu_{B,c} > 450$  MeV with a  $2\sigma$  confidence [25].

Experiments, too, seek to chart the QCD phase diagram and possibly locate the chiral critical endpoint, which indeed has been a major motivation behind several generations of collider experiments. Among the wealth of data collected in two decades of the Beam Energy Scan program at RHIC, let us highlight two classes of observables particularly relevant for QCD thermodynamics. First, it was observed that the global abundance of hadrons can be modeled by a thermal ensemble. The associated grand canonical parameters  $T$  and  $\mu_B$  provide a snapshot of the chemical freeze-out, the moment when inelastic scatterings cease. The data points in the left panel of Fig. 1 show such conditions for different collision energies at different facilities. For small through intermediate chemical potentials, where lattice data are available, the freeze-out line closely follows the chiral transition line.

The other class of observables is based on event-by-event fluctuations of conserved charges. These were advocated for their sensitivity to criticality if freeze-out occurs at near-critical parameters [26]. In fact, high order fluctuations of the net proton number have the advantage to be accessible to experiment and to diverge with a high inverse power of the correlation length [27]. If the crossover line Fig. 1 ends in a chiral critical point, a non-monotonic pattern in the fourth-to-second cumulant (or factorial cumulant) is expected, based on computations in effective models [28]. The STAR experiment at RHIC has measured the energy dependence of high order proton fluctuations [29–31]. Even in the latest update [32] no unambiguous critical signal was found.

While the search for the chiral critical point of QCD intensifies, another, well established critical endpoint exists at low temperature: it corresponds to the liquid-gas transition of nuclear matter. The lightest hadrons that carry baryon charge are the nucleons with a mass  $m_N \approx 940$  MeV, which up to a small binding energy sets the threshold for the baryo-chemical potential where nucleons can form a condensate. This happens in a first order transition at  $\mu^{LG} \approx 924$  MeV, which for increasing temperature weakens and eventually terminates in an endpoint at  $T_c^{LG} = 17.9(4)$  MeV, as found by low energy heavy ion collision experiments [14]. This transition and the end-point have also been located by lattice simulations of the low energy effective theory of baryons [33]. Additionally, functional methods in QCD can also provide quantitative predictions in this region of the phase diagram [34].

One may notice that the freeze-out line in Fig. 1 appears to approach the cross-over line emerging from the liquid-gas critical point. Since chiral symmetry is broken on both sides of this crossover, it must be distinct from the chiral transition line. The latter – be it first order or crossover – has to separate from the liquid-gas crossover line somewhere between  $T \approx 145 - 20$  MeV. It is possible that the chiral endpoint exists but is far from the conditions accessible at chemical freeze-out. In this case, new means to detect it need to be found, otherwise it would be entirely out of the reach of heavy ion collision experiments.

While the well established facts on the QCD phase diagram are not many, several different approaches provide insight into the behavior of the theory in different regimes. This is summarized in the right panel of Fig. 1, from the MUSES collaboration [15], where the chemical potential axis is replaced by the net baryon density, expressed in units of the nuclear saturation density  $\sim 0.17 \text{ fm}^{-3}$ . While this phase diagram does not reveal any features, it displays the validity range of several complementary approaches: i) perturbative methods (red) are reliably applicable at very high temperature or density, thanks to asymptotic freedom; ii) lattice QCD simulations (green) are most successful at zero density, in the transition region or above, and finite-density extrapolations rely on expansions in  $\mu_B/T$ , hence the range in  $\mu_B$  increases at high temperature; iii) heavy ion collisions (orange) explore intermediate densities near and above the transition, but can hardly go beyond saturation density; iv) chiral effective theories and lattice simulations where gluons are not resolved are limited to very low temperatures (blue), but cover nuclear physics up to twice saturation density; v) neutron stars probe the equation of state of nuclear matter to even higher densities; vi) the upcoming generation of gravitational wave observations promises abundant merger signals, which will give us experimental access to the white region in the center of the diagram [15].

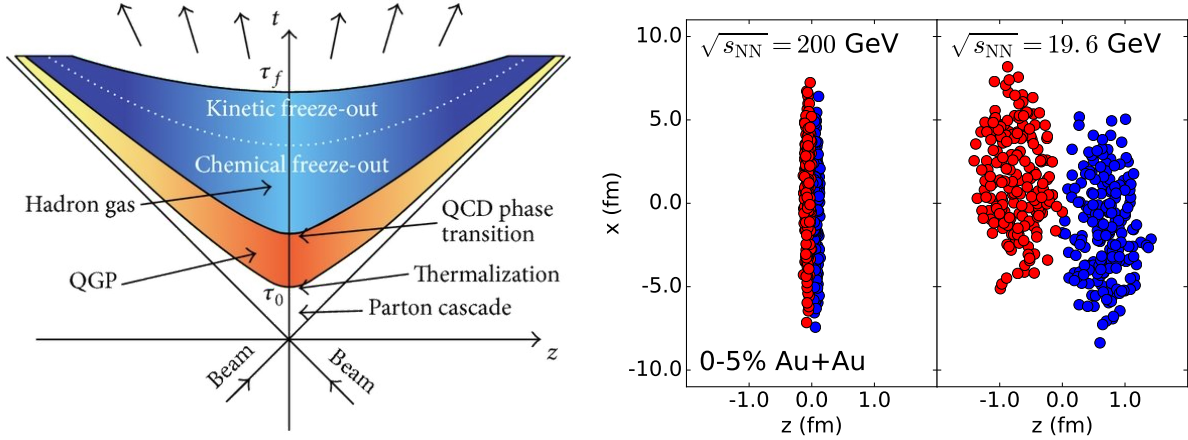


**Fig. 2** Left: schematic spacetime evolution of the system created in a heavy ion collision. Right: initial position of the nucleons in the laboratory frame for different collision energies [35].

We start this chapter with a phenomenological review of available evidence from experiments, lattice results and other theoretical computations on the phase diagram in Section 2. Much of the research on the phase diagram is centered on the hypothetical chiral critical endpoint. We discuss its theoretical motivation and the expected structure of the phase diagram in general in Section 3. While the phase diagram is most frequently presented in the temperature vs baryochemical plane, more external variables can be considered, such as other chemical potentials (e.g. isospin) or the strength of an external magnetic field. The phase diagram in these alternative representations will be addressed in Section 4. The densities that we can study in an Earth-bound laboratory are limited below the nuclear saturation density. Beyond that, astrophysical observation will let us explore the remote parts of the phase diagram. In Section 5 we briefly summarize the theoretical knowledge toward the high density limit, where exotic phases are expected.

## 2 Phenomenology of the phase diagram

### 2.1 Evidence based on collision experiments

Heavy ion collisions are the tool of choice for experimentally investigating the thermodynamics of QCD for densities up to around nuclear saturation density, and temperatures up to a few times larger than the QCD transition temperature. They are carried out in the largest particle accelerators in the world, like the Large Hadron Collider (LHC) and the Super Proton Synchrotron (SPS) at CERN and the Relativistic Heavy Ion Collider (RHIC) at the Brookhaven National Laboratory, as well as future facilities such as the Facility for Antiproton and Ion Research (FAIR) at GSI and the Japan Proton Accelerator Research Complex (J-PARC).

Heavy atomic nuclei, typically lead or gold, are collided at ultrarelativistic speeds, with beam energies ranging from a few GeV to a few TeV. Immediately after the collision, a large amount of energy is deposited in a very small volume in the form of color fields. The subsequent evolution of the medium created in heavy ion collisions is commonly divided in a few steps, schematically pictured with a spacetime diagram in Fig. 2. Within a very short time, typically less than 1 fm/c, the system reaches an approximate thermal equilibrium, and – if the energy density is sufficient – a quark gluon plasma state is formed. At top LHC energies the initial temperature can easily exceed 400 MeV [36, 37]. This very hot and dense medium then expands very quickly, driven by the internal pressure gradients, and accordingly cools down. The quark gluon plasma phase of this evolution is now successfully described by means of relativistic hydrodynamic simulations (see e.g. Refs. [38, 39] for a review). Comparison of hydrodynamic simulations and experimental results has led to the discovery that the quark gluon plasma is the most perfect fluid currently known, as its specific shear and bulk viscosities (namely, normalized by the entropy density,  $\eta/s$ ,  $\zeta/s$ ) are extremely small, more than an order of magnitude smaller than in superfluid helium. This stage of the evolution ends around 6 – 10 fm/c ( $\sim 2 - 3 \cdot 10^{-23}$  s) [40], when the temperature eventually drops below the QCD transition temperature  $T_c$  and quarks and gluons become confined, at the so-called *hadronization*. The still very hot and dense medium is at this point characterized by both elastic and inelastic collisions, which can alter the system's chemical composition. The latter cease at a stage named chemical freeze-out, after which the relative abundance of different hadron species is fixed. Finally, also elastic collisions cease as the system becomes very dilute, and thus particle spectra, too, are fixed at the kinetic freeze-out, after which only strong or electromagnetic decay processes may take place before the particles reach the detector. The characteristic time of weak decay processes is too long for them to take place during the system's evolution, of the order of about  $\sim 10^{-22}$  seconds. It is remarkable that most of current experimental knowledge on the structure of the QCD phase diagram was inferred from the measurement of final state hadrons in such events.

By varying the system's colliding energy, the net density of the medium created can be modified. While at very large energy the nuclei are essentially transparent due to the extreme Lorentz contraction (see Fig. 2, right), and only color fields are left behind at the collision site, when the energy is lowered Lorentz contraction is smaller, and the overlap time significantly increases. This results in baryon stopping, i.e.

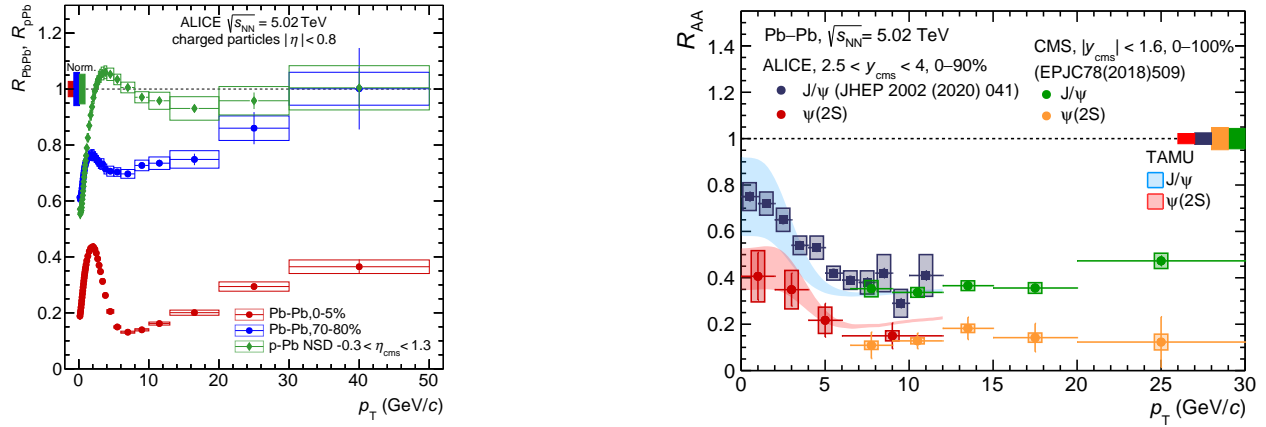


**Fig. 3** Left: jet nuclear modification factor in p-Pb as well as peripheral and central Pb-Pb collisions at the LHC [41]. Right: charmonium nuclear modification factor in Pb-Pb collisions for  $1S$  and  $2S$  states at CMS [42] and ALICE [43].

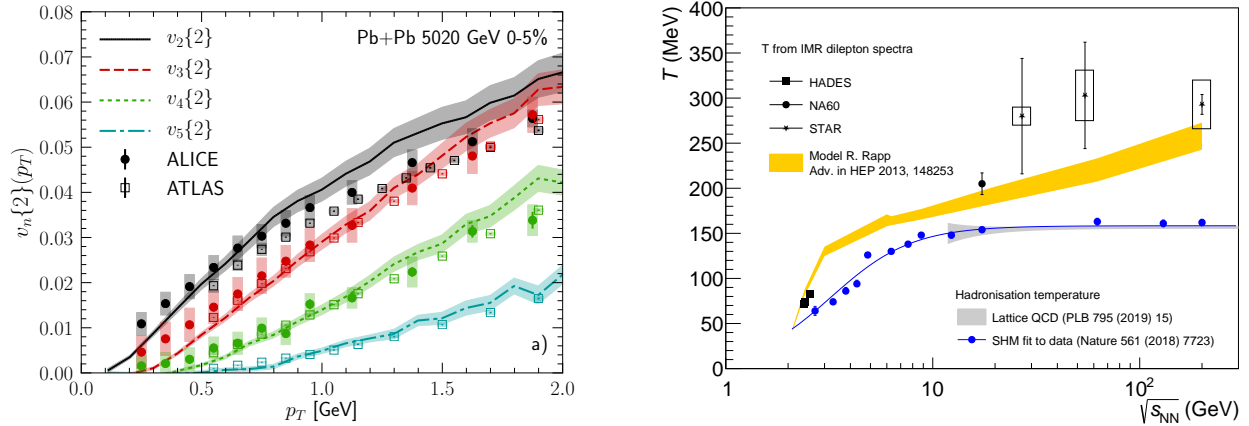


**Fig. 4** Left: flow coefficients in semi-central Pb-Pb collisions at the LHC, compared to results from a hybrid formalism including a viscous hydrodynamics description of the QGP phase [45]. Right: temperatures extracted from dilepton invariant mass spectra from NA60, STAR and HADES, compared to chemical freezeout temperatures and model expectations. Figure from Ref. [46].

a deposition of baryon number at mid-rapidity, increasing with decreasing collision energy, which drives the net baryon density to positive values. This allows to probe the phase diagram over a broad range of chemical potential.

### 2.1.1 QGP formation in experiments

Evidence of the production in the lab of a deconfined medium comes from a number of different signatures [36, 44] and the strong synergy with a comprehensive theoretical description which was built in the past decades. Among the most popular effects attributed to QGP formation are jet-quenching, the suppression (and re-generation) of quarkonium and flow.

Jet quenching is the reduction in the energy of high momentum partons (jets) as they travel through the deconfined medium, mostly due to collisions and gluon emission. This results in a reduced jet yield, and can be quantified by the relative number of high momentum hadrons compared to properly scaled p-p collisions, usually referred as the nuclear modification factor  $R_{AA}$ . A value below one indicates that, differently from p-p collisions, the produced medium has caused a yield reduction. This is shown in Fig. 3 (left) for different colliding systems at the LHC, highlighting how the effect increases when a larger – and longer-lasting – QGP phase is produced [41].

A similar argument is the basis of  $J/\psi$  suppression. Matsui and Satz [47] suggested that in a deconfined medium quarkonium would melt because of the screening of the color force. Based on this argument, a smaller yield of quarkonium states would be expected in heavy-ion collisions, compared to p-p ones, which again could be quantified through a nuclear modification factor. Additionally, the effect would be larger for more weakly bound states, a phenomenon known as sequential suppression. This can be seen in Fig. 3 (right), where  $R_{AA}$  at LHC is shown for  $J/\psi$  (a  $1S$  state) and  $\psi(2S)$ , in both cases smaller than one, and displaying a more pronounced suppression for the  $2S$  state. In Fig. 3 (right) a complementary effect is also visible at low- $p_T$ : quarkonium regeneration. Bound states can form by a recombination mechanism between the  $c$  and  $\bar{c}$  quarks, during the deconfined phase and/or at the hadronisation of the system. This effect

is sizable for charmonium at high LHC energies due to the large density of  $c\bar{c}$  pairs, while for bottomonium states it's negligible, because the density of  $b\bar{b}$  pairs is much lower [48]. The original view on quarkonium suppression has been revisited in recent years to include the effect of dissociation due to collisions with the medium on top (or instead [49]) of color screening, which can be encoded in an imaginary potential [50, 51] and described within the formalism of open quantum systems [52–55].

While these observables were proposed decades ago, new opportunities for QGP signaling were provided more recently by flow observables. Collectively, they relate to the fact that the strongly coupled nature of the deconfined medium results in the appearance of collective behavior; in short, the QGP “flows”. A quantitative description is made possible by the flow coefficients  $v_n$ , namely the Fourier coefficients of the azimuthal distribution of final state particles. Non-zero values for these coefficients reflect the anisotropy of particle emission driven by the initial spatial anisotropy of the medium. If the QGP were not strongly coupled, or not present, free streaming would result in a washing away of these anisotropies. In Fig. 4 (left) results from ALICE [43] and ATLAS [56] for the first flow coefficients of charged hadrons are shown, and compared to results from a hybrid model including viscous hydrodynamic description of the plasma phase, with excellent agreement [45].

Evidence on the formation of a thermalized medium at temperatures well exceeding the transition temperature predicted by lattice QCD can be provided by photon and dilepton spectra [57–64]. Photons and dileptons are radiated by the medium throughout the system's evolution, and their thermal distributions can be reconstructed from momentum and invariant mass spectra, respectively. However, while photons spectra are heavily affected by the “blue shift” effect due to the rapid expansion of the system, dilepton measurements allow for a clean determination of the temperature of the medium. In recent years, such measurements have been carried out by the NA60 [65, 66], STAR [67–69] and HADES [70] collaborations, yielding results consistently above the chemical freeze-out and QCD transition lines, see Fig. 4 (right).

### 2.1.2 Phase separation and critical point

From an experimental standpoint, it is not possible to directly locate the QCD phase transition on the phase diagram. However, by comparing results to theoretical models for the production of hadrons, it is possible to estimate the location of the chemical freeze-out in different experimental setups. Thermal fits, i.e. fits to hadron yields based on thermal models such as the hadron resonance gas (HRG) model (see Sec. 2.4.1) have been widely employed to chart the location of chemical freeze-out in high energy collisions. A collection of these from different collision energies and experimental facilities is shown in Fig. 1 (left), returning a consistent picture that is also in quite good agreement with current results for the QCD transition temperature at finite density. At large collision energies, the chemical freeze-out occurs shortly after hadronization, at temperatures around  $T = 150 - 160$  MeV, due to the explosive expansion of the fireball that cause a quick dilution of the system. At larger chemical potentials, the line of freeze-out points approaches the location of ordinary, cold and dense nuclear matter. While results for the transition temperature above  $\mu_B \approx 400$  MeV are not available, it is expected that the two curves detach at some point, due to the fact that lower collision energies create a less explosive system which ultimately freezes out at a lower temperature.

Chemical freeze-out has also been investigated by studying low order net-particle fluctuations [71–73], namely proton, pion, kaon, lambda serving as proxies for conserved  $B, Q, S$  charges as functions of the collision energy, and yielding comparable results as thermal fits to yields. Often, separate fits to strange and non-strange degrees of freedom result in improved fit quality and a consistent temperature gap between the freeze-out of strange and light particles, in a picture dubbed flavour hierarchy, which appears present at different collision energies in yields and fluctuations alike [72–75].

The rather complete picture of where collision systems freeze out in the phase diagram clashes with the fact that it is not known whether the QCD transition in its close vicinity is a true phase transition or not. While it is well established that at small chemical potential QCD undergoes a smooth transition, at larger density the transition might be of the first order. Should there be a critical point separating the two regimes, as many models of QCD suggest, at some intermediate collision energy the system would be bound to evolve in its vicinity. Identifying signals of criticality in experimental measurements is largely based on the corresponding divergence in the correlation length, which should result in large fluctuations across the system. In particular, event-by-event fluctuations in the baryon number have been identified as the most promising observables, with higher order fluctuations diverging with increasing powers of the correlation length [27]. Arguments based on the universality of critical behavior made it possible to identify a non-monotonic dependence on the collision energy as the typical smoking gun signature of criticality [28]. State-of-the-art results for net-proton fluctuation ratios from the STAR collaboration [32] are shown in Fig. 5 together with existing estimates of a non-critical baseline. It has been pointed out that factorial cumulants are likely to be more sensitive to criticality, as they isolate irreducible particle correlations of order  $n$ . Results from the HADES collaboration at  $\sqrt{s} = 2.4$  GeV appear to follow a similar trend. Although the quality of the data has sensibly increased thanks to the new fixed target program at RHIC, identifying a clear pattern for criticality is not straightforward. Though deviations from the baseline below  $\sqrt{s} \approx 10$  GeV are certainly suggestive, better precision from the data, and more importantly a firmer hold on the correct non-critical baseline will be needed to draw more precise conclusions. Additional data from the HADES and CBM experiments are expected in the future, as well as increased statistics on the STAR data.

## 2.2 Evidence based on lattice QCD

The theoretical investigation of the QCD phase diagram can count on a number of different approaches, each with its advantages and limitations. In Section 2.3 we will describe a number of methods to study the thermodynamics of QCD in different regimes, retaining more or less of the rich physics the theory entails. In this Section, we discuss the large body of evidence gathered in the past decades from the most robust method to study it, namely lattice simulations. In fact, lattice QCD translates the problem of solving the theory of strong interactions into a numerical experiment. Most of the established features of QCD thermodynamics are indeed due to lattice simulations.

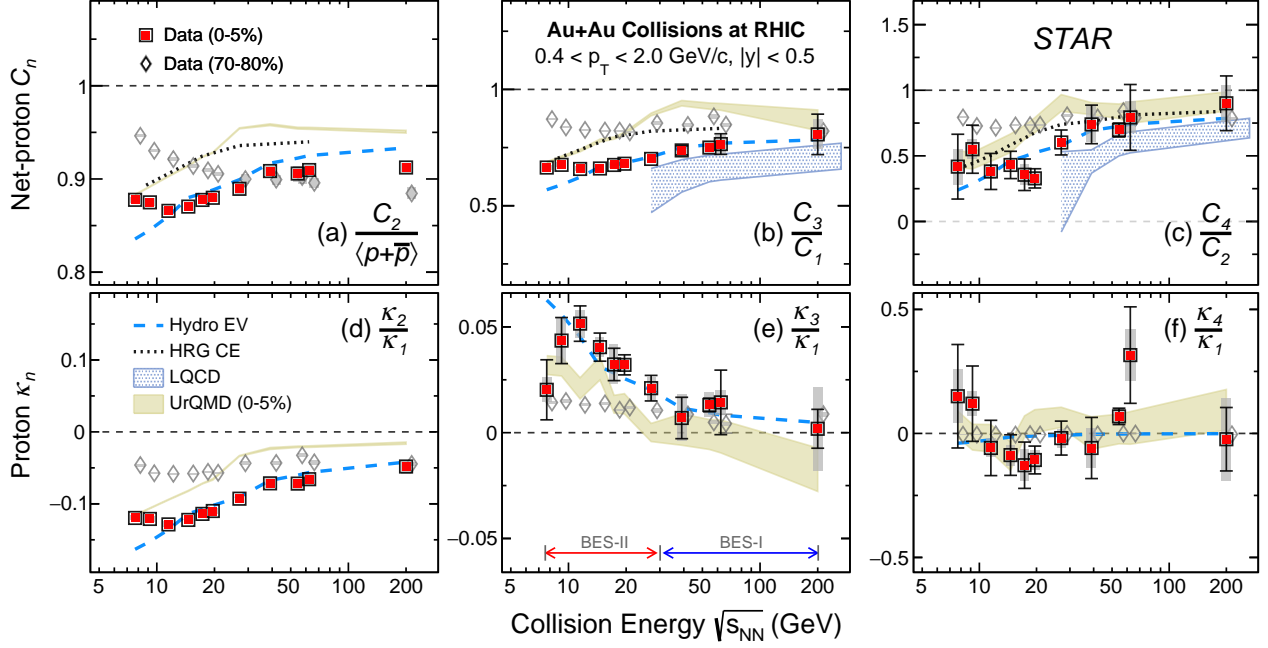


**Fig. 5** Net proton cumulant ratios (top) and proton factorial cumulant ratios (bottom) as functions of the collision energies from the STAR collaboration [32], together with non-critical baselines.

In short, the formulation of QCD on a lattice amounts to calculating *euclidean* path integrals like:

$$\mathcal{Z} = \int \mathcal{D}U \mathcal{D}\bar{\psi} \mathcal{D}\psi e^{-S_G[U]} e^{-S_F[U, \bar{\psi}, \psi]} \quad (1)$$

where  $U$  are the gauge fields and  $\bar{\psi}, \psi$  the fermion fields, and  $S_G, S_F$  are the gauge and fermion actions. The fermion part is bilinear in the fermion fields, and can thus be integrated analytically, yielding:

$$\mathcal{Z} = \int \mathcal{D}U e^{-S_G[U]} \det M[U] \quad (2)$$

where  $M$  is the Dirac matrix involving all fermion fields on the lattice, and its determinant depends only on the gauge configuration  $\{U\}$ . The path integral in Eq. (1) is formally analogous to the partition function of a statistical system [76], thus expectation values can be evaluated as:

$$\langle \hat{O} \rangle = \frac{1}{\mathcal{Z}} \int \mathcal{D}U \hat{O} e^{-S_G[U]} \det M[U]. \quad (3)$$

By discretizing spacetime, the integral over the field configurations becomes numerically tractable and can be computed by means of Monte Carlo methods by identifying  $e^{-S_G[U]} \det M[U]$  with a statistical weight assigned to configuration  $U$ . In practice, importance sampling methods are employed to estimate the integral by summing over only a small portion of statistically relevant configurations. This approach breaks down when a real chemical potential is included because then  $\det M[U]$  becomes complex making the would-be probability weight of a gauge configuration complex. This is the complex action problem in lattice QCD. Alternatives have been developed over the years to circumvent this problem and somehow bridge the gap between the theory accessible to simulations ( $\mu_B = 0$ ) and the theory of interest ( $\mu_B > 0$ ). These include Taylor expansion around  $\mu_B = 0$  [24, 77–85] and analytic continuation from imaginary chemical potential [6, 22, 23, 83, 86–94]. Reweighting methods have also been widely employed [95–101], and have recently enjoyed increased interest [102–106].

Most notably for the thermodynamics of QCD, lattice results include the determination of the transition line, the equation of state, and fluctuations of conserved charges, which are the main topics of this Section.

### 2.2.1 QCD transition

The fate of the hadronic phase at increasing temperature was initially proposed by Hagedorn to be a limiting temperature [107], known as Hagedorn temperature. Cabibbo and Parisi later showed that a more likely scenario would be the existence of a phase transition to a deconfined state of matter [108]. The nature and location of the transition remained uncertain for about 30 more years, until lattice simulations became powerful enough to provide definitive answers.

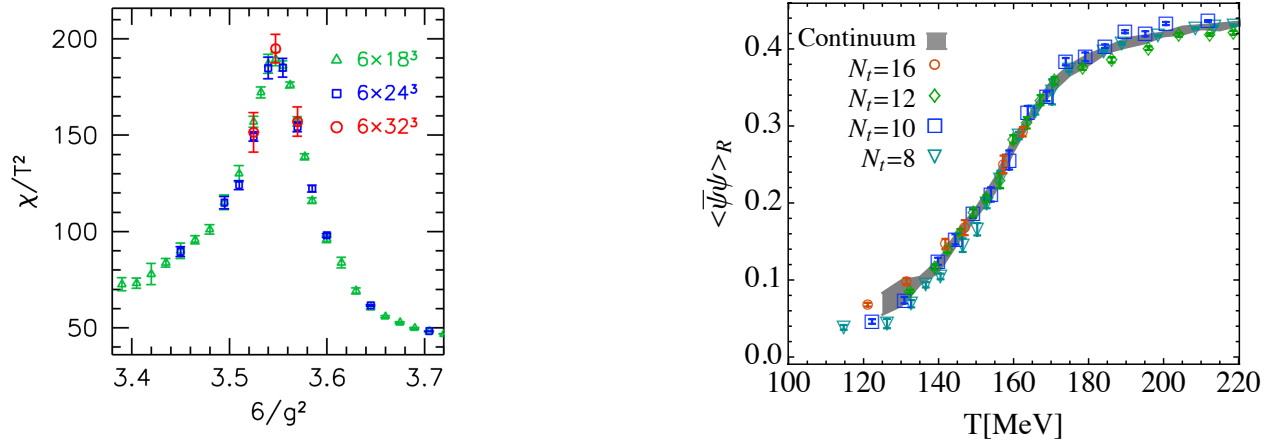


**Fig. 6** Left: chiral susceptibility as a function of the gauge coupling (equivalently, of the temperature) for different volumes. Figure from Ref. [3]. Right: chiral condensate as functions of the temperature, at finite lattice spacing and in the continuum. Figure from Ref. [4].

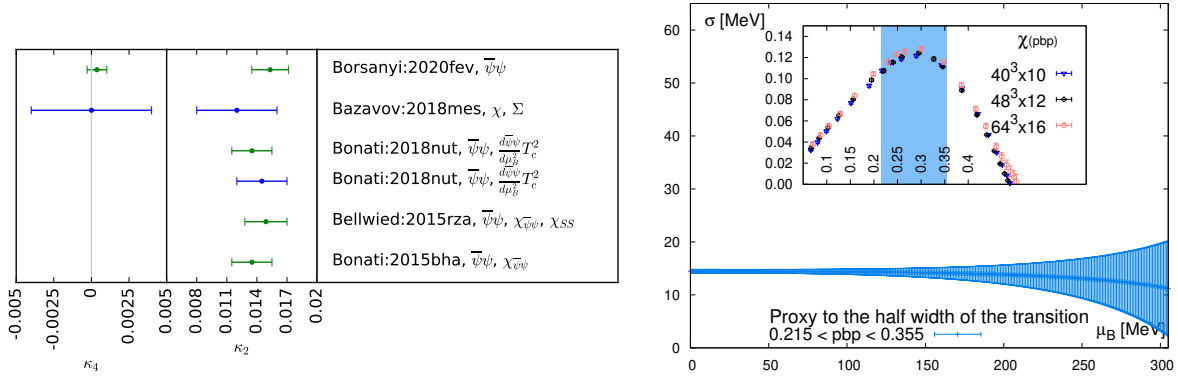


**Fig. 7** Left: world plot of the coefficients  $\kappa_2, \kappa_4$  of Eq. 4 (Taylor method in blue, imaginary  $\mu_B$  in green). Right: width of the transition at real chemical potential. Figures from Ref. [6].

Simulations of the pure Yang-Mills theory have quickly shown that the QCD transition at vanishing baryon density is of the first order [109, 110], yet it was a much harder task to apply lattice methods to full QCD with physical quark masses. By means of a finite size scaling of continuum extrapolated results it was shown in Ref. [3], that in full QCD the transition is a smooth crossover. In general, the susceptibility peak of the order parameter of a first-order transition is expected to grow in height and shrink proportionally to the system's volume, while in a crossover the susceptibilities converge. The left panel of Fig. 6 shows this for the chiral susceptibility with no visible dependence on the volume, indicating that the transition with Nature's choice of quark masses is a crossover.

The transition separating the hadronic phase from the quark gluon plasma is, in fact, related to two distinct, albeit related, phenomena, namely the restoration of chiral symmetry and deconfinement, see Section 3. In the right panel of Fig. 6 we show the temperature dependence of the pseudo-order parameter of the chiral transition, the renormalized chiral condensate. One observes a smooth rise around  $T \approx 155$  MeV, as expected in a crossover. Determinations of the pseudocritical temperature have been based on different observables, yielding slightly different values [4, 5, 111, 112]. More recent results based on chiral observables yield  $T \sim 157$  MeV with uncertainties around 1 MeV [6, 24]. The deconfinement aspect of the transition is more subtle, as will be discussed in Section 3.1.

At finite chemical potential, it is customary to express the transition temperature as an expansion:

$$T_c(\hat{\mu}_B) = T_c(0) \left( 1 - \kappa_2 \hat{\mu}_B^2 - \kappa_4 \hat{\mu}_B^4 + \mathcal{O}(\hat{\mu}_B^6) \right), \quad (4)$$

where  $\hat{\mu}_B = \mu_B/T$ , and the coefficients  $\kappa_n$  encode the chemical potential dependence of  $T_c$ . Results have been obtained making use of simulations at zero chemical potential, and directly evaluating the coefficients  $\kappa_n$ , or by determining the transition temperature for imaginary chemical potentials and analytically continuing to  $\mu_B^2 > 0$  [22–24, 83, 113]. Results based on chiral observables from several groups and both methods are shown in Fig. 7 (left), displaying good agreement. The NLO coefficient  $\kappa_4$  appears to be sensibly smaller than  $\kappa_2$ , and compatible with zero at the current precision. The transition line shown in Fig. 1 was obtained from analytical continuation in Ref. [6]. While estimates for the transition temperature have become extremely precise, this does not imply that the transition takes place over such a narrow range in temperature. The crossover transition is rather broad, and its width was estimated in Ref. [6] as a function of the chemical

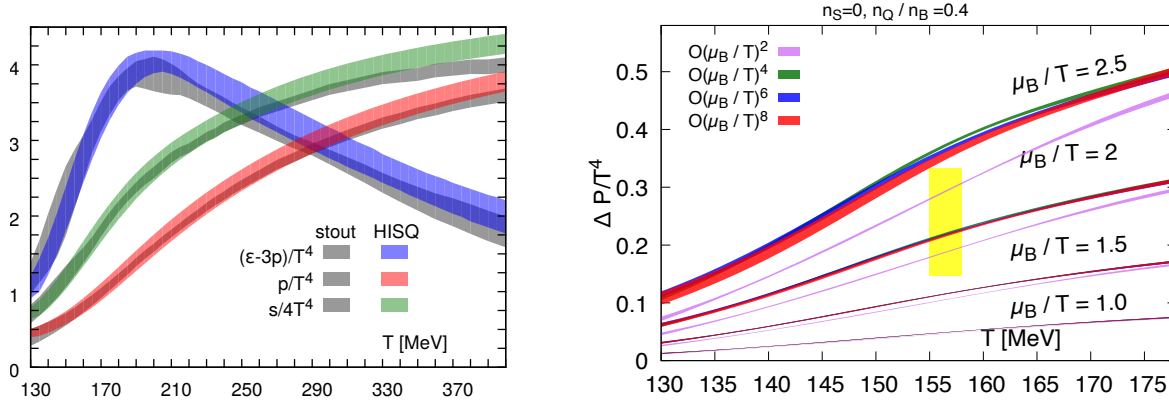


**Fig. 8** Left: equation of state at  $\mu_B = 0$  from the hotQCD and Wuppertal-Budapest collaborations, showing excellent agreement. Figure from [117]. Right: reduced pressure as a function of the temperature for different chemical potentials and orders of the Taylor expansion [118].

potential, by studying the chiral susceptibility peak. As shown in Fig. 7 (right), the half-width of the crossover stays constant around  $\Delta T \approx 15$  MeV for  $\mu_B < 300$  MeV, showing no hint of strengthening of the transition. Similarly, the chiral transition peak height is shown to remain constant in the same range. The extrapolation to higher chemical potentials is extremely difficult, but a proxy to the transition temperature could be computed in a smaller volume ( $16^3 \times 8$ ) up to 400 MeV in  $\mu_B$  [114]. The chosen proxy was the peak of the static quark entropy  $S_Q \sim \partial \ln L / \partial T$  as suggested in Ref. [115], because its value is more stable under the reduction of volume than the direct chiral observables [116]. The peak of  $S_Q(T)$  is found to roughly follow the chiral transition line of Ref. [6].

### 2.2.2 Equation of state

The equation of state is the fundamental quantity to describe the thermodynamic behavior of a system in different conditions. Its qualitative features can provide information on the effective degrees of freedom in a system, and help locate where phase transitions occur. For the modeling of heavy ion collisions, the equation of state of QCD is a fundamental quantity, which allows to take into account the thermodynamics of the theory and to close the set of equations to solve. Given the values of the volume  $V$  and of the control parameters  $T, \mu_B$ , the equation of state is uniquely determined by the partition function  $Z(V, T, \mu_B)$ , from which the free energy  $f = -T \ln Z(V, T, \mu_B)$  is defined. The pressure is (minus) the derivative of  $f$  with respect to the volume, which under the assumption of a homogeneous system simply amounts to  $p = -f/V = T/V \ln Z$ . All thermodynamic quantities are then defined as derivatives of  $p$ .

On the lattice, it is not possible to calculate the pressure directly. Most commonly, the integral method [119] is employed, writing the pressure as:

$$\frac{p(T)}{T^4} = \frac{p(T_0)}{T^4} + \int_{T_0}^T \frac{dT}{T} \frac{I(T)}{T^4}, \quad (5)$$

where the trace anomaly  $I(T)$  is determined by the renormalized values of the chiral condensates and the gauge action, and the integration constant  $p(T_0)/T^4$  is determined e.g., as an integral of the chiral condensates in the quark masses.

For about a decade now there has been substantial agreement over the equation of state of QCD at vanishing density between different collaborations, with physical values of the quark masses and in the continuum limit, see e.g. Fig. 8 (left) [117, 120]. A new determination was presented in a recent work [25], with smaller uncertainties but compatible with the previous ones.

At finite density the equation of state can be determined as a Taylor expansion [78, 121]:

$$\frac{p(T, \mu_B)}{T^4} = \sum_n \frac{1}{n!} \chi_n^B(T) \left( \frac{\mu_B}{T} \right)^n, \quad \text{with} \quad \chi_n^B(T) = T^n \frac{\partial^n (p/T^4)}{\partial \mu_B^n}, \quad (6)$$

where only even coefficients contribute due to charge conjugation symmetry. The determination of the susceptibilities  $\chi_n^B$  is very costly when the order is increased, and convergence of the series is usually checked by comparing subsequent orders. Results for coefficients up to order 8 have been published [24, 79–85], but only up to order 4 were continuum extrapolated (and order 6 in a smaller volume [122]). Fig. 8 shows the baryon density as a function of the temperature, for different chemical potentials and different expansion orders, obtained from a Taylor expansion in Ref. [118]. A multidimensional Taylor expansion of the QCD pressure was constructed in Refs. [123, 124] to cover the full 3D space of chemical potentials  $\mu_B, \mu_Q, \mu_S$  needed in the hydrodynamic description of heavy ion collisions with multiple conserved charges.

Imaginary  $\mu_B$  simulations have been used in the past to determine fluctuation observables [125, 126]. In Ref. [93] an alternative approach – sometimes dubbed  $T'$ -expansion and generalized in Refs. [94, 127] – was developed to extrapolate the equation of state to finite chemical

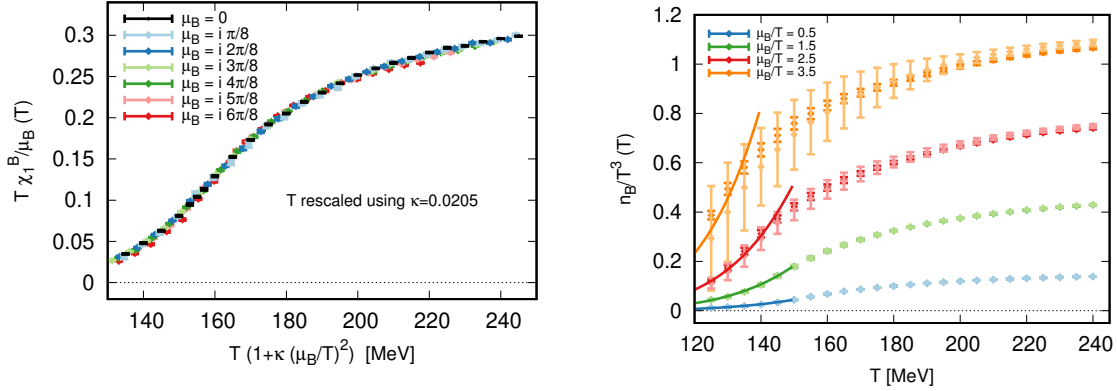


**Fig. 9** Left: collapse of curves of  $n_B/\hat{\mu}_B$  for different imaginary valued  $\mu_B$  when  $T$  is replaced by  $T' = T(1 + 0.0205\hat{\mu}_B^2)$ . Right: baryon density in the continuum limit, for different chemical potentials, at two subsequent orders in the expansion (darker shade is  $O(\hat{\mu}_B^2)$ , lighter shade is  $O(\hat{\mu}_B^4)$ ). The perfect agreement up to  $\hat{\mu}_B = 3.5$  shows the good convergence of the series. Figures from Ref. [93].

potential. This approach is based on the ansatz of a simplified  $\mu_B$  dependence of the baryon density in the vicinity of  $\mu_B = 0$ :

$$n_B(T, \mu_B) = \hat{\mu}_B \chi_2^B(T', 0) \quad \text{with} \quad T' = T(1 + \kappa_2(T)\hat{\mu}_B^2 + \kappa_4(T)\hat{\mu}_B^4 + O(\hat{\mu}_B^6)), \quad (7)$$

where the coefficients  $\kappa_n(T)$ , similarly to Eq. (4), encode the  $\mu_B$  dependence, but here are crucially  $T$ -dependent themselves to define the expansion rigorously. This expansion amounts to a reorganization of the Taylor series, carried out along lines of constant  $n_B/\hat{\mu}_B$ . This results in better convergence, and smaller uncertainties, as shown in Fig. 9 (right).

## 2.3 Diagrammatic approaches to QCD

### 2.3.1 Weak coupling expansion

Asymptotic freedom relates large temperatures to small values of the running coupling. However, at phenomenological temperatures of the high temperature phase the couplings are of  $O(1)$ , and it is not natural to expect a well converging perturbative series. Subsequent orders of the expansion of the thermodynamic potential in the coupling constant  $\alpha_s$  exhibit a wildly oscillating pattern (see Fig. 10 left). We know this to order  $\alpha_s^3 \log \alpha_s$  [128] and there is no hope for higher orders with perturbative methods. Their computation is prevented by the magnetic mass problem [129, 130], which limits the calculable order in this case to  $\alpha_s^3$  due to infrared divergences in the Feynman diagrams: an additional power of the effective infrared cutoff ( $\sim g^2 T$ ) contributes to the denominator for each new loop order.

Hard thermal loop perturbation theory (HTLpt) has brought much improvement to the poor prospects of ordinary perturbation theory. The idea is to consider massive quasi-particles instead of massless gluons and quarks as the basis of the expansion, thus, moving the expansion point. While such shifting by a mass term can be easily introduced in a scalar theory, the gauge invariant equivalent is more elaborate [131], but still depends on a mass parameter  $m_D$ . The expansion scheme has been implemented to two-loop [132] and three-loop [133] order. The loop order does not completely determine the procedure, because there are multiple schemes for selecting the optimal  $m_D$ . One option is to use the mass parameter of the effective theory obtained by dimensional reduction [134].

The improved behaviour of the HTLpt is shown in the right panel of Fig. 10. Note, that these results are phenomenologically relevant only if calculated to three-loop order. Higher loop results are not expected since HTLpt suffers from the magnetic mass problem just as ordinary perturbation theory does [133, 136]. Also, the results shown in Fig. 10 exhibit a large renormalization scale dependence. Renormalization is typically performed at the energy scale of  $\mu = 2\pi T$ , but variations by a factor two on both sides are also shown, to estimate the systematic errors of the truncation.

The formalism was extended to finite quark-chemical potential and quark number susceptibilities [137–141]. Especially the fourth-order baryon and isospin fluctuations exhibit very small scale dependence. Dedicated lattice studies computed these at high temperatures in the continuum limit and found good agreement with HTLpt down to 250 MeV temperature [142, 143].

The framework of electrostatic QCD (EQCD) [147–149] offers a systematic approach to weak coupling expansion. It is based on the reduction of the four dimensional full theory to a three dimensional bosonic gauge theory with a scalar field in the adjoint representation. Even the order  $\alpha_s^3$  can be included by simulating the reduced theory on the lattice. Among other applications, such results are available for the pressure [145, 150] and quark number susceptibilities [151, 152]. The use of non-zero quark masses was discussed in Ref. [153]. In Fig. 11 we show a comparison of results on light quark number susceptibilities with lattice data [143, 146].

### 2.3.2 Functional QCD

Hard thermal loop thermodynamics is just one example for the resummation schemes that approximate the QCD thermodynamical functional. In this section, we discuss two generic approximation schemes that run under the common label of functional methods for QCD. In these schemes, equations for the  $n$ -point functions of the underlying quantum field theory are constructed; this often starts with  $n = 2$ ,

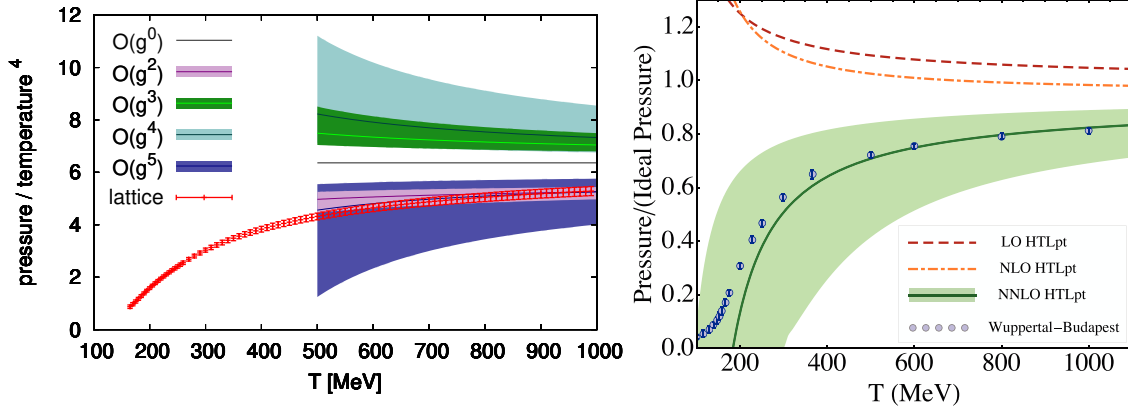


**Fig. 10** The normalized QCD pressure ( $p/T^4$ ) as a function of temperature (4-flavor case). The pressure approaches the Stefan-Boltzmann limit at high  $T$ . The pace at which this happens should be controlled by perturbation theory, but its orders show an oscillatory pattern (left panel). Three-loop hard thermal loop perturbation theory cures this and agrees with lattice data, though with large theoretical uncertainties [133]. (Lattice data taken from Ref. [135]).

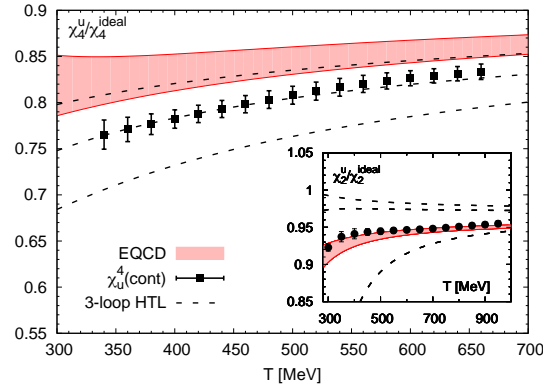


**Fig. 11** Fourth and second order (in the inset) quark number susceptibilities found with two approaches to weak coupling expansion: 3-loop HTLpt [144] and EQCD [145, 146], compared with lattice data [143, 146]. The uncertainties of EQCD are smaller than in the case of HTLpt (the latter shown with dashed lines).

that is, the propagators. However, these equations depend on higher-point functions, such that an infinite hierarchy of equations arises, that requires a truncation for practical use. The various approaches clearly differ in technical terms, but the resummation they implement is often guided by the same principle.

The functional renormalization group (FRG) offers a self-consistent framework for solving a quantum field theory. It integrates the path integral starting with the UV degrees of freedom and sequentially progressing towards the infrared. This is done by solving a flow equation, e.g. the Wetterich equation [154] (see also [155, 156]), that describes the response of the effective action or its derivatives to the inclusion of a new momentum scale as the infrared cutoff of the theory is reduced towards zero. This principle has already been used successfully applied in several field theories, including those with phase transitions [157]. For a detailed discussion of the systematics of this approach in the QCD context, see Ref. [158].

An initial success in the application to strong interactions was the computation of the gauge and ghost propagators in the vacuum of the Yang-Mills theory [159]. These are, by now, consistent among different functional methods, agree with lattice and satisfy the criteria for color confinement [160, 161]. Quark confinement and the deconfinement transition at finite temperature were shown to follow from the features of these propagators by solving the flow equation for the effective potential of the temporal gauge background, strongly related to the Polyakov loop [162].

A key feature in the FRG approach to full QCD is dynamical hadronization [163, 164] (see Ref. [165] for a detailed discussion). This means that the flow equations for the gluon, ghost and quark correlators are extended with fields representing composite (meson) operators (see Ref. [166] for the generalization to other channels). As the infrared cut-off is reduced, these degrees of freedom are automatically activated and account for the dynamical breaking of chiral symmetry and the emergence of hadrons [167]. For this to happen, one formulates coupled flow equations for the propagators and vertices of the fundamental theory (QCD) and of the composite operators in some parametrized form [167, 168]. This is unlike effective models (to be discussed in section 2.4.2) where the gauge fields are already integrated,

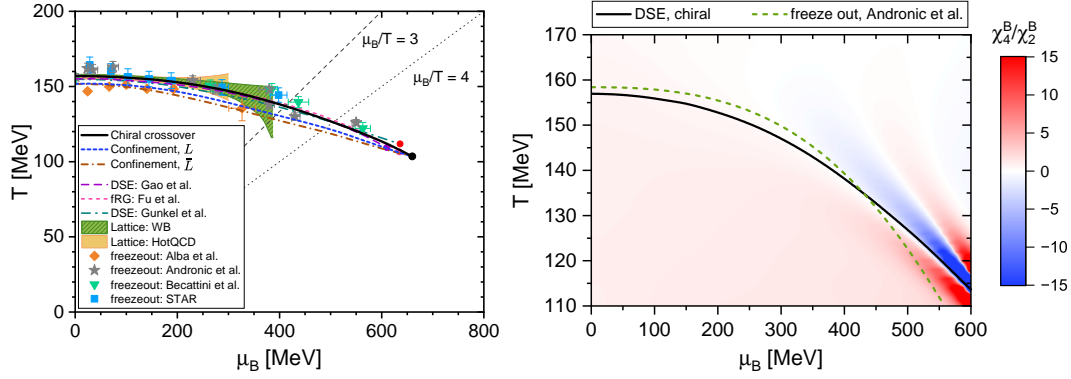


**Fig. 12** Left: Summary plot of the QCD phase diagram based on functional approaches. The additional data points refer to the empirical chemical freeze-out parameters. Right: baryon cumulant ratio  $\chi_4^B/\chi_2^B$  on the phase diagram ( $\mu_S = 0$  setup). (Plots taken from Ref. [189])

leaving a handful of pre-set hadrons as degrees of freedom. It is also in contrast with the brute force approach of lattice QCD, that computes the hadronic phase solely in terms of gluonic and quark variables.

The state-of-the-art formulation of the truncated flow equations is the result of decades of research [166–170]. The transition temperature in Yang-Mills theories [162] and in the two-flavor theory [171] were important milestones. By today, functional results for the QCD transition with 2+1 flavors include the chiral condensate as a function of temperature, which agrees with lattice results [4, 168]. The chemical potential dependence can also be studied, from which the curvature of the transition line emerges ( $\kappa = 0.0142(2)$  in the  $\mu_S = 0$  scheme, close to lattice results [90, 113]). The location of the critical end-point was computed to be  $(T_{\text{CEP}}, \mu_{B,\text{CEP}}) = (107, 635) \text{ MeV}$  [168]. Note, that to demonstrate the critical behaviour itself would require further ingredients.

Another successful guiding principle for resummation schemes is offered by the Dyson-Schwinger approach [172]. Dyson-Schwinger equations are path integrals of total derivatives that reveal non-trivial identities between the full, non-perturbative  $n$ -point functions. These can be conveniently set up in the Landau gauge. A notable feature of these equations is that they can be solved in the infrared limit and the solution is consistent with certain confinement criteria [159]. The momentum scales achievable by this scaling solution is, however, below what is relevant for the phase diagram ( $\Lambda_{\text{QCD}}$ ). Unlike the  $n$ PI effective actions, a truncation is introduced through the use of an approximate full vertex [173]. One example is the rainbow ladder truncation, where the  $qq$  interaction is reduced to an effective gluon exchange. Due to the complexity of the gluon self-interaction, in one possible approach the gluon propagator is taken from finite-temperature Yang-Mills lattice simulations [174]. The gluon propagators (electric and magnetic) are unquenched by solving a coupled propagator equation for gluons and quarks. This approximation misses implicit, in  $1/N_c$  subleading quark loop effects in the Yang-Mills self-energies. Nevertheless, the first order transition of the Yang-Mills theory as well as the existence of a heavy critical mass (see section 3.1) including its chemical potential dependence could be calculated with these equations [175]. Addressing the chiral limit with the Dyson-Schwinger equations is more challenging. The rainbow-ladder truncation correctly predicts the second order transition in the chiral limit, although with mean field exponents [176]. It is crucial for the study of the chiral transition to include the pion and sigma propagators in the quark equations [177].

The Dyson-Schwinger equations were first solved for the 2+1 flavor case with physical quark masses in Refs. [178, 179], and later extended with the charm quarks in Ref. [180]. While resulting transition temperature agrees with lattice by construction, the quantitative agreement of the chiral condensate as a function of temperature with lattice simulations is non-trivial. The solution features a chiral crossover and a critical end-point in the phase diagram at  $\mu_B \approx 500 \text{ MeV}$ . Later, to refine the quantitative analysis, baryon effects were considered in the quark-gluon vertex [181]. In Ref. [182] the quark self-energy was extended with mesonic backcoupling terms, simplifying the vertex at the same time. In this approximation the critical end-point is predicted to be at  $(T_{\text{CEP}}, \mu_{B,\text{CEP}}) = (117, 600) \text{ MeV}$ .

Apart from the location of the critical point, many observables have been computed using the Dyson-Schwinger equations. The equation of state was extracted using a 2PI effective action of the quark sector in the rainbow-ladder truncation [183]. The fluctuations of conserved charges were computed in detail in a more elaborate approximation of the quark-gluon vertex in Ref. [184].

Thanks to new solutions to the functional renormalization group equations the vacuum quark-gluon vertex and the unquenched gluon propagator are available for use in the Dyson-Schwinger equations [185]. The latter can be matched with the propagator from lattice [186]. This way new forms of the Dyson-Schwinger equations have been introduced and solved [187]. With the new truncation the equation of state [188] and fluctuations of net-baryon number could be computed at finite temperature and density [189]. Most importantly a new result on the transition line (with the curvature parameter  $\kappa = 0.0147(5)$ ) and the critical end-point was found in [190] at  $(T_{\text{CEP}}, \mu_{B,\text{CEP}}) = (109, 610) \text{ MeV}$  (see Fig. 12). Remarkably, in the works here cited, the crossover temperatures from the chiral observables and the Polyakov loop are always close and are equal at the critical endpoint.

Functional approaches to QCD have presented a consistent view on the QCD phase diagram. This is summarized in the left panel of Fig. 12. All approximations feature a chiral critical endpoint near  $(T, \mu_B) \approx (105 - 115 \text{ MeV}, 600 - 650 \text{ MeV})$ . The right panel shows the net-baryon cumulant ratio  $\chi_4^B/\chi_2^B$  from the most recent DSE computation. This is the central observable for the experimental search (then replacing baryons by protons) [189], it was previously mapped by low energy models embedded in functional QCD [191, 192].

## 2.4 Models that approximate QCD

### 2.4.1 Hadron resonance gas model

The better known limits of the thermodynamic structure of QCD matter correspond to large or small temperature and chemical potential.

When both are small, QCD matter is in a hadron gas phase, in which quarks and gluons are *confined* inside composite particles with neutral color charge called hadrons, like protons and neutrons. At very low temperature and density, this phase is very dilute, interactions are negligible and the thermodynamics is dominated by the lightest degrees of freedom, namely pions. When either  $T$  or  $\mu_B$  is increased, heavier states are thermally excited and interactions become more prominent. Before the advent of QCD, Hagedorn proposed [193] that a thermally excited strongly interacting medium would be made up of composite objects populating an exponentially growing spectrum for increasing masses. While in Hagedorn's view this was a continuous "effective" spectrum modeling the formation of strongly interacting objects, it predicted a maximum possible temperature for strongly interacting matter of the order of  $T \approx 200$  MeV, which now can be seen as a surprisingly accurate estimate for the transition to the *deconfined* phase [108].

In the modern view, this spectrum is replaced by the actually observed hadrons, which indeed populate an exponentially growing spectrum. The modern version of Hagedorn's model is the hadron resonance gas (HRG) model, which in its simplest (ideal) version describes an interacting hadron gas in terms of a non-interacting gas of hadrons and all their resonant states. The system's partition function factorizes into single-particle contributions as  $\ln Z(T, \mu_B, V) = \sum_i \ln Z_i(T, \mu_B, V)$  with:

$$\ln Z_i(T, \mu_B, V) = \pm \frac{d_i V}{2\pi^2} \int_0^\infty dp p^2 \ln \left( 1 \pm e^{\frac{\sqrt{p^2 + m_i^2} - \mu_i}{T}} \right), \quad (8)$$

where the sum runs over all hadron states and  $d_i$ ,  $m_i$ ,  $\mu_i$  are the spin degeneracy, mass and single-particle chemical potential of species  $i$ . Even with its rather crude setup, the HRG model has proven extremely successful in reproducing experimental results as well as theoretical predictions in the low temperature phase. This is quite impressive, considering that the model has virtually no free parameter: given a value for the temperature, the baryon chemical potential and the system volume, all thermodynamic quantities are determined.

Perhaps the most striking success of the model is its ability to *simultaneously* describe the abundances of detected hadrons in heavy ion collisions over several orders of magnitude, from pions to omega baryons and even light nuclei, with a single temperature, baryon chemical potential and volume [12, 71]. Among the perks of this model, especially useful when comparing to experimental measurements, is the possibility to take into account genuine experimental effects, such as the contributions from decay feed-down and the implementation of acceptance cuts. These effects cannot easily be included in other theoretical approaches to the study of QCD thermodynamics. Although initially the model has been applied to large colliding systems in the grand canonical formulation, it has been later shown that canonical corrections can – and should – be included for smaller colliding systems, such as heavy ion collisions at lower energy and proton-proton or proton-nucleus collisions at high energies [194, 195]. With these corrections, a good description is achieved for a huge variety of colliding setups. Furthermore, the comparison with other theoretical calculations is another great success of the HRG model, which can precisely reproduce most thermodynamics results from lattice QCD [105, 142, 196–198].

Although the HRG has proven extremely successful even in its ideal form, a more realistic treatment of interactions is necessary to describe observables which are very sensitive to the details of the hadron spectrum or the strength of interactions in the medium [85, 91, 118, 199], as for example high order fluctuations of conserved charges [200]. In the S-matrix approach to relativistic statistical mechanics based on the virial expansion, first introduced by Dashen, Ma and Bernstein [201], information on the phase shifts due to hadron interactions can be used to construct the second virial coefficient. The ideal HRG model thus corresponds to the leading order of the virial expansion, in which it also includes contributions by all known resonant states. However, all interactions not related to resonance formation are neglected. It was later shown that a large cancellation appears in the pressure between non resonant attractive and repulsive contributions [202]. The virial expansion in the S-matrix formalism was employed e.g. to study the effect of interactions on baryon fluctuations [200], and to investigate the existence of unknown strange baryon states [203]. In Ref. [204] it was argued that the quality of thermal fits to particle yields can be dramatically improved by including the phase shift information on pion-nucleon scattering. The main limitation of the S-matrix approach is the limited available information on hadronic scattering phase shifts, which have to be modeled when not experimentally available.

For this reason, a number of modifications have been considered to further improve the accuracy of HRG model predictions. The hadron spectrum employed in the model can be adjusted by explicitly including additional states [205–208], for example those predicted by theoretical models [209–211]. Repulsive mean field interactions were included in Ref. [200], showing that the effect on baryon fluctuations is the same as in the relativistic virial expansion, and later employed to study the equation of state [212]. The same setup was applied in Ref. [213] – also including additional hadronic states – to study the equation of state and the chiral transition line at finite baryon chemical potential, finding good agreement with lattice results. In a similar fashion, repulsive excluded-volume and attractive van der Waals-like interactions have also been extensively studied in recent years (see Ref. [199] for a review), which also provide an improved description of lattice QCD fluctuations data over the ideal formulation. An advantage of the van der Waals approach is the natural emergence of the liquid-gas transition and associated critical point, which can be reproduced by tuning the values of the repulsive and attractive terms [91].

### 2.4.2 Effective models

Due to the difficulty in solving the full theory of strong interactions, one has often resorted to low-energy effective theories to predict the features of the QCD phase diagram. Such models are sharing the symmetries of the full theory, and go beyond the claim of being in the universality class of QCD near some critical point. Effective models identify the relevant degrees of freedom and formulate a field theory

in terms of these. The resulting field theory is not always renormalizable, a cut-off scale is needed, above which the model is not defined. Typical cut-off scales are below 1 GeV.

Effective models can be classified by their principal ingredients. One of the earliest is the linear sigma model where the pions and an isospin singlet sigma are combined to model the chiral symmetry breaking as in a scalar  $O(4)$  model [214]. Integrating out the sigma degree of freedom defines the non-linear sigma model. Chiral perturbation theory, too, expresses QCD in terms of its lightest degree of freedom, the pions, or light pseudoscalar mesons, in general [215]. This leading Lagrangian coincides with the non-linear sigma model [216]. A chiral transition was predicted to happen at 190 MeV in a low temperature expansion of the two-flavor theory to three-loop order [217]. In the chiral limit the transition temperature would be 20 MeV lower.

The Nambu–Jona–Lasino model is also an effective theory for chiral symmetry breaking [218, 219]. The principal degrees of freedom are fermions that form, in analogy to superconducting, quark-antiquark pairs as composite particles, the light mesons. (see Ref. [220] for a historic review). Effective models are often solved in the mean field approximation, where the operator valued equations of motions are linearized around a nontrivial (mean field) value of composite operators, facilitating an order parameter for chiral symmetry breaking. A shortcoming of the NJL model is the lack of confinement: in the chirally broken phase the fermions describe the constituent quarks. In this framework the QCD phase diagram was sketched in the  $T - \mu_B$  plane for the two flavor theory [221]. This diagram featured a first order transition at finite  $\mu_B$  and  $T = 0$  and a smooth transition at finite  $T$  and  $\mu_B = 0$ , indicating the necessity of an end-point on the  $T - \mu_B$  plane. The position of the end-point can be tuned with the parameters, and it could be removed entirely if we consider a sufficient repulsive vector interaction among the possible four-fermion terms [222].

If we explicitly include the pion and sigma fields together with the quark fields in the effective Lagrangian, with the gluon fields already integrated, we get the quark meson model. Here the phase structure has been computed in Ref. [223] using a renormalization group method. They find a second order transition in the chiral limit that smoothens into a crossover for physical pion mass. This crossover also turns first order in an end-point, however, the structure at low temperature, high density is more complicated.

Since neither the Nambu–Jona–Lasino, nor the quark meson model can account for the deconfinement, newer models include the order parameter of the deconfinement, the Polyakov loop as a dynamical variable in the effective Lagrangian. At the heart of these models there is a potential for the Polyakov loop with a temperature dependent parametrization such that the center symmetry is respected and the lattice results for the quarkless gauge theory are reproduced. The Polyakov loop is then brought into direct connection with the temporal gauge field, which is fed into the Dirac operator of the quarks degrees of freedom. These extended models, dubbed PNJL and PQM, respectively, have been used extensively in the literature to explore the phase diagram (see [224–226] for the PNJL model and [227–229] for the PQM).

A common feature in these results is the existence of a critical end-point that separates the crossover at high temperature from the first order line at high density. Although the position of the end-point varies, one can conclude with the semi-quantitative picture of Fig. 13. The most distinctive feature is the blue transition line that separates nuclear matter from quark matter. The labels suggest deconfinement, but the definition is based on chiral symmetry breaking. The phase in the right end of the diagram (Color Flavor Locking) is a superconducting phase [230, 231], see Section 5.2.

The predictive power of such effective models has been greatly enhanced by their embedding into the functional renormalization group framework. The two-flavor PQM model was revisited in this sense in Ref. [232] and found a chiral crossover and a critical end-point near the expected position of the liquid-gas transition. Several improvements have been introduced to the truncation of the effective action: the inclusion of quark backreaction to the Polyakov loop potential [228], the use of the ‘t Hooft determinant to consider the  $U(1)_A$  breaking [233]. Thanks to the fluctuations included by the FRG formalism a smooth transition is obtained in accordance with lattice simulations. The slopes of the remnant order parameters were larger in the mean field approach. Using a simple approximation for the strange degree of freedom this effective model was used to derive very high order fluctuations, showing promising smoking-gun signal for the baryon cumulant ratio  $\chi_4^B/\chi_2^B$  on the phase diagram in a large region around the critical end-point [191]. These results were further refined by directly evolving the RG flow of quark-meson scattering processes with a new result for the critical endpoint at  $T_{CEP} = 98$  MeV and  $\mu_B = 643$  MeV [192], which is fairly close to what was found in full functional QCD [168] of Section 2.3.2.

A different class of models of QCD are those based on the gauge-gravity duality, in particular the Einstein–Maxwell–Dilaton (EMD) type models [234–236]. In these models the QCD phase diagram is mapped onto asymptotically Anti-de Sitter (AdS) charged black hole geometries in five dimensions. They are constructed with the explicit intent to reproduce the observed features of the QCD equation of state at zero chemical potential. The minimal ingredients they contain are the bulk metric field, a Maxwell field whose value at the boundary sets the chemical potential, and a dilaton field to break conformal invariance. A number of free parameters are fixed by requiring agreement with lattice QCD results at zero chemical potential. These models inherently include the almost perfect fluidity of the QGP, and in all different realizations predict the existence of a critical point [237, 238]. They have been employed to determine transport coefficients of the QGP [239–242], the location of the critical point [243, 244] and the equation of state of QCD at finite density [245], showing agreement with lattice simulations where results from the latter are available.

### 3 Theory of the phase diagram

#### 3.1 Quark masses and symmetries: the Columbia plot

In the following discussion, we review the phase diagram in a specific representation: instead of temperature and chemical potential, the axes indicate the values of the strange and light quark masses, thus positioning QCD in theory space. This is the famous Columbia plot [247], see Fig. 14. The physics of the transition can be vastly different in different corners of this diagram: in the top right corner all quark

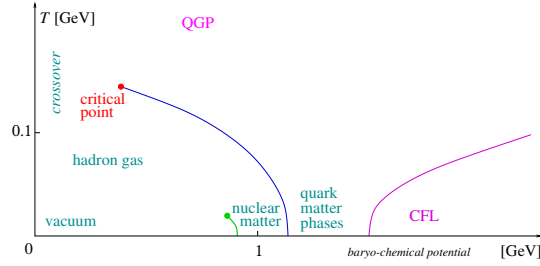


Fig. 13 The standard view on the QCD phase diagram as suggested by several effective theories [246].

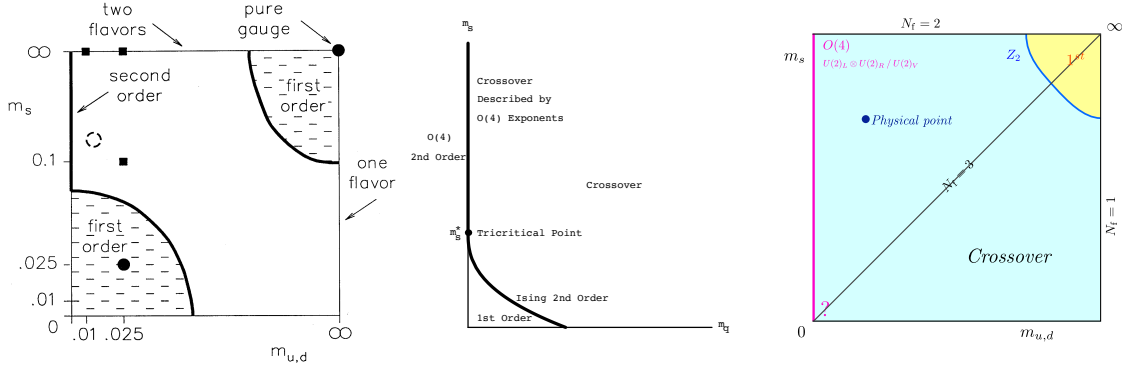


Fig. 14 The Columbia plot in its original version (left) with a handful of simulation points (black dots) [247], in agreement with the theoretical arguments of [248]. The middle panel shows the detailed theoretical expectations for the lower left corner [249]. New lattice results challenge the original view and propose a new version (right) [250]. Recent effective model studies find room in the parameter space for this scenario, too (see e.g. [251]).

masses are infinite, and purely the dynamics of gluons determine how confinement stops as temperature increases. However, in the lower left corner, light quarks take the dominant role and restore chiral symmetry at high temperature. QCD with physical quark masses resides in the bulk of the diagram where the transition is a crossover driven by an interplay of deconfinement and chiral dynamics. In the Columbia plot the order of the transition is marked for each possible pair of light and strange masses. The left panel shows the first attempt to explore this vast range of parameters [247]. Even after 35 years there are still unsettled issues, mostly centered around its lower left corner.

### 3.1.1 The deconfinement transition

A key feature of QCD is the running of the coupling constant, that is, the effective coupling depends on the energy scale. A generic feature of non-abelian quantum field theories (below a threshold in the number of flavours) is asymptotic freedom, which means that the coupling goes to zero in the ultraviolet. Thus, at extreme temperatures, the theory is weakly coupled where the fundamental degrees of freedom (quarks and gluons) are also the relevant ones. By their nature, these are color-nonsinglets. This is in contrast to color confinement at low temperatures with color singlet effective degrees of freedom. Whether or not the two temperature regions are separated by a phase transition depends on the presence of matter fields.

Specifically for the quark-less case (Yang-Mills theory), the path integral has an exact symmetry related to the center of the gauge group ( $Z(N_c)$ ). This means, that for every gauge configuration, there are two others with the same weight. The expectation value of the temporal Wilson line (the Polyakov loop) [252]

$$L(\vec{x}) = \frac{1}{N_c} \text{Tr} \mathcal{P} \exp \left[ \int_0^{1/T} A_0(t, \vec{x}) dt \right] \quad (9)$$

transforms non-trivially, a non-vanishing expectation value signals the spontaneous breaking of the center symmetry. ( $N_c$  stands for the number of colors and  $\mathcal{P}$  prescribes path ordering). At the same time, the expectation value of the Polyakov loop is related to the free energy of a static color source  $F_q$  [252], with  $\langle L \rangle = e^{-F_q/T}$ . A zero value can be identified with a divergent free energy associated with a color-nonsinglet static (infinitely heavy) quark. This idea connects the center symmetry breaking with quark deconfinement. The perturbative vacuum is clearly not center symmetric. A highly non-trivial feature of  $SU(N_c)$  theories is the restoration of this symmetry at low temperature. The determination of the temperature dependence of  $\langle L \rangle$ , and thus the numerical observation of the deconfinement transition, was the first successful application of lattice simulations to QCD thermodynamics [253, 254]. The order of the deconfinement transition depends on the number of colors. Monte Carlo simulations with finite size scaling have established that the transition is second order for  $N_c = 2$  [255] and first order for  $N_c = 3$  [109, 110], which persists for larger  $N_c$  [256]. The first order nature was predicted by Svetitsky

and Yaffe based on generic arguments on the effective potential of the Polyakov loop [257]. In fact, the cubic term in  $L$ , as required by the  $Z(3)$  symmetry, is not compatible with a continuous transition and  $Z(3)$  is not among the known universality classes. Detailed studies of the latent heat [258, 259] have showed that among the  $SU(N)$  theories the transition in  $SU(3)$  is weak, with a latent heat 3–4 times smaller than in the large- $N$  limit  $L_h/T_c^4 \approx 0.42(7)N_c^2$  [258]. It was recently determined to be  $L_h/T_c^4 = 1.025(21)_{\text{(stat)}}(27)_{\text{(sys)}}$  [259] (see also [260, 261]). The pressure function  $p/T^4$  versus  $T$  has been a subject of several large-scale lattice studies up to perturbative temperatures [262–264].

The temperature of this first-order transition is sometimes quoted in MeV units. Since lattice simulations can only produce dimensionless ratios or products, this assumes the universality of a reference scale, that can be also defined in full QCD with 2+1+1 flavors, where it is then given in MeV. By choosing the reference scale (spatial string tension, Sommer scale ( $r_0$ ), or the flow-based scales  $w_0$  and  $\sqrt{t_0}$ ) one gets 275 MeV, 322 MeV, 344 MeV and 285 MeV, respectively. This ambiguity is inevitable when the running of the coupling differs between the simulated theory and Nature.

Matter fields break the center symmetry explicitly. To be precise, a center transformation can be re-interpreted as a shift in the quark chemical potential by the imaginary value  $\mp i2\pi T/N_c$ . Due to the explicit breaking of this symmetry, the Polyakov loop ceases to be an exact order parameter for the transition. In the language of an effective potential this means a linear tilt in the effective potential towards positive real values to leading order in the hopping parameter expansion [265]. Allowing for a continuous dependence of the latent heat as a function of control parameters, such as the inverse mass, one can expect a finite first-order region in the top-right corner of the Columbia plot (Fig. 14). This region is delimited by a line of critical masses stretching between the two-flavor (top) and single-flavor (right) edges of the diagram. Along this critical line the effective potential of the real part of the Polyakov loop is akin to that of the Ising model, where the quark masses provide the fine-tuning to make the positive and negative valued minima of equal statistical weight. Without quarks the negative minimum has double weight at high temperatures, reflecting an intact  $Z(3)$  symmetry. In this context QCD can be mapped to a three state Potts model in an external field that also features an Ising end-point [266]. Lattice studies have confirmed this, by finding (for two flavors) a critical point in the Ising class at the pseudo-scalar (“pion”) mass  $m_\pi/T_c \approx 18.1$  [267, 268], which is compatible with earlier estimates based on random matrix theory [269].

The meaning of the Polyakov loop, which is the order parameter in the heavy quark limit, is less clear in the case of physical quark masses. Its renormalized expectation value is related to the free energy ( $F_Q$ ) of a static quark as  $L_{\text{ren}} = \exp(-F_Q/T)$ , which in turn, admits the definition of the entropy of the static quark as  $S_Q = -\partial F_Q/\partial T$ . While  $F_Q(T)$  is very smooth and monotonic across the cross-over, and its value is subject to an arbitrary constant shift,  $S_Q(T)$  is well defined and features a peak at  $T_c$  [115]. Actually, Ref. [115] observes, that the peak position is consistent with the chiral susceptibility’s peak for various quark masses, while the more obvious choices (e.g. the susceptibility of the Polyakov loop) did not give a conclusive result. It was pointed out in Ref. [270] that  $F_Q$  behaves as an energy-like observable in the vicinity of the chiral phase transition temperature, and for small quark masses the corresponding  $O(4)$  scaling applies to its derivatives.

### 3.1.2 QCD in the chiral limit

As we have already discussed in Section 2.2, QCD with physical quark masses exhibits a crossover transition. It was not a simple achievement to establish this fact from lattice simulations, but it also turns out to be a robust statement, as the transition remains a crossover for a very broad range of parameters, as shown in Fig. 14.

While the upper right corner of the Columbia plot refers to the Yang-Mills theory, the lower left corner corresponds to the chiral limit with three flavors. However, let us consider the two-flavor chiral limit (left edge) first. As long as the third (strange) quark is much heavier than the light flavors it will have no impact on symmetry considerations. In the low temperature phase the massless QCD Lagrangian has a  $U(N_f) \times U(N_f)$  symmetry, where the left and right-handed (or, equivalently, the axial and vector combinations) can be rotated in flavor space independently. The  $U(1)_V$  symmetry (charge conservation) is a true symmetry. We can also regard the isospin symmetry as unbroken, as long as the light flavors are degenerate ( $m_u = m_d$ ) and QED effects are neglected. Note that also a spontaneous symmetry breaking of the vector symmetries is ruled out [271]. On the other hand, the chiral symmetry  $SU(2)_A$  is spontaneously broken, with the pseudo-scalar pions playing the role of Goldstone bosons, as they are the lightest hadrons even in the presence of an explicit breaking due to finite quark masses [272]. The last element of the classical symmetry group is the flavor singlet chiral symmetry  $U(1)_A$ . This is broken by a quantum anomaly, resulting in a large mass for the  $\eta'$  meson. The mechanism of this anomaly is the existence of topologically non-trivial configurations in the path integral. The localized finite-action solutions of the Euclidean gauge theory with non-trivial topology are called instantons – the reader is referred to the in-depth review on the subject in this volume or in Ref. [273].

The fate of the flavor-singlet and non-singlet chiral symmetries determines the order of the transition in the QCD phase diagram. At perturbative temperatures the  $SU(N_f)_A$  symmetry is completely restored if the explicit breaking is strictly zero. This requires at least a continuous transition between the chirally broken and unbroken phases at  $T_\chi$ . If the  $U(1)_A$  symmetry is also restored at the chiral transition  $T_\chi$ , such transition may be either first or second order [274, 275]. If, however, the breaking of the  $U(1)_A$  axial symmetry persists for  $T > T_\chi$ , the transition is of second order in the  $O(4)$  universality class. Recent lattice simulations agree with the  $O(4)$  hypothesis and determine  $T_\chi$  in the chiral limit to be  $T_\chi \approx 132$  MeV [276, 277]. Truncated functional approximations to QCD have also determined the critical temperature in the chiral limit, with results varying between 141 and 147 MeV [278–280], however, the critical region was found to be much smaller than the pion masses used by any lattice group [281]. A likely scenario for the embedding of this critical point in the broader picture of the phase diagram is shown in Fig. 15.

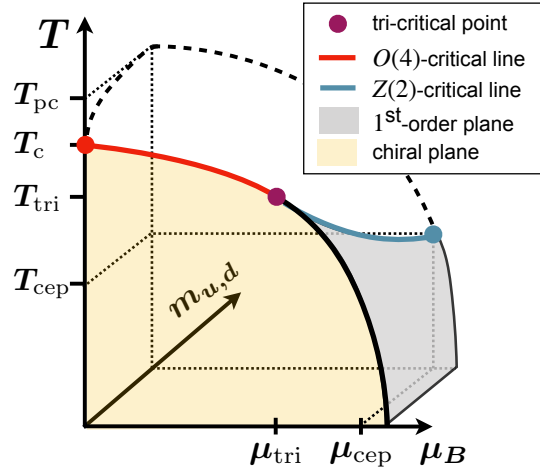


**Fig. 15** The phase diagram extended to three dimensions: temperature ( $T$ ), light quark mass (normalized to the strange mass  $h = m_l/m_s$ ) and baryo-chemical potential ( $\mu_B$ ). The front plane at  $h = 0$  shows the 2nd order chiral transition line in red, starting at the  $O(4)$  critical temperature  $T_c$ . Two dashed lines indicate the chiral crossover surface: i) the quark mass is varied keeping  $\mu_B = 0$ , ii) the chemical potential is varied with physical quark masses, starting at the pseudocritical temperature  $T_{pc}$  at  $\mu_B = 0$  and ending at the chiral critical endpoint at  $T_{cep}$ . The universality class of the second order line where these two examples of a crossover end is different, but can be connected in a tri-critical point at  $T_{tri}$ . (Plot from Ref. [113])

### 3.1.3 Instantons and the fate of the $U(1)_A$ symmetry

Several lattice groups have studied the effective restoration of the  $U(1)_A$  symmetry. The qualifier “effective” refers to the fact, that anomalous fluctuations break the  $U(1)_A$  at any temperature. For physical quark masses the instanton density, observed through the topological susceptibility, does not completely vanish at perturbative temperatures, but drops with temperature according to a power law with an exponent that depends on the number of flavors as given by the theory of the dilute instanton gas [130], and was also computed on the lattice [135, 282].

The question of effective restoration of the  $U(1)_A$  symmetry is usually posed in the massless limit. This is understood as a limit of QCD theories with light quarks, where first the infinite volume limit is taken, then the chiral limit ( $m_u = m_d \rightarrow 0$ ). Performing the limits in reverse order the zero quark masses would suppress all instantons. The question to be answered is whether the  $U(1)_A$  (chiral singlet) and  $SU(2)_A$  (chiral nonsinglet) symmetries are restored at the same temperature in this particular limit, or not.

If present, the effective restoration of the  $U(1)_A$  symmetry can be observed in the mesonic correlators as the degeneracy of the pion and the scalar iso-triplet  $a_0$  meson [283]. To find a direct evidence for the restoration from lattice QCD is extremely difficult, since this requires simulations at very small quark masses and large volumes, while the effect of  $U_A(1)$  breaking may be very small (but non-zero) in the chiral limit. Several lattice groups have made significant progress, but there is no conclusive answer found yet [284–289]. Initially, works with chiral fermions saw a restoration, and those working with an improved staggered discretization did not. It is also not clear how an effective restoration can be established at a given temperature based on finite-error data points.

The quantitative study of the anomalous breaking of  $U(1)_A$  requires good control on the low lying eigenvalues of the Dirac operator, since these determine the statistical weight of configurations with instantons. Staggered fermions are known to be prone to severe discretization effects at the low end of the Dirac spectrum. A recent work with domain wall fermions at finite lattice spacing [290] has presented new results that are likely to be unaffected from such errors, yet in agreement with the staggered results [289], supporting on the non-restoration scenario. Let us remark, though, that the actual temperature where the  $U(1)_A$  symmetry is approximately restored is very similar in the pro-restoration [287] and non-restoration [289] papers, but the pro-restoration papers consistently use a 2 flavor setup (top left corner) while the non-restoration papers work with physical strange mass (middle left edge). In the latter case the chiral transition temperature can be about 30 MeV lower.

In view of the available evidence a picture with interacting quasi-instantons emerges [291]. In the deconfined phase the field configurations in the pure gluonic theory are characterized with a non-interacting gas [292] of topological defects, instantons and anti-instantons. Their density approximately follows a power law in the temperature [130]. Instantons (anti-instantons) contribute with a positive (negative) integer to the topological charge of the configuration. By means of the index theorem [293] the number of zero eigenvalues of the Dirac operator  $D$  is given by the difference between the number of instantons and anti-instantons, i.e. the topological charge. In addition to the exact zero modes, a peak appears in the infrared end of the Dirac spectral density [294]. This peak can be explained by the non-interacting instanton gas picture [295–297].

In dynamical QCD the statistical weight of a gauge configuration is given by the fermion determinant  $\det(D + m)^{N_f}$ , where  $m$  is the bare quark mass and  $N_f$  is the number of light flavors. In a sufficiently large volume the zero mode zone of the spectral density is dominated by eigenvalues below the quark mass, numbering  $\sim V\chi_0$  where  $V$  is the four-volume and  $\chi_0$  is the topological susceptibility of the quark-less theory. Configurations with  $n_i$  instantons and  $n_a$  anti-instantons are, thus, suppressed by  $n_i + n_a$  factors of the bare quark mass. If this

mass is small (near the chiral limit), configurations with many instantons are suppressed by a higher factor, and those configurations will be favored where instantons are sparse [130].

The Banks-Casher relation is known to connect the spectral density  $\rho(\lambda)$  at zero eigenvalue with the value of the chiral condensate [298]. Indeed, in the low temperature phase, chiral symmetry breaking is manifest through a finite limit of  $\rho(\lambda)$  at  $\lambda \rightarrow 0$ . Above the actual chiral transition temperature we are now confronted with a power law with negative exponent, thus, a divergent limit at  $\lambda \rightarrow 0$ . It is tempting to think, that what we are facing is a new "anomalous" phase [299]. A closer look, however, reveals that a re-derivation of the Banks-Casher relation in the presence of an instanton-gas yields a chiral condensate proportional to  $\sim m^{N_f-1}$  [297], admitting a zero value in the chiral limit, corresponding to the complete restoration of the chiral symmetry. At the same time, specific mesonic correlators, often used to characterize the  $U(1)_A$  breaking, are predicted to have a finite value for  $N_f = 2$  [297].

It is, thus, likely, that the  $U(1)_A$  restoration happens gradually as temperature is increased. Its significance may depend on innocuous parameters, like the strange quark mass that sets the temperature of interest, that, in turn, controls the instanton density. In this scenario, QCD transition belongs to  $O(4)$  universality class for two massless flavors.

### 3.1.4 Lower left corner of the Columbia plot

The order of the transition with three light flavors is also much debated. The standard picture in the three flavor chiral limit of QCD is shown in the middle panel of Fig. 14. The detailed discussion in Ref. [249] is partly based on the seminal work of Pisarski and Wilczek [248]. The latter solves an effective theory in  $\epsilon$ -expansion, that is, working in  $d = 4 - \epsilon$  dimensions, expanding in  $\epsilon$  and setting  $\epsilon = 1$ . Modeling the axial anomaly and the chiral symmetry breaking and their relation to actual hadron masses a first order transition was suggested for the chiral limit. The first order nature persists for small perturbations in the mass. The middle panel of Fig. 14 shows a second order boundary that ends in a tri-critical point where the boundary line touches the chiral edge of the Columbia plot.

The standard picture with the first order transition was challenged by lattice studies that did not find the predicted first order region [250], suggesting the right panel of Fig. 14. This results, as well as earlier unsuccessful searches for the first order region using improved quarks [300, 301] are likely to be influenced by severe cut-off effects. The difficulty that lattice QCD faces in the lower left corner of the Columbia plot is similar to those hindering the conclusive study of the effective  $U(1)_A$  restoration.

The doubt in the existence of the first order corner in the Columbia plot sparked a new wave of interest in effective models and advanced solution techniques. For example, in the case of restored  $U(1)_A$  symmetry the existence of an infrared fixed point is suggested, admitting the possibility of a 2nd order transition [302]. In the non-restoration scenario, however, the first order prediction can be confirmed with renormalization group equations (without relying on the  $\epsilon$  expansion) [303]. The first order region also appears in model computations, see Ref. [304] for an FRG based solution of the quark-meson model. The full computation suggests the a small critical pseudo-scalar mass of 17 MeV, which is currently out of reach for lattice. An effective model with a more generic  $U(1)_A$  breaking finds parameters for both first and second order [251]. If, however, effective models find a sensitivity to the tunable parameters, lattice artefacts may also shift the order of the transition, as it has already happened when unimproved quarks were used with coarse lattices in the past.

We conclude this section admitting that the lower left corner of the Columbia plot is one of the remaining white spots on our map of the QCD phase diagram. Lattice studies, though they are not hindered by a sign problem, struggle to make predictions for small quarks and extrapolate to the continuum. Firm knowledge in this region would tightly constrain effective models, and concrete predictions could be inferred for the hypothetical chiral critical endpoint in the  $T - \mu_B$  phase diagram.

## 3.2 Imaginary valued chemical potentials

We do not study imaginary valued chemical potentials of pure academic interest, but to gain valuable insight for the analytic structure of the QCD partition function, which is immediately related the QCD phase diagram in the phenomenological domain. The significance of imaginary  $\mu_B$  is further raised by the applicability of Monte Carlo simulations on the lattice: purely imaginary chemical potentials do not invoke the sign problem. Their use in practical simulations open the possibility of gaining information in the phenomenological domain via analytical continuation. In this section we will mainly address an imaginary baryo-chemical potential ( $\mu_B$ ) defined along with the electric charge ( $\mu_Q$ ) and strangeness chemical potentials ( $\mu_S$ ) as

$$\begin{aligned}\mu_u &= \frac{1}{3}\mu_B + \frac{2}{3}\mu_Q, \\ \mu_d &= \frac{1}{3}\mu_B - \frac{1}{3}\mu_Q, \\ \mu_s &= \frac{1}{3}\mu_B - \frac{1}{3}\mu_Q - \mu_S,\end{aligned}\tag{10}$$

The basic expectations for the phase diagram in the  $T - \text{Im}(\mu_B/T)$  plane were formulated in the seminal work of Roberge and Weiss [305]. The quark chemical potential  $\mu_q$  appears as the pre-factor of a simple density term  $\sim \psi^\dagger \psi$  in the Lagrangian. This  $\mu_q$  plays the role of a homogeneous imaginary  $A_0$  field of a  $U(1)$  gauge theory, and can be transformed such that it only affects the boundary condition of the quark field as

$$\psi(x, 0) = -\exp(i\mu_q/T)\psi(x, 1/T)\tag{11}$$

This formula has a trivial symmetry for each quark flavor, independently:  $\mu_q \rightarrow \mu_q + i2\pi T$ . More importantly, though, the simultaneous shift of all quark chemical potential  $\mu_q \rightarrow \mu_q + i2\pi T/N_c$  is also an exact symmetry even in the presence of quarks, as it can be compensated

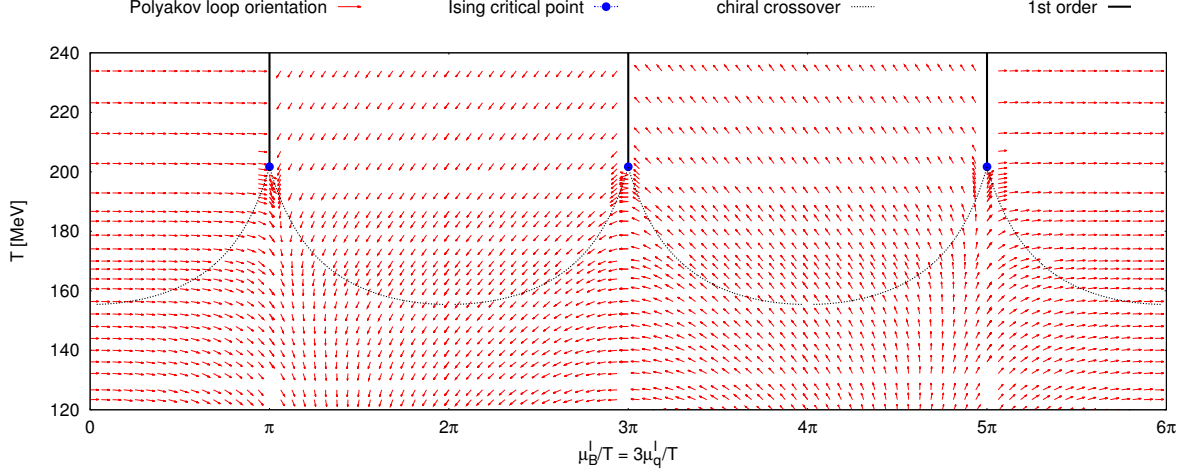


**Fig. 16** The phase diagram at imaginary chemical potential with physical quark masses in the temperature – imaginary  $\mu_B$  plane. The thermodynamic potential is periodic,  $\mu_B \rightarrow \mu_B + i2\pi T$ , though after such a shift in imaginary  $\mu_B$  the Polyakov loop is rotated by a center element. The phase diagram features a first order line at  $\mu_B = i\pi T + i2n\pi T$  for any integer  $n$  above a critical temperature  $T_{RW} = 208 \pm 5$  MeV [306]. The small red arrows show the orientation of the Polyakov loop.

by a center transformation of the gauge field. The same transformation can be simpler expressed as  $\mu_B \rightarrow \mu_B + i2\pi T$ , the corresponding periodicity is visible in Fig. 16. Only color-non-singlet observables, such as the Polyakov loop are affected by this transformation. A look at the definitions in Eq. (10) reveals that not just  $\mu_B$ , but  $\mu_S$  and  $\mu_Q$ , too, are periodic with a period of  $i2\pi T$ .

A further noteworthy feature of the partition sum  $Z(\mu_B, \mu_Q, \mu_S)$  is charge conjugation symmetry, that leaves  $Z$  invariant to a *simultaneous* sign flip in *all* chemical potentials. For example, with  $\mu_S = \mu_Q = 0$ , the  $\mu_B$  dependence of  $Z$  is entirely encoded in the range  $\mu_B = 0 \rightarrow i\pi T$ . We know the grand canonical potential  $\sim \log Z(\mu_B)$  at asymptotic temperatures analytically [307]. For QCD ( $N_c = 3$ ) we have

$$\frac{1}{VT^3} \log Z(\mu_B) = \frac{8\pi^2}{45} + \frac{7\pi^2 N_f}{60} + \frac{1}{2} \sum_f \left( \frac{\mu_f^2}{T^2} + \frac{\mu_f^4}{2\pi^2 T^4} \right) \quad (12)$$

which is a polynomial in  $\mu_B$  and is valid between  $-\pi < \text{Im}\mu_B/T < \pi$ . The imaginary baryon density  $n_B = \mu_B/3 + \mu_B^3/27\pi^2$  is monotonic and periodic at the same time, thus, it must be discontinuous at  $\mu_B/T = i\pi + 2\pi n$ , for all integer  $n$ . For this reason the phase diagram in the  $T - \text{Im} \mu_B$  plane features a vertical first order line, that is repeated periodically (see Fig. 16). This figure is a simulation result on a  $32^3 \times 8$  lattice with staggered fermions in the physical point. The high and low temperature phases are separated by a crossover. The red arrows show the orientation of the Polyakov loop. Notice, that below and above the chiral transition temperature the Polyakov loop follows a different pattern. This reflects the different behavior in the imaginary  $n_B(\mu_B)$  function (see Fig. 17). The Polyakov loop has a discontinuity where  $n_B$  has, and both disappear in the same critical point  $T_{RW} = 208 \pm 5$  MeV [306]. The same study has investigated the universality class of the Roberge-Weiss critical point and found compatible results with an Ising-like critical endpoint.

In a cluster or fugacity expansion – closely related to the virial expansion discussed in section 2.4.1, the (imaginary) baryon density at imaginary valued baryo-chemical potential reads

$$\text{Im} \frac{n_B}{T^3} = \sum_{k=1}^{\infty} b_k \sin(k \text{Im} \mu_B) \quad (13)$$

ignoring the other chemical potentials. In the HRG model  $b_{k+1} \ll b_k$ , thus in practice only  $b_1$  contributes to baryon-related observables. In Fig. 17 we show the function  $n_B(\mu_B)$  for imaginary arguments and its Fourier coefficients. The breakdown of the HRG model can be observed at  $T_c$  where  $b_2(T)$  and then at  $T_{RW}$  all higher coefficients become relevant.

In the context of the Columbia plot (see section 3.1) the fate of the Roberge-Weiss critical point is often discussed near the chiral limit [308]. In one possible scenario, the Roberge-Weiss point turns into a first order triple point, while two critical end-points progress along the crossover line towards the  $\mu_B = 0$  as all quark masses are simultaneously reduced, eventually turning the chiral transition entirely first order. This picture is consistent with the hypothetical existence of a first order region on the lower left corner of the Columbia plot, and also predicts a first order triple-point already for not-yet-chiral quark masses. As of today most lattice studies addressing it use coarse lattices with non-chiral (Wilson or staggered) discretizations, thus, the conclusions are not final. A first order triple-point was observed only with un-improved actions on coarse lattices. In more modern setups the Roberge-Weiss transition was always 2nd order, even for very small quark masses [309]. Nevertheless, it was suggested that at  $\mu_B = i\pi T$  the Roberge-Weiss critical point is also a chiral critical point [309, 310].

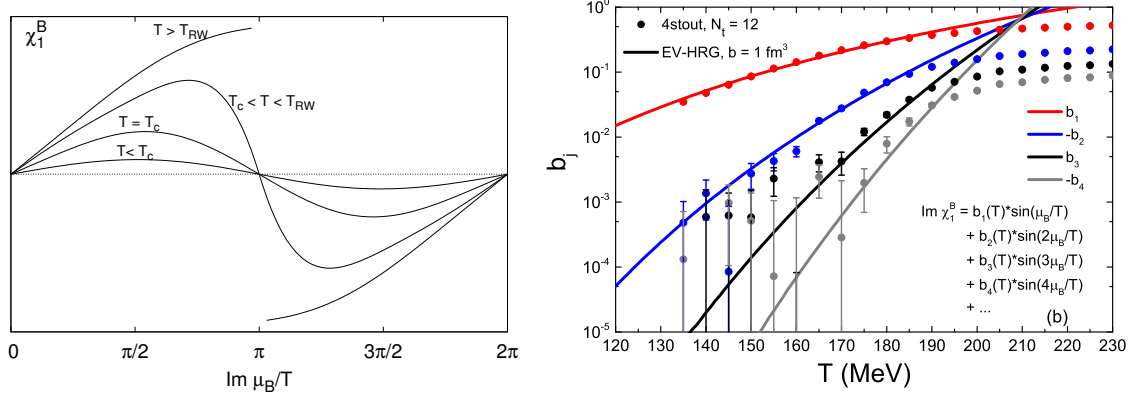


**Fig. 17** Left: The imaginary valued baryon density as a function of the imaginary chemical potential. Above the critical temperature  $T_{RW}$  the baryon number shows a discontinuity, and indicates a first order transition. Below the chiral transition  $T_c$  this is a sine function to very good approximation. Right: The function in the left panel is periodic, its Fourier components on logarithmic scale are shown as a function of temperature [91]. (In the latter the performance of a HRG-motivated excluded volume model is also shown.)

### 3.3 Yang-Lee edge singularities

In recent years, the search for the QCD critical point saw the advent of a new method based on the study of the analytic structure of the theory's partition function. In a couple of seminal papers [311, 312] Lee and Yang showed the profound connection between the analytic structure of the partition function and the presence and location of phase transitions. They showed that, although in finite systems a true phase transition cannot take place, the partition function of a physical system always has zeroes (the Lee-Yang zeroes) for complex values of the control parameter (in our case, the chemical potential  $\mu_B$ ). The zeroes of the partition function correspond to singularities of the free energy, and thus to phase transitions. In the thermodynamic limit, an infinite number of Lee-Yang zeroes appear, which accumulate onto a branch cut in the complex  $\mu_B$  plane, that terminates at branch points called Yang-Lee edge (YLE) singularities. In the presence of a critical point, these singularities fall onto the real axis at the critical value of  $\mu_B$ . Crucially, even away from a critical point, the YLE singularities are present in the complex  $\mu_B$  plane, and are continuously connected to the critical point itself.

The location of the YLE singularities is universal when expressed in terms of the scaling variable  $z = h/t^{\beta\delta}$ , at:

$$z_c = |z_c| \exp\left(\frac{i\pi}{2\beta\delta}\right), \quad (14)$$

where  $|z_c|$  is a non-universal quantity which has only recently been estimated with functional methods and on the lattice [313–316]. Not just the branch point, but the other zeros on the branch cut follow a universal pattern, and the ratios of subsequent Lee-Yang zeros can be used to locate the critical point [317].

The presence and universal behavior of the branching point allows new strategies to locate critical points in the QCD phase diagram [318]. Near the critical point, one can create a map between the QCD phase diagram and the Ising model one:

$$\begin{aligned} t &= a\Delta T + b\Delta\mu_B \\ h &= c\Delta T + d\Delta\mu_B \end{aligned} \quad (15)$$

where  $t$  and  $h$  are the reduced temperature and magnetic field in the Ising model, while  $\Delta T$  and  $\Delta\mu_B$  are the coordinates in the QCD phase diagram relative to the critical point. Once the YLE singularity is located on the complex plane, the expected behavior for the approach towards the critical point is known. Exploiting the relation between  $z, h, t$  and then  $T, \mu_B$ , it follows that (see e.g., [318]):

$$(a\Delta T + b\Delta\mu_B) = i|z_c|^{\beta\delta} (c\Delta T + d\Delta\mu_B)^{\beta\delta}, \quad (16)$$

from which one can show that, as a function of the temperature, the real and imaginary parts of the critical chemical potential follow:

$$\begin{aligned} \text{Re}\Delta\mu_B &= \mu_{B,c} + c_1\Delta T, \\ \text{Im}\Delta\mu_B &= c_2\Delta T^{\beta\delta}, \end{aligned} \quad (17)$$

where  $\mu_{B,c}$  is the chemical potential at the critical point.

It is not necessarily the chiral critical endpoint that dominates the parameter space where observations are made. For example, above 160 MeV Ref. [319] finds evidence for the Yang-Lee edge corresponding to the Roberge-Weiss critical point from lattice simulations at imaginary  $\mu_B$ . In a finite volume, the closest singularity of the free energy is located on the complex  $\mu_B$  plane and interpreted as the branching point. This implies an extrapolation from imaginary to complex valued  $\mu_B$ , performed by fitting some ansatz that can account for poles to the imaginary density. The systematics of this *first extrapolation* is less controlled in the vicinity of the chiral critical endpoint, where the magnitude of  $|\mu_B|$  is challenging. Once the leading singularity is found for the temperature where we have a crossover, Eq. (17)

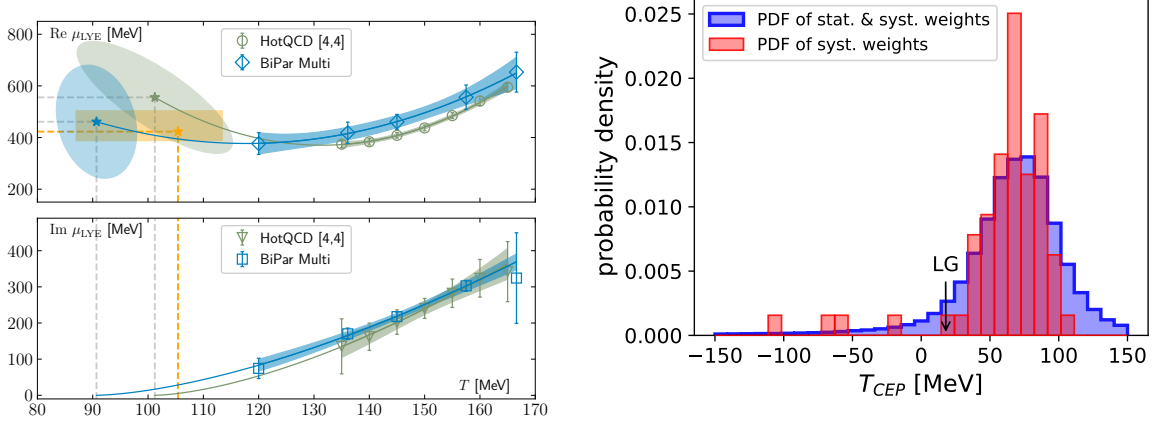


**Fig. 18** Left: estimates for the YLE singularities from Refs. [85, 320], and their  $T$ -extrapolations. Right: systematic analysis of the critical temperature from Ref. [321].

is applied as a *second extrapolation*. As of this writing, lattice studies have not yet been able to perform the first extrapolations at low enough temperatures to guarantee the success of the second extrapolation. In practice, additional terms can be included when fitting this temperature dependence, and a potentially infinite number of functional forms ought to yield the same estimates for  $T_c, \mu_{B,c}$ .

Most commonly, a rational ansatz is applied to the free energy or its derivatives to estimate the YLE singularities locations. In the left panel of Fig. 18 results for the real and imaginary parts are shown for different temperatures, together with their extrapolation in  $T$  based on Eq. (17) [85, 320]. In Ref. [322], the procedure was modified by first applying a uniformizing map to the complex  $\mu_B$  plane, then carrying out the YLE singularities estimation, before mapping back to  $\mu_B$ ; this alternative yielded comparable results.

The authors of [320] estimated the location of the critical point based on large volume simulations on a coarse lattice. Their main analysis gives the estimate  $(T_c, \mu_{B,c}) = (105^{+8}_{-18}, 422^{+80}_{-35})$  MeV, while further systematic effects are expected that could push the critical chemical potential towards  $\mu_{B,c} \approx 650$  MeV. Uncertainty estimation is all but obvious, given that both the YLE singularities estimation, as well as the temperature extrapolation can in principle be carried out in an infinite number of ways. The authors of Ref. [323] attempted to probe the predictive power of such a strategy, based on high statistics,  $N_\tau = 8$  lattice results. In particular, different sources of systematics were considered: i) the rational ansatz was applied either to the free energy, to its first or second  $\mu_B$ -derivative; ii) the  $T$  dependence was modeled by different functional forms, and iii) the fits carried out over different  $T$ -ranges. Moreover, differently from previous determinations, the rational ansätze for locating the YLE singularities were chosen to explicitly reflect CP symmetry, i.e. to be even in  $\mu_B$ . The results for the estimated value of the critical temperature are summarized in the histogram in the right panel of Fig. (18), while no results were reported for the critical chemical potential, as the corresponding uncertainty would be very large. The main result is an upper bound for the location of the critical endpoint, which at the  $1\sigma$  level is either below  $T = 103$  MeV or it does not exist. It should be reminded that, although quite promising, at present the strategy of locating the critical point by means of the YLE singularities hinges on substantial caveats. First, the continuum and infinite volume limits ought to be taken. Second, the systematics due to a truncated expansion and, most importantly, on the temperature range from which the extrapolation is carried out, ought to be quantified.

## 4 The multidimensional phase diagram

### 4.1 External magnetic fields

Let us now consider a new axis in the QCD phase diagram, the strength of an external homogeneous magnetic field. The strength of the magnetic field is often expressed as the rooted product with the elementary charge in MeV units: typical values in the interior of magnetars are  $\sqrt{eB} \sim 1$  MeV ( $\sim 10^{15}$  G), but in the early Universe much larger fields were realized, such as  $\sqrt{eB} \gtrsim 1$  GeV. Transient magnetic fields are present in non-central collision experiments [324] are expected to be of order  $\sqrt{eB} \sim 0.1 - 0.5$  GeV. These have impact on the early plasma phase, the hydrodynamic evolution or possibly even the chemical freeze-out.

The magnetic field is time dependent in the examples above. In contrast, in theoretical models we assume a constant background field in equilibrium. The reader will find a summary of the theoretical work in Ref. [325] or with a focus at lattice QCD in Ref. [326]. As opposed to electric fields or a baryo-chemical potential, magnetic fields can be simulated on the lattice without encountering a sing problem. One important restriction is that in a finite volume the total flux, thus, the  $B$  field, too, is quantized.

Near the chiral transition, we have to study its order parameter, the chiral condensate, as a function of the magnetic field. In the QCD vacuum the condensate is enhanced, this is the *magnetic catalysis* [327]. At finite temperature the situation is more complicated: the magnetic catalysis is still active for valence quarks, however, sea quarks behave differently [328]. While the former is a monotonic function of  $B$  at all temperatures, the sea quark contribution exhibits a reversal of the trend in the transition region and gives the dominant effect

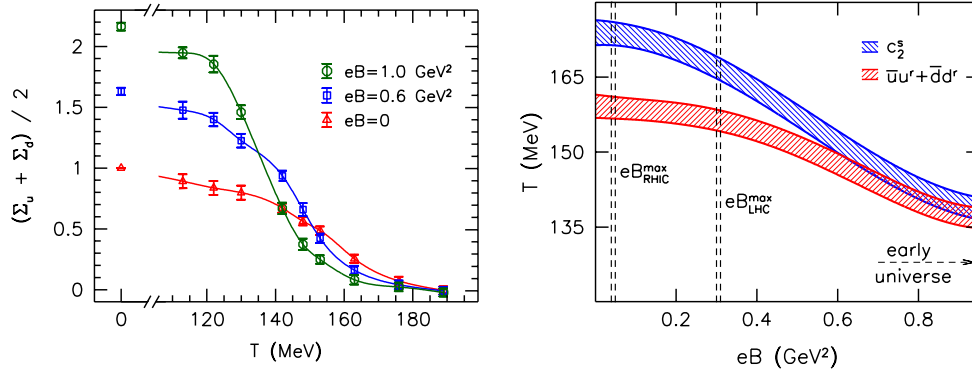


**Fig. 19** Left: The renormalized chiral condensate (averaged over the two light flavors) as a function of the magnetic field for temperatures below and above the crossover. One observes the magnetic catalysis at low temperatures. This trend reverses near  $T_c$  [334]. Right: The QCD phase diagram in the  $T - B$  plane from continuum extrapolated lattice simulations [332].

[329]. This is the *inverse magnetic catalysis* and works towards chiral symmetry restoration. In the case of inhomogeneous magnetic fields the spatial response of the sea quarks follows a broadening pattern. Together with the more localized valence quarks a non-uniform response emerges [330].

The magnetic fields have an impact not just on chiral symmetry, but an analogous effect can be observed on the order parameter of the center symmetry, the Polyakov loop, too. Small values of the Polyakov loop, characteristic to confinement, correlate with an abundance of small eigenvalues ( $\lambda_{\min}$ ) of the Dirac operator. The statistical weight of a configuration can be approximated as  $\lambda_{\min}^{q|B|}$ , thus, suppressing small values of the Polyakov loop in the ensemble [331].

These effects lead to a monotonic decrease of the transition temperature with  $B^2$  as first demonstrated on the lattice in Ref. [332]. The main result of Ref. [332] is shown in Fig. 19. Due to their different electric charge, the up and down chiral condensates show a slightly different pattern, the extracted transition temperatures are still compatible [333]. In the same work the outlined behaviour of the Polyakov loop was confirmed.

Whether the crossover line in Fig. 19 ends in a new critical point has been subject to various speculations [335]. The phase diagram was later extended towards stronger magnetic fields. With increasing  $B$  the crossover temperature further decreases, and so does its width [333]. Simulating at isolated choices of  $B$  Ref. [336] has found evidence for a first-order transition at  $eB = 9 \text{ GeV}^2$  and  $T_c = 63 \pm 5 \text{ MeV}$ . Thus, a second-order endpoint is expected to be between 4 and 9  $\text{GeV}^2$  in  $B$ . It is an intriguing question, whether this new critical point is analytically connected to the expected chiral endpoint on the  $T - \mu_B$  phase diagram, or perhaps it is related to the Roberge-Weiss transition at  $\mu_B = \pi i T$ , see illustration in Fig. 20. If it was connected to the chiral critical point at  $\mu_B > 0$  one might attempt an analytical continuation of the crossover line (with question marks) using imaginary  $\mu_B$  simulations. Very recently, an argument was presented for this being unlikely. Ref. [337] follows the critical point at  $\mu_B = \pi i T$  in a finite magnetic field, observes the drop in the critical temperature, and finds that it turns first order at  $B < 2.5 \text{ GeV}^2$ . In Fig. 20 we show a possible scenario where the end-point in the  $T - B$  plane is connected to the Roberge-Weiss point with a critical line. Direct evidence for this connection has not yet been found.

## 4.2 Isospin chemical potential

In the space of the quark chemical potentials ( $\mu_u, \mu_d, \mu_s$ ) the baryon-chemical potential ( $\mu_B$ ) represents a direction with  $\mu_u = \mu_d$ . The orthogonal combination ( $\mu_u = -\mu_d$ ) corresponds to the third component of the isospin. If there is no other source of isospin breaking (non-degenerate up and down quarks, QED effects) any other component can be considered. The third component is particularly interesting, e.g. in neutron stars with  $\mu_l < 0$  due to the weak interaction. In that case  $\mu_B \gg \mu_l$ , however, we consider the (unstable)  $\mu_B = 0$  setup here.

The motivation behind the phase diagram with an isospin chemical potential ( $\mu_I$ ) axis with fixed  $\mu_B = 0$  comes from theory:

- i) There is no sign problem in this setup; thus, lattice simulations are possible. In general, a real quark chemical potential introduces a complex fermion determinant after quark degrees of freedom are integrated. However, as long as the up and down quarks are degenerate in mass, the complex phase of these two determinants exactly cancel, leaving us with a positive semidefinite combined quark matrix.
- ii) The grand canonical pressure function  $p_I(\mu)$  at  $\mu = \mu_u = -\mu_d = \mu_I/2$  is always greater than or equal to the pressure  $P_B(\mu)$  with  $\mu = \mu_u = \mu_d = \mu_B/3$  at the same temperature. This is a simple path integral relation: we can rewrite the partition sum of baryon-dense matter to isospin-dense matter simply by replacing the complex determinant of the  $u, d$  quark pair  $(\det M)^2$  by its modulus  $|\det M|^2$ . In the process, both the partition sum  $Z$  and its logarithm, the pressure, increase.

These points were used to constrain the QCD pressure at zero temperature, for finite  $\mu_B$  through the inequality  $p_B \lesssim p_I$  using continuum extrapolated lattice results in  $p_I$  [338, 339]. The resulting equation of state (see Fig. 21) shows a speed of sound that exceeds the conformal limit  $c_s^2 > 1/3$  over a large range of  $\mu_I$ . The right panel indicates the exclusion region from the isospin constraint.

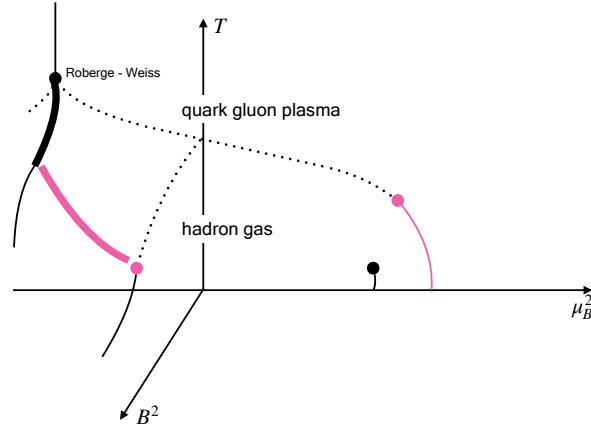


**Fig. 20** The three dimensional phase diagram with temperature, magnetic field and chemical potential (left imaginary, right real) on the axis. The  $B$  and  $\mu_B$  variables are squared to reflect symmetries. The magenta features are hypothetical.

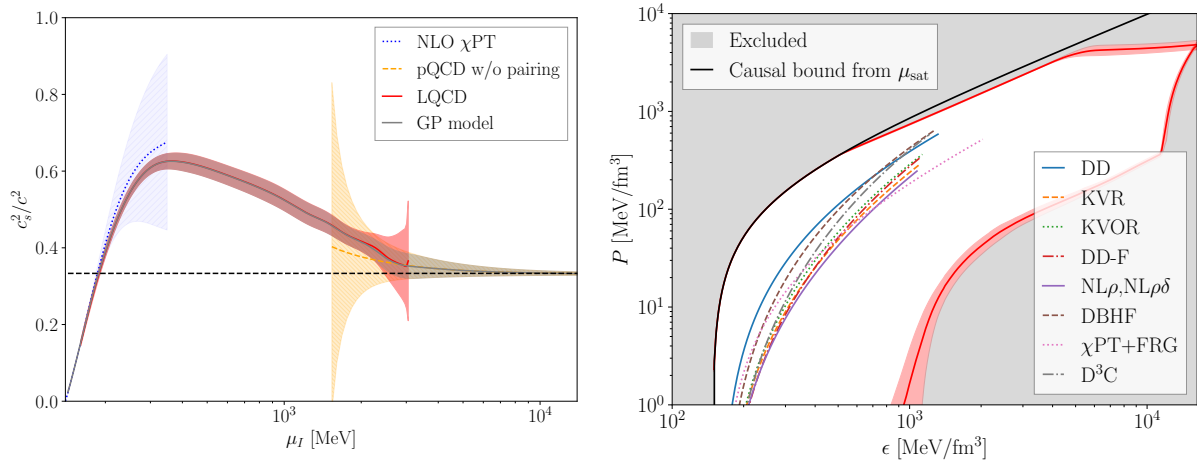


**Fig. 21** Left: The squared speed of sound ( $c_s^2$ ) as a function of the isospin chemical potential ( $\mu_I$ ). The lattice QCD determination (red), pQCD determination (orange), and  $\chi$ PT determination (blue) are combined into a model (GP for Gaussian Process). Right: Constrain to the equation of state for baryon-dense matter (the border of the possible range is marked by the red bands). Several phenomenological equations of states are shown in the non-excluded region [339].

Besides these results at zero temperature, the phase diagram in the  $T - \mu_I$  plane also received attention from theorists. The expected structures were discussed in Ref. [340]. For this one considers three regions in  $\mu_I$ . In the first region near  $\mu_I < m_\pi$  an ordinary hadron gas is expected. At the threshold value of  $m_\pi$  pions condensate, and the  $SU(2)$  isospin symmetry spontaneously breaks to the  $U(1)$  subgroup generated by  $I_3$ . A Goldstone boson appears, while two other pions remain massive, their masses will approach  $|\mu_I|$  for large densities. The order parameter of this phase is  $\langle \bar{u}\gamma_5 d \rangle \sim \Delta$ . The non-zero gap  $\Delta$  persists for large values of  $\mu_I$ . Eventually, the phase will exhibit Cooper pairs of color singlet combinations of the  $\bar{u}$  and  $d$  quarks. The order parameter of this phase is not different from the pion condensation, thus, no real transition is expected to separate the large- $\mu_I$  superconducting phase from the pion condensation at  $\mu_I \gtrsim m_\pi$ . The gap  $\Delta$  is much larger in comparison to the analogous phase of baryon-dense matter [340].

The progress in lattice QCD at finite temperature and isospin density was, indeed, quick exploring the phase diagram. Polynomial extrapolation from  $\mu = 0$  as well as direct simulations are unproblematic up to onset of the condensation phase. The Taylor coefficients indicate a divergence of the series for  $\mu_I > m_\pi$  [341, 342]. In the pion condensation phase non-trivial technical issues have to be addressed: the presence of a Goldstone boson hinders the convergence of the iterative solver of the Dirac equation: the number of iterations is proportional to the reciprocal of the (square root of the) smallest eigenvalue of the fermion matrix, and the latter is zero in the condensation phase [343]. The authors of Ref. [343] offered a solution in form of an infrared regulator term in the action that is removed in a second, reweighting-based step. The resulting phase diagram together is shown together with the prediction of [340] in Fig. 22. On the phase boundary between the hadron gas and pion condensation phases the Polyakov loop indicates no deconfinement, as expected. The order of

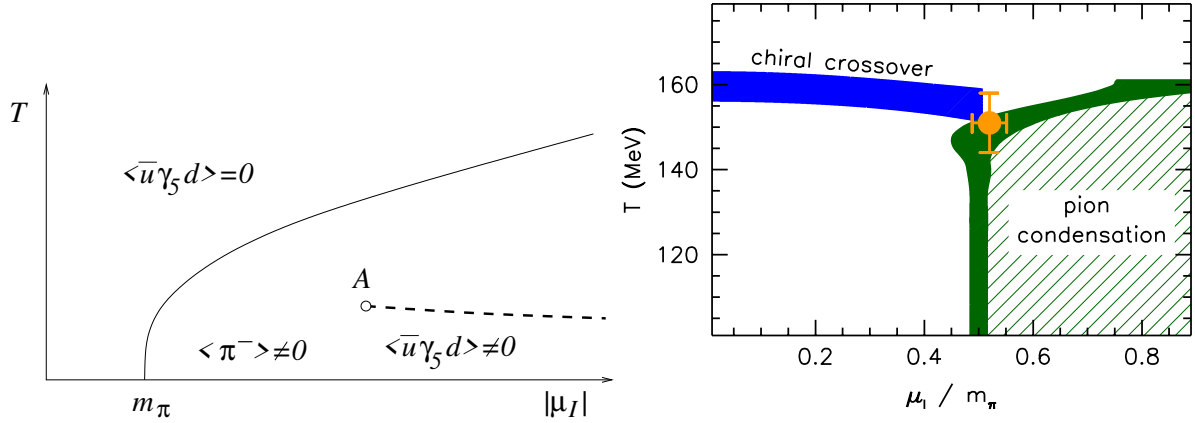


**Fig. 22** The QCD phase diagram in the temperature – isospin chemical potential plane. The left panel shows the theoretical expectation based on effective field theory in Ref. [340]. The gross picture was confirmed on the lattice [343] (right panel, this plot introduces an extra factor two in the definition of  $\mu_I$ , thus, the onset of the condensation appears to be at  $m_\pi/2$ ).

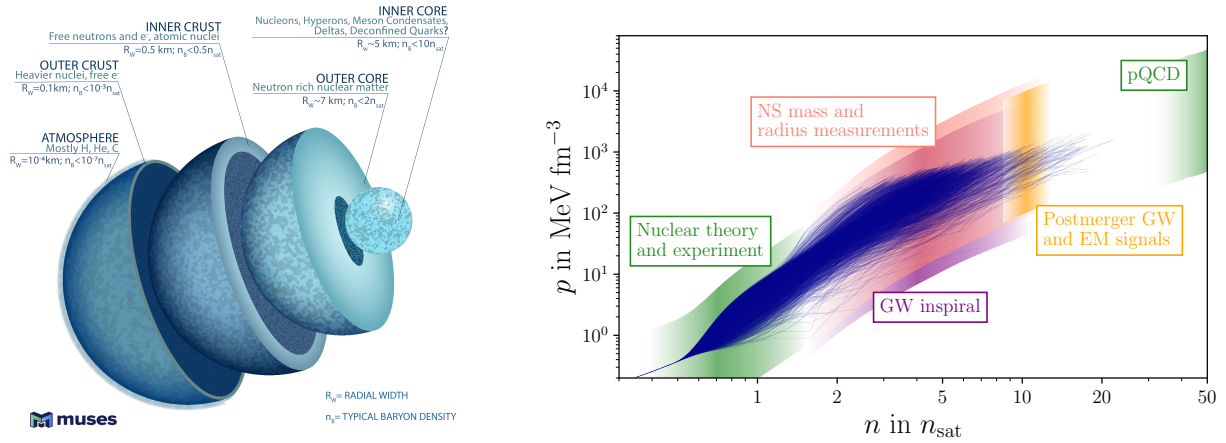


**Fig. 23** Left: internal stratified structure of a neutron star [15]. Right: possible interpolations of dense matter equation of state between the nuclear and perturbative regimes, and a summary of the regions where different possible measurements can provide constraints on the equation of state, from Ref. [344].

the transition is second order in the  $O(2)$  universality class due to the pattern of symmetry breaking, and this, too was confirmed on lattice [343]. At higher temperatures, in the absence of pions, the condensation does not occur.

## 5 Phase diagram of dense matter

### 5.1 Dense matter equation of state

Since matter above saturation density cannot be created in the laboratory, the only available testbed for dense matter thermodynamics are neutron stars. These cold objects have typical radii of the order of 10 km, masses around  $1 - 2M_\odot$  ( $M_\odot$  is the Sun's mass), and thus are the second-densest known objects, after black holes. They are globally neutral objects with a stratified structure as sketched in Fig. 23 (left). The outer portion is mostly composed of heavy nuclei, and moving inward one finds more and more neutron-rich nuclei which do not exist in isolation. The inner layers comprise a rich structure, with possibly a neutron-pair superfluid [345] and “nuclear pasta” phases [346]. The outer core contains mostly neutrons, with electrons, muons and protons contributing to *beta*-equilibrium. The inner core reaches densities up to a few times nuclear saturation density [344], and it is unclear what the effective degrees of freedom might be in this regime, as several different scenarios have been proposed. These include the existence of pions or kaon condensates, as well as nuclei including hyperons (strange baryons), which would be stable in a large density environment due to Pauli blocking [347]. Another possibility is provided by *quarkyonic* matter [348], a conjectured phase where quarks populate the Fermi sea, and baryons live on the Fermi surface. Since baryons only populate a thin outer layer of the Fermi sphere, as the chemical potential (and thus the Fermi momentum) is increased, baryons can

reach high momenta, thus increasing the pressure, without correspondingly increasing the energy density. This provides a mechanism for a very stiff equation of state [349]. Originally based on large- $N_c$  arguments, it is not clear whether it does exist in QCD with  $N_c = 3$ . Finally, densities might also be large enough that quarks become deconfined [350].

Regardless of the effective degrees of freedom, neutron stars owe their existence to the delicate equilibrium between the inward gravitational force and the outward force due to the pressure. Measurements of neutron stars masses and radii can provide significant constraints on the equation of state of dense matter, as the latter must be such to support star masses at least up to the observed ones, which currently lie at  $m_{\text{NS}} = 2.01 - 2.35 M_\odot$  [351–354]. For non-rotating isolated neutron stars, the Tolman-Oppenheimer-Volkoff (TOV) equations [355, 356] relate the core density of the star to its radius and mass. A given equation of state is then one-to-one mapped onto a mass-radius curve  $M(R)$  [357]. Also when not in isolation, and/or rotating, different solutions of Einstein’s equations can relate the equation of state to the mass and radius, but also the moment of inertia and tidal deformability of the star, which can be constrained through gravitational wave detection [358]. Through gravitational wave and electromagnetic astronomy, mergers of neutron stars and neutron star-black hole mergers can be observed, and numerical relativity simulations showed that temperatures up to  $T \sim 80 - 100$  MeV can be reached in these events [359–361]. In particular, the gravitational wave signal from the inspiral stage can probe the regime  $\sim 2 - 3n_{\text{sat}}$ . On the other hand, post-merger signals would provide much more stringent constraints – as their morphology is more sensitive to the equation of state than its pre-merger counterpart – though their observation with current detectors is unlikely [362].

From the theoretical side, the cold matter equation of state is constrained at the lower density end by chiral effective theory, and in the opposite regime by perturbation theory. While astrophysical observations can provide insights into the nuclear equation of state in the density range covered by neutron stars cores, above 10 times saturation densities they have little constraining power, which leaves a gap stretching from a few to a few tens of times saturation density. Since thermodynamic relations (e.g. causality bounds on the speed of sound) cause perturbative QCD constraints to propagate to lower energy scales, modeling of the intermediate regions have been constructed to produce a posterior distribution for the pressure-energy density  $p(\epsilon)$  relation [344, 363–366], see Fig. 23 (right), possibly hinting at the existence of deconfined matter in neutron stars cores [364]. How much the equation of state in this regime is constrained by perturbative QCD results is however still unclear [367].

## 5.2 Color superconductivity

The expectation, that asymptotic freedom also applies to superdense matter, not just high temperatures or momentum scales, promising an analytically tractable region for QCD, has a long history [368]. The dense phase, however, is less trivial than its high temperature counterpart. Around the Fermi surface of dense quark matter, even the smallest attractive interactions can introduce instabilities [369]. Unlike conventional superconductivity, here a diquark pair is formed, and instead of phonons a gluon exchange is sufficient to induce the bound state. We know that gluon exchange is attractive in some channels, e.g. in those that bind baryons. Such pairs, being bosonic, can form a condensate, the phase with such a condensate is called color superconductivity [370]. In presence of a diquark condensate perturbation theory is still possible, though around an improved ground state [371]. This state is characterized by broken chiral and color symmetries. Most strikingly, the originally massless gluons and quarks become massive. See Refs. [231, 372] for in-depth reviews.

The pattern of symmetry breaking depends on the channel of attractive interaction. At asymptotic densities of the three-flavor theory the most symmetric option is the color-flavor locked phase [373] with the condensate form

$$\langle \psi_i^a C \gamma_5 \psi_j^b \rangle \sim \Delta_{\text{CFL}} \epsilon^{abc} \epsilon_{ijc} + \Delta_{\text{CFL}} \kappa \left( \delta_i^a \delta_j^b + \delta_j^a \delta_i^b \right). \quad (18)$$

Here  $a, b$  are color indices and  $i, j$  are flavor indices, both running from 1 to 3.  $C$  is the Dirac charge conjugation matrix, and  $\Delta_{\text{CFL}}$  is the dimensionful gap parameter. The pattern of symmetry breaking is then

$$[SU(3)_c] \times U(1)_B \times SU(3)_L \times SU(3)_R \rightarrow SU(3)_{c+L+R} \times Z_2 \quad (19)$$

The attractive interaction is through the first term, which is antisymmetric both in color and flavor. From the Dirac structure it is a parity-even spin-singlet. Unlike the QCD vacuum, the chiral symmetry breaking is not caused by the pairing of left-handed quarks with right-handed antiquarks, here the pairs are formed by quarks of equal chirality. The breaking occurs due to the locking of the flavor-space and color-space rotation, and is manifest in an order parameter of  $\langle \bar{\psi} \psi \rangle$  type. Even the  $U(1)_B$  is broken and reduced to  $Z_2$ , the quantum numbers of the associated order parameter matches the di-Lambda condensate  $\langle \Lambda \Lambda \rangle$  [374]. While the gluon fields produce an octet of massive spin 1 bosons through the Meissner effect and fermionic excitations have a gap [375, 376], there will also be Goldstone bosons associated with the broken symmetries. Those associated with chiral symmetry breaking will be lifted by the small quark masses, but the scalar singlet coming from the  $U(1)_B$  stays massless (baryon number superfluidity).

There are several effective models that can address superconducting phases. For example in Ref. [377] the Goldstone bosons are explicitly represented. The NJL model was also extended with the diquark channel to describe superconductivity [222, 378]. The order of magnitude estimates for the superconducting gap hint for the extension of these phases to finite temperature, as high as 50 MeV [379, 380]. The emerging picture is shown in the high density side of Fig. 13, where color-flavor-locking is labeled as CFL. In this figure, other possibilities at lower densities, such as the locking of the up and down quarks with two of the colors in a 2SC phase is omitted, as its significance is questionable for the most important inhabitants of the intermediate density part of the diagram, the charge neutral neutron stars [379]. There are many other phases suggested for the high density region of the phase diagram (see [222] for a review). Presently, these are far from the range of applicability of first principles non-perturbative approaches, such as lattice QCD.

## 6 Conclusions

The study of the QCD phase diagram over the past few decades has gathered an enormous amount of information, from the theory community as well as from experiment. As a result, we can draw a quantitative picture of the phase structure and thermodynamic features of strongly interacting matter under extreme conditions.

The existence of the QGP has been established thanks to huge experimental efforts at several generation of accelerator facilities, such as SPS, RHIC and LHC. Moreover, the experimental description of the QGP and of the conditions needed to produce it have developed to a precision science. Thanks mostly to lattice QCD simulations, the low net-density region of the phase diagram is quantitatively well established, with precise determinations of the QCD transition line and the equation of state. At the same time, other diagrammatic techniques emerged in the form of the functional renormalization group and Dyson-Schwinger equations that are in quantitative agreement with lattice simulations.

The search for the conjectured critical end-point has dominated the recent years of research in the community, with RHIC's beam energy scan program ultimately producing hints for its existence, though not unambiguous evidence. Various models, functional methods and indirect evidence from lattice simulations suggest a possible location in the chemical potential range ( $\mu_B \approx 550 - 650$  MeV) available to fixed-target heavy ion experiments. Current lattice methods do not extend to this range but, at the very least, the critical point's existence could be excluded up to  $\mu_B = 450$  MeV.

The structures on the phase diagram with physical quark masses can be viewed as a point in a quark-mass-dependent diagram (Columbia plot). How the physical critical point is connected with other critical lines at zero chemical potential and smaller quark masses is known only in some effective models. In view of the latest lattice results it is not clear whether such a critical surface exists at all. If not the case, the existence of the critical point would be less likely. These findings call for further investigations, which remain challenging not only because of the finite density, but the proximity to the chiral limit.

In fact, although experiment and theory alike seem to be closing in on the QCD critical point, it should be stressed that it is still not settled whether it exists or not. In the coming years, more data from fixed-target experiments at RHIC and CBM will help clarify whether the hints we see now are indeed signatures of critical behavior. At the same time, theoretical predictions will become more accurate, refining the region where the critical point is more likely expected to be. As the reach of lattice QCD continues to grow to larger chemical potentials, thanks to new methods and more computing power, precise quantitative knowledge of QCD phases keeps extending.

The larger phase diagram of QCD, including finite isospin density or magnetic fields, has also been thoroughly explored in recent years via lattice methods, and can now provide a comprehensive picture on the thermodynamic properties of the theory in more exotic scenarios, which are nonetheless relevant for experimental and astrophysical conditions. As a welcome by-product, the equation of state of QCD is now known over a very broad range of conditions, which is crucial for charting QCD phases, as well as for implementations in hydrodynamic simulations of different systems.

Since the first observation of gravitational waves from a neutron star merger, stronger constraints have been placed on the equation of state of dense matter, which needs to be stiff enough to support very dense stars. Whether the inner cores of neutron stars are formed by hadrons, quark matter or other exotic phases of high-density QCD, and whether these phases are separated by a first order transition, remain crucial open questions.

## Acknowledgments

We thank Anton Andronic, Roberta Arnaldi, Andrea Beraudo, Livio Bianchi, Gergely Endrődi, Tetyana Galatyuk, Tamás G. Kovács, Jan Pawłowski, Péter Petreczky and Enrico Scapparini for their feedback and enlightening discussions while preparing this manuscript.

## References

- [1] B. P. Abbott, et al. (LIGO Scientific, Virgo), GW170817: Observation of Gravitational Waves from a Binary Neutron Star Inspiral, *Phys. Rev. Lett.* 119 (16) (2017) 161101, doi:10.1103/PhysRevLett.119.161101, 1710.05832.
- [2] B. P. Abbott, et al. (LIGO Scientific, Virgo, Fermi GBM, INTEGRAL, IceCube, AstroSat Cadmium Zinc Telluride Imager Team, IPN, Insight-Hxmt, ANTARES, Swift, AGILE Team, 1M2H Team, Dark Energy Camera GW-EM, DES, DLT40, GRAWITA, Fermi-LAT, ATCA, ASKAP, Las Cumbres Observatory Group, OzGrav, DWF (Deeper Wider Faster Program), AST3, CAASTRO, VINROUGE, MASTER, J-GEM, GROWTH, JAGWAR, CaltechNRAO, TTU-NRAO, NuSTAR, Pan-STARRS, MAXI Team, TZAC Consortium, KU, Nordic Optical Telescope, ePESSTO, GROND, Texas Tech University, SALT Group, TOROS, BOOTES, MWA, CALET, IKI-GW Follow-up, H.E.S.S., LOFAR, LWA, HAWC, Pierre Auger, ALMA, Euro VLBI Team, Pi of Sky, Chandra Team at McGill University, DFN, ATLAS Telescopes, High Time Resolution Universe Survey, RIMAS, RATIR, SKA South Africa/MeerKAT), Multi-messenger Observations of a Binary Neutron Star Merger, *Astrophys. J. Lett.* 848 (2) (2017) L12, doi:10.3847/2041-8213/aa91c9, 1710.05833.
- [3] Y. Aoki, G. Endrődi, Z. Fodor, S.D. Katz, K.K. Szabo, The Order of the quantum chromodynamics transition predicted by the standard model of particle physics, *Nature* 443 (2006) 675–678, doi:10.1038/nature05120, hep-lat/0611014.
- [4] Szabolcs Borsanyi, et al. (Wuppertal-Budapest Collaboration), Is there still any  $T_c$  mystery in lattice QCD? Results with physical masses in the continuum limit III, *JHEP* 1009 (2010) 073, doi:10.1007/JHEP09(2010)073, 1005.3508.
- [5] A. Bazavov, T. Bhattacharya, M. Cheng, C. DeTar, H.T. Ding, et al., The chiral and deconfinement aspects of the QCD transition, *Phys. Rev. D* 85 (2012) 054503, doi:10.1103/PhysRevD.85.054503, 1111.1710.

- [6] Szabolcs Borsanyi, Zoltan Fodor, Jana N. Guenther, Ruben Kara, Sandor D. Katz, Paolo Parotto, Attila Pasztor, Claudia Ratti, Kalman K. Szabo, The QCD crossover at finite chemical potential from lattice simulations, *Phys. Rev. Lett.* 125 (2020) 052001, 2002.02821.
- [7] J. Cleymans, K. Redlich, Unified description of freezeout parameters in relativistic heavy ion collisions, *Phys. Rev. Lett.* 81 (1998) 5284–5286, doi:10.1103/PhysRevLett.81.5284, nucl-th/9808030.
- [8] V. Vovchenko, V. V. Begun, M. I. Gorenstein, Hadron multiplicities and chemical freeze-out conditions in proton-proton and nucleus-nucleus collisions, *Phys. Rev. C* 93 (6) (2016) 064906, doi:10.1103/PhysRevC.93.064906, 1512.08025.
- [9] F. Becattini, J. Steinheimer, R. Stock, M. Bleicher, Hadronization conditions in relativistic nuclear collisions and the QCD pseudo-critical line, *Phys. Lett. B* 764 (2017) 241–246, doi:10.1016/j.physletb.2016.11.033, 1605.09694.
- [10] Volodymyr Vovchenko, Mark I. Gorenstein, Horst Stoecker, Finite resonance widths influence the thermal-model description of hadron yields, *Phys. Rev. C* 98 (3) (2018) 034906, doi:10.1103/PhysRevC.98.034906, 1807.02079.
- [11] L. Adamczyk, et al. (STAR), Bulk Properties of the Medium Produced in Relativistic Heavy-Ion Collisions from the Beam Energy Scan Program, *Phys. Rev. C* 96 (4) (2017) 044904, doi:10.1103/PhysRevC.96.044904, 1701.07065.
- [12] Anton Andronic, Peter Braun-Munzinger, Krzysztof Redlich, Johanna Stachel, Decoding the phase structure of QCD via particle production at high energy, *Nature* 561 (7723) (2018) 321–330, doi:10.1038/s41586-018-0491-6, 1710.09425.
- [13] Artemiy Lysenko, Mark I. Gorenstein, Roman Poberezhniuk, Volodymyr Vovchenko, Chemical freeze-out curve in heavy-ion collisions and the QCD critical point, *Phys. Rev. C* 111 (5) (2025) 054903, doi:10.1103/PhysRevC.111.054903, 2408.06473.
- [14] J. B. Elliott, P. T. Lake, L. G. Moretto, L. Phair, Determination of the coexistence curve, critical temperature, density, and pressure of bulk nuclear matter from fragment emission data, *Phys. Rev. C* 87 (5) (2013) 054622, doi:10.1103/PhysRevC.87.054622.
- [15] Rajesh Kumar, et al. (MUSES), Theoretical and experimental constraints for the equation of state of dense and hot matter, *Living Rev. Rel.* 27 (1) (2024) 3, doi:10.1007/s41114-024-00049-6, 2303.17021.
- [16] Franz Gross, et al., 50 Years of Quantum Chromodynamics, *Eur. Phys. J. C* 83 (2023) 1125, doi:10.1140/epjc/s10052-023-11949-2, 2212.11107.
- [17] S. Durr, Z. Fodor, J. Frison, C. Hoelbling, R. Hoffmann, et al., Ab-Initio Determination of Light Hadron Masses, *Science* 322 (2008) 1224–1227, doi:10.1126/science.1163233, 0906.3599.
- [18] Sz. Borsanyi, S. Durr, Z. Fodor, C. Hoelbling, S.D. Katz, et al., Ab initio calculation of the neutron-proton mass difference, *Science* 347 (2015) 1452–1455, doi:10.1126/science.1257050, 1406.4088.
- [19] Timo A. Lähde, Evgeny Epelbaum, Hermann Krebs, Dean Lee, Ulf-G. Meißner, Gautam Rupak, Lattice Effective Field Theory for Medium-Mass Nuclei, *Phys. Lett. B* 732 (2014) 110–115, doi:10.1016/j.physletb.2014.03.023, 1311.0477.
- [20] H. T. Ding, et al., Chiral phase transition temperature in (2+1)-flavor QCD, *Phys. Rev. Lett.* 123 (2019) 062002, doi:10.1103/PhysRevLett.123.062002, 1903.04801.
- [21] M. A. Stephanov, QCD critical point and complex chemical potential singularities, *Phys. Rev. D* 73 (2006) 094508, doi:10.1103/PhysRevD.73.094508, hep-lat/0603014.
- [22] Claudio Bonati, Massimo D’Elia, Marco Mariti, Michele Mesiti, Francesco Negro, Francesco Sanfilippo, Curvature of the chiral pseudocritical line in QCD: Continuum extrapolated results, *Phys. Rev. D* 92 (5) (2015) 054503, doi:10.1103/PhysRevD.92.054503, 1507.03571.
- [23] R. Bellwied, S. Borsanyi, Z. Fodor, J. Guenther, S. D. Katz, C. Ratti, K. K. Szabo, The QCD phase diagram from analytic continuation, *Phys. Lett. B* 751 (2015) 559–564, doi:10.1016/j.physletb.2015.11.011, 1507.07510.
- [24] A. Bazavov, et al., Chiral crossover in QCD at zero and non-zero chemical potentials, *Physics Letters B* 795 (2019) 15–21, 1812.08235.
- [25] Szabolcs Borsanyi, Zoltan Fodor, Jana N. Guenther, Paolo Parotto, Attila Pasztor, Claudia Ratti, Volodymyr Vovchenko, Chik Him Wong, Lattice QCD constraints on the critical point from an improved precision equation of state (2025), 2502.10267.
- [26] Misha A. Stephanov, K. Rajagopal, Edward V. Shuryak, Event-by-event fluctuations in heavy ion collisions and the QCD critical point, *Phys. Rev. D* 60 (1999) 114028, doi:10.1103/PhysRevD.60.114028, hep-ph/9903292.
- [27] M.A. Stephanov, Non-Gaussian fluctuations near the QCD critical point, *Phys. Rev. Lett.* 102 (2009) 032301, doi:10.1103/PhysRevLett.102.032301, 0809.3450.
- [28] M.A. Stephanov, On the sign of kurtosis near the QCD critical point, *Phys. Rev. Lett.* 107 (2011) 052301, doi:10.1103/PhysRevLett.107.052301, 1104.1627.
- [29] L. Adamczyk, et al. (STAR Collaboration), Energy Dependence of Moments of Net-proton Multiplicity Distributions at RHIC, *Phys. Rev. Lett.* 112 (2014) 032302, doi:10.1103/PhysRevLett.112.032302, 1309.5681.
- [30] Mohamed Abdallah, et al. (STAR), Measurement of the Sixth-Order Cumulant of Net-Proton Multiplicity Distributions in Au+Au Collisions at  $\sqrt{s_{NN}} = 27, 54.4$ , and 200 GeV at RHIC, *Phys. Rev. Lett.* 127 (26) (2021) 262301, doi:10.1103/PhysRevLett.127.262301, 2105.14698.
- [31] Mohamed Abdallah, et al. (STAR), Cumulants and correlation functions of net-proton, proton, and antiproton multiplicity distributions in Au+Au collisions at energies available at the BNL Relativistic Heavy Ion Collider, *Phys. Rev. C* 104 (2) (2021) 024902, doi:10.1103/PhysRevC.104.024902, [Erratum: *Phys. Rev. C* 111, 029902 (2025)], 2101.12413.
- [32] B. E. Aboona, et al. (STAR), Precision Measurement of Net-Proton-Number Fluctuations in Au+Au Collisions at RHIC, *Phys. Rev. Lett.* 135 (14) (2025) 142301, doi:10.1103/PhysRevLett.135.142301, 2504.00817.
- [33] Bing-Nan Lu, Ning Li, Serdar Elhatisari, Dean Lee, Joaquín E. Drut, Timo A. Lähde, Evgeny Epelbaum, Ulf-G. Meißner, *AbInitio* Nuclear Thermodynamics, *Phys. Rev. Lett.* 125 (19) (2020) 192502, doi:10.1103/PhysRevLett.125.192502, 1912.05105.
- [34] Kenji Fukushima, Jan Horak, Jan M. Pawłowski, Nicolas Wink, Carl Philipp Zelle, Nuclear liquid-gas transition in QCD, *Phys. Rev. D* 110 (7) (2024) 076022, doi:10.1103/PhysRevD.110.076022, 2308.16594.
- [35] Lipei Du, Agnieszka Sorensen, Mikhail Stephanov, The QCD phase diagram and Beam Energy Scan physics: a theory overview, *Int. J. Mod. Phys. E* 33 (07) (2024) 2430008, doi:10.1142/S021830132430008X, 2402.10183.
- [36] John W. Harris, Berndt Müller, “QGP Signatures” Revisited, *Eur. Phys. J. C* 84 (3) (2024) 247, doi:10.1140/epjc/s10052-024-12533-y, 2308.05743.
- [37] Christopher Plumberg, et al., Conservation of B, S, and Q charges in relativistic viscous hydrodynamics solved with smoothed particle hydrodynamics, *Phys. Rev. C* 111 (4) (2025) 044905, doi:10.1103/PhysRevC.111.044905, 2405.09648.
- [38] Charles Gale, Sangyong Jeon, Bjoern Schenke, Hydrodynamic Modeling of Heavy-Ion Collisions, *Int. J. Mod. Phys. A* 28 (2013) 1340011, doi:10.1142/S0217751X13400113, 1301.5893.
- [39] Xin An, et al., The BEST framework for the search for the QCD critical point and the chiral magnetic effect, *Nucl. Phys. A* 1017 (2022) 122343, doi:10.1016/j.nuclphysa.2021.122343, 2108.13867.
- [40] Mike Lisa, Timescales in heavy ion collisions, *Acta Phys. Polon. B* 47 (2016) 1847, doi:10.5506/APhysPolB.47.1847, 1607.06188.
- [41] Shreyasi Acharya, et al. (ALICE), The ALICE experiment: a journey through QCD, *Eur. Phys. J. C* 84 (8) (2024) 813, doi:10.1140/epjc/s10052-024-12935-y, 2211.04384.
- [42] Albert M. Sirunyan, et al. (CMS), Measurement of prompt and nonprompt charmonium suppression in PbPb collisions at 5.02 TeV, *Eur. Phys. J. C* 78 (6) (2018) 509, doi:10.1140/epjc/s10052-018-5950-6, [Erratum: *Eur. Phys. J. C* 83, 145 (2023)], 1712.08959.

- [43] S. Acharya, et al. (ALICE), Energy dependence and fluctuations of anisotropic flow in Pb-Pb collisions at  $\sqrt{s_{NN}} = 5.02$  and 2.76 TeV, JHEP 07 (2018) 103, doi:10.1007/JHEP07(2018)103, 1804.02944.
- [44] John W. Harris, Berndt Muller, The Search for the quark - gluon plasma, Ann. Rev. Nucl. Part. Sci. 46 (1996) 71–107, doi:10.1146/annurev.nucl.46.1.71, hep-ph/9602235.
- [45] Bjoern Schenke, Chun Shen, Prithwish Tribedy, Running the gamut of high energy nuclear collisions, Phys. Rev. C 102 (4) (2020) 044905, doi:10.1103/PhysRevC.102.044905, 2005.14682.
- [46] C Ahdida, G Alocco, M Arba, R Arnaldi, S Beole, J Bernhard, L Bianchi, I Bilinskyi, E Borisova, S Bressler, S Bufalino, R Cerri, M Ciacco, C Cicalo, S Coli, P Cortese, A Dainese, H Danielsson, J Datta, A De Falco, A Drees, L Epshteyn, A Ferretti, F Fionda, M Gagliardi, G M Galimberti, S Girod, T Gunji, G Jin, F Geurts, L Hu, L Levinson, F Li, W Li, Z Liu, D Marras, M Masera, A Masoni, F Mazzaschi, P Mereu, J Metselaar, L Micheletti, A Milov, L Mirasola, A Mulliri, L Musa, E Nowak, C Oppedisano, N Pacifico, M Ploskon, T Prebibaj, F Prino, M Puccio, C Puggioni, A Rossi, V Sarritzu, B Schmidt, E Scomparin, D Sekihata, Q Shou, R Shahoyan, M Shoa, S Siddhanta, X Su, Z Tang, S Trogolo, M Tuveri, A Uras, G Usai, M Van Dijk, E Vercellin, I Vorobyev, B Yankovsky, D Zavazieva (NA60+/DiCE), NA60+/DiCE: study of rare probes of the Quark-Gluon Plasma at SPS energies, tech. rep., CERN, Geneva 2025, URL <https://cds.cern.ch/record/2932302>.
- [47] T. Matsui, H. Satz,  $J/\psi$  Suppression by Quark-Gluon Plasma Formation, Phys.Lett. B178 (1986) 416, doi:10.1016/0370-2693(86)91404-8.
- [48] Anton Andronic, Roberta Arnaldi, Quarkonia and Deconfined Quark-Gluon Matter in Heavy-Ion Collisions, Ann. Rev. Nucl. Part. Sci. 75 (1) (2025) 351–375, doi:10.1146/annurev-nucl-121423-101041, 2501.08290.
- [49] Alexei Bazavov, Daniel Hoying, Rasmus N. Larsen, Swagato Mukherjee, Peter Petreczky, Alexander Rothkopf, Johannes Heinrich Weber (HotQCD), Unscreened forces in the quark-gluon plasma?, Phys. Rev. D 109 (7) (2024) 074504, doi:10.1103/PhysRevD.109.074504, 2308.16587.
- [50] M. Laine, O. Philipsen, P. Romatschke, M. Tassler, Real-time static potential in hot QCD, JHEP 03 (2007) 054, doi:10.1088/1126-6708/2007/03/054, hep-ph/0611300.
- [51] A. Beraudo, J. P. Blaizot, C. Ratti, Real and imaginary-time Q anti-Q correlators in a thermal medium, Nucl. Phys. A806 (2008) 312–338, doi:10.1016/j.nuclphysa.2008.03.001, 0712.4394.
- [52] Yukinao Akamatsu, Heavy quark master equations in the Lindblad form at high temperatures, Phys. Rev. D 91 (5) (2015) 056002, doi:10.1103/PhysRevD.91.056002, 1403.5783.
- [53] Nora Brambilla, Miguel A. Escobedo, Joan Soto, Antonio Vairo, Quarkonium suppression in heavy-ion collisions: an open quantum system approach, Phys. Rev. D 96 (3) (2017) 034021, doi:10.1103/PhysRevD.96.034021, 1612.07248.
- [54] Yukinao Akamatsu, Quarkonium in quark-gluon plasma: Open quantum system approaches re-examined, Prog. Part. Nucl. Phys. 123 (2022) 103932, doi:10.1016/j.pnpnp.2021.103932, 2009.10559.
- [55] Nora Brambilla, Miguel Ángel Escobedo, Ajaharul Islam, Michael Strickland, Anurag Tiwari, Antonio Vairo, Peter Vander Griend, Regeneration of bottomonia in an open quantum systems approach, Phys. Rev. D 108 (1) (2023) L011502, doi:10.1103/PhysRevD.108.L011502, 2302.11826.
- [56] Morad Aaboud, et al. (ATLAS), Measurement of the azimuthal anisotropy of charged particles produced in  $\sqrt{s_{NN}} = 5.02$  TeV Pb+Pb collisions with the ATLAS detector, Eur. Phys. J. C 78 (12) (2018) 997, doi:10.1140/epjc/s10052-018-6468-7, 1808.03951.
- [57] Edward V. Shuryak, Quark-Gluon Plasma and Hadronic Production of Leptons, Photons and Psions, Phys. Lett. B 78 (1978) 150, doi:10.1016/0370-2693(78)90370-2.
- [58] Hendrik van Hees, Ralf Rapp, Comprehensive Interpretation of Thermal Dileptons Measured at the CERN Super Proton Synchrotron, Phys. Rev. Lett. 97 (2006) 102301, doi:10.1103/PhysRevLett.97.102301, URL <https://link.aps.org/doi/10.1103/PhysRevLett.97.102301>.
- [59] Ralf Rapp, Hendrik van Hees, Thermal Dileptons as Fireball Thermometer and Chronometer, Phys. Lett. B 753 (2016) 586–590, doi:10.1016/j.physletb.2015.12.065, 1411.4612.
- [60] Florian Seck, Tetyana Galatyuk, Ayon Mukherjee, Ralf Rapp, Jan Steinheimer, Joachim Stroth, Maximilian Wiest, Dilepton signature of a first-order phase transition, Phys. Rev. C 106 (1) (2022) 014904, doi:10.1103/PhysRevC.106.014904, 2010.04614.
- [61] Piotr Salabura, Joachim Stroth, Dilepton radiation from strongly interacting systems, Prog. Part. Nucl. Phys. 120 (2021) 103869, doi:10.1016/j.pnpnp.2021.103869, 2005.14589.
- [62] Frank Geurts, Ralf-Arno Tripolt, Electromagnetic probes: Theory and experiment, Prog. Part. Nucl. Phys. 128 (2023) 104004, doi:10.1016/j.pnpnp.2022.104004, 2210.01622.
- [63] N. Xu, et al., Nuclear Matter at High Density and Equation of State 2022 doi:10.1007/978-981-19-4441-3\_4.
- [64] Oleh Savchuk, Anton Motornenko, Jan Steinheimer, Volodymyr Vovchenko, Marcus Bleicher, Mark Gorenstein, Tetyana Galatyuk, Enhanced dilepton emission from a phase transition in dense matter, J. Phys. G 50 (12) (2023) 125104, doi:10.1088/1361-6471/acfcf, 2209.05267.
- [65] R Arnaldi, et al. (NA60), Evidence for the production of thermal-like muon pairs with masses above 1-GeV/c<sup>2</sup> in 158-A-GeV Indium-Indium Collisions, Eur. Phys. J. C 59 (2009) 607–623, doi:10.1140/epjc/s10052-008-0857-2, 0810.3204.
- [66] Hans J. Specht (NA60), Thermal Dileptons from Hot and Dense Strongly Interacting Matter, AIP Conf. Proc. 1322 (1) (2010) 1–10, doi:10.1063/1.3541982, 1011.0615.
- [67] L. Adamczyk, et al. (STAR), Energy dependence of acceptance-corrected dielectron excess mass spectrum at mid-rapidity in Au+Au collisions at  $\sqrt{s_{NN}} = 19.6$  and 200 GeV, Phys. Lett. B 750 (2015) 64–71, doi:10.1016/j.physletb.2015.08.044, 1501.05341.
- [68] M. I. Abdulhamid, B. E. Aboona, J. Adam, L. Adamczyk, J. R. Adams, I. Aggarwal, M. M. Aggarwal, Z. Ahammed, D. M. Anderson, E. C. Aschenauer, S. Aslam, J. Atchison, V. Bairathi, W. Baker, J. G. Ball Cap, K. Barish, R. Bellwied, P. Bhagat, A. Bhasin, S. Bhatta, J. Bielcik, J. Bielcikova, J. D. Brandenburg, J. Butterworth, X. Z. Cai, H. Caines, M. Calderón de la Barca Sánchez, D. Cebra, J. Ceska, I. Chakaberia, P. Chaloupka, B. K. Chan, Z. Chang, A. Chatterjee, D. Chen, J. Chen, J. H. Chen, Z. Chen, J. Cheng, Y. Cheng, S. Choudhury, W. Christie, X. Chu, H. J. Crawford, M. Csanád, G. Dale-Gau, A. Das, M. Dagherity, I. M. Deppner, A. Dhamija, L. Di Carlo, L. Didenko, P. Dixit, X. Dong, J. L. Drachenberg, E. Duckworth, J. C. Dunlop, J. Engelage, G. Eppley, S. Esumi, O. Evdokimov, A. Ewigleben, O. Eyser, R. Fatemi, S. Fazio, C. J. Feng, Y. Feng, E. Finch, Y. Fisyak, F. A. Flor, C. Fu, C. A. Gagliardi, T. Galatyuk, F. Geurts, N. Ghimire, A. Gibson, K. Gopal, X. Gou, D. Grosnick, Y. Guo, A. Gupta, W. Guryn, A. Hamed, Y. Han, S. Harabasz, M. D. Harasty, J. W. Harris, H. Harrison-Smith, W. He, X. He, Y. He, N. Herrmann, L. Holub, C. Hu, Q. Hu, Y. Hu, B. Huang, H. Z. Huang, S. L. Huang, X. Huang, Y. Huang, P. Huck, T. J. Humanic, D. Isenhowe, M. Isshiki, W. W. Jacobs, A. Jalta, C. Jena, A. Jentsch, Y. Ji, J. Jia, C. Jin, X. Ju, E. G. Judd, S. Kabana, M. L. Kabir, S. Kagamaster, D. Kalinkin, K. Kang, D. Kapukchyan, K. Kauder, H. W. Ke, D. Keane, M. Kelsey, Y. V. Khyzhniak, D. P. Kikola, B. Kimelman, D. Kincses, I. Kisel, A. Kiselev, A. G. Knospe, H. S. Ko, L. K. Kosarzewski, L. Kramarik, L. Kumar, S. Kumar, R. Kunnawalkam Elayavalli, R. Lacey, J. M. Landgraf, J. Lauret, A. Lebedev, J. H. Lee, Y. H. Leung, N. Lewis, C. Li, W. Li, X. Li, Y. Li, Y. Li, Z. Li, X. Liang, Y. Liang, R. Licens, T. Lin, M. A. Lisa, C. Liu, F. Liu, G. Liu, H. Liu, H. Liu, L. Liu, T. Liu, X. Liu, Y. Liu, Z. Liu, T. Ljubicic, W. J. Llope, O. Lomicky, R. S. Longacre, E. M. Lloyd, T. Lu, N. S. Lukow, X. F. Luo, L. Ma, R. Ma, Y. G. Ma, N. Magdy, D. Mallick, S. Margetis, C. Markert, H. S. Matis, J. A. Mazer, G. McNamara, K. Mi, S. Mioduszewski, B. Mohanty, M. M. Mondal, I.

- Mooney, A. Mukherjee, M. I. Nagy, A. S. Nain, J. D. Nam, Md. Nasim, D. Neff, J. M. Nelson, D. B. Nemes, M. Nie, T. Niida, R. Nishitani, T. Nonaka, G. Odyniec, A. Ogawa, S. Oh, K. Okubo, B. S. Page, R. Pak, J. Pan, A. Pandav, A. K. Pandey, T. Pani, A. Paul, B. Pawlik, D. Pawlowska, C. Perkins, J. Pluta, B. R. Pokhrel, M. Posik, T. Protzman, V. Prozorova, N. K. Pruthi, M. Przybycien, J. Putschke, Z. Qin, H. Qiu, A. Quintero, C. Racz, S. K. Radhakrishnan, N. Raha, R. L. Ray, R. Reed, H. G. Ritter, C. W. Robertson, M. Robotkova, M. A. Rosales Aguilar, D. Roy, P. Roy Chowdhury, L. Ruan, A. K. Sahoo, N. R. Sahoo, H. Sako, S. Salur, S. Sato, W. B. Schmidke, N. Schmitz, F.-J. Seck, J. Seger, R. Seto, P. Seyboth, N. Shah, P. V. Shanmuganathan, T. Shao, M. Sharma, N. Sharma, R. Sharma, S. R. Sharma, A. I. Sheikh, D. Y. Shen, K. Shen, S. S. Shi, Y. Shi, Q. Y. Shou, F. Si, J. Singh, S. Singha, P. Sinha, M. J. Skoby, N. Smirnov, Y. Söhngen, Y. Song, B. Srivastava, T. D. S. Stanislaus, M. Stefaniak, D. J. Stewart, B. Stringfellow, Y. Su, A. A. P. Suaide, M. Sumera, C. Sun, X. Sun, Y. Sun, Y. Sun, B. Surrow, Z. W. Sweger, P. Szymanski, A. Tamis, A. H. Tang, Z. Tang, T. Tarnowsky, J. H. Thomas, A. R. Timmins, D. Tlusty, T. Todoroki, C. A. Tomkiel, S. Trentalange, R. E. Tribble, P. Tribedy, T. Truhlar, B. A. Trzeciak, O. D. Tsai, C. Y. Tsang, Z. Tu, T. Ullrich, D. G. Underwood, I. Upsal, G. Van Buren, J. Vanek, I. Vassiliev, V. Verkest, F. Videbæk, S. A. Voloshin, F. Wang, G. Wang, J. S. Wang, X. Wang, Y. Wang, Y. Wang, Y. Wang, Z. Wang, J. C. Webb, P. C. Weidenkaff, G. D. Westfall, D. Wielanek, H. Wieman, G. Wilks, S. W. Wissink, R. Witt, J. Wu, J. Wu, X. Wu, Y. Wu, B. Xi, Z. G. Xiao, G. Xie, W. Xie, H. Xu, N. Xu, Q. H. Xu, Y. Xu, Z. Xu, Z. Xu, G. Yan, Z. Yan, C. Yang, Q. Yang, S. Yang, Y. Yang, Z. Ye, Z. Ye, L. Yi, K. Yip, Y. Yu, H. Zbroszczyk, W. Zha, C. Zhang, D. Zhang, J. Zhang, S. Zhang, W. Zhang, X. Zhang, Y. Zhang, Y. Zhang, Y. Zhang, Z. J. Zhang, Z. Zhang, Z. Zhang, F. Zhao, J. Zhao, M. Zhao, C. Zhou, J. Zhou, S. Zhou, Y. Zhou, X. Zhu, M. Zurek, M. Zyzak (STAR Collaboration), Measurements of dielectron production in Au + Au collisions at  $\sqrt{s_{NN}} = 27, 39$ , and 62.4 GeV from the STAR experiment, *Phys. Rev. C* 107 (2023) L061901, doi:10.1103/PhysRevC.107.L061901, URL <https://link.aps.org/doi/10.1103/PhysRevC.107.L061901>.
- [69] B. E. Aboona, et al. (STAR), Temperature measurement of Quark-Gluon plasma at different stages, *Nature Commun.* 16 (1) (2025) 9098, doi:10.1038/s41467-025-63216-5, 2402.01998.
- [70] J. Adamczewski-Musch, et al. (HADES), Probing dense baryon-rich matter with virtual photons, *Nature Phys.* 15 (10) (2019) 1040–1045, doi:10.1038/s41567-019-0583-8.
- [71] Paolo Alba, Wanda Alberico, Rene Bellwied, Marcus Bluhm, Valentina Mantovani Sarti, et al., Freeze-out conditions from net-proton and net-charge fluctuations at RHIC, *Phys. Lett. B* 738 (2014) 305–310, doi:10.1016/j.physletb.2014.09.052, 1403.4903.
- [72] Rene Bellwied, Jacquelyn Noronha-Hostler, Paolo Parotto, Israel Portillo Vazquez, Claudia Ratti, Jamie M. Stafford, Freeze-out temperature from net-kaon fluctuations at energies available at the BNL Relativistic Heavy Ion Collider, *Phys. Rev. C* 99 (3) (2019) 034912, doi:10.1103/PhysRevC.99.034912, 1805.00088.
- [73] Rene Bellwied, Szabolcs Borsanyi, Zoltan Fodor, Jana N. Guenther, Jacquelyn Noronha-Hostler, Paolo Parotto, Attila Pasztor, Claudia Ratti, Jamie M. Stafford, Off-diagonal correlators of conserved charges from lattice QCD and experiment, *Physical Review D* 101 (3) (2020), 1910.14592.
- [74] Marcus Bluhm, Marlene Nahrgang, Freeze-out conditions from strangeness observables at RHIC, *Eur. Phys. J. C* 79 (2) (2019) 155, doi:10.1140/epjc/s10052-019-6661-3, 1806.04499.
- [75] Fernando Antonio Flor, Gabrielle Olinger, Rene Bellwied, Flavour and Energy Dependence of Chemical Freeze-out Temperatures in Relativistic Heavy Ion Collisions from RHIC-BES to LHC Energies, *Phys. Lett. B* 814 (2021) 136098, doi:10.1016/j.physletb.2021.136098, 2009.14781.
- [76] Kenneth G. Wilson, Confinement of Quarks, *Phys. Rev. D* 10 (1974) 2445–2459, doi:10.1103/PhysRevD.10.2445.
- [77] C. R. Allton, S. Ejiri, S. J. Hands, O. Kaczmarek, F. Karsch, E. Laermann, C. Schmidt, The Equation of state for two flavor QCD at nonzero chemical potential, *Phys. Rev. D* 68 (2003) 014507, doi:10.1103/PhysRevD.68.014507, hep-lat/0305007.
- [78] C. R. Allton, M. Doring, S. Ejiri, S. J. Hands, O. Kaczmarek, et al., Thermodynamics of two flavor QCD to sixth order in quark chemical potential, *Phys. Rev. D* 71 (2005) 054508, doi:10.1103/PhysRevD.71.054508, hep-lat/0501030.
- [79] O. Kaczmarek, F. Karsch, E. Laermann, C. Miao, S. Mukherjee, et al., Phase boundary for the chiral transition in (2+1)-flavor QCD at small values of the chemical potential, *Phys. Rev. D* 83 (2011) 014504, doi:10.1103/PhysRevD.83.014504, 1011.3130.
- [80] G. Endrodi, Z. Fodor, S. D. Katz, K. K. Szabo, The QCD phase diagram at nonzero quark density, *JHEP* 1104 (2011) 001, doi:10.1007/JHEP04(2011)001, 1102.1356.
- [81] Sz. Borsanyi, G. Endrodi, Z. Fodor, S. D. Katz, S. Krieg, et al., QCD equation of state at nonzero chemical potential: continuum results with physical quark masses at order  $mu^2$ , *JHEP* 1208 (2012) 053, doi:10.1007/JHEP08(2012)053, 1204.6710.
- [82] A. Bazavov, et al., The QCD Equation of State to  $O(mu_B^6)$  from Lattice QCD, *Phys. Rev. D* 95 (5) (2017) 054504, doi:10.1103/PhysRevD.95.054504, 1701.04325.
- [83] Claudio Bonati, Massimo D'Elia, Francesco Negro, Francesco Sanfilippo, Kevin Zambello, Curvature of the pseudocritical line in QCD: Taylor expansion matches analytic continuation, *Phys. Rev. D* 98 (5) (2018) 054510, doi:10.1103/PhysRevD.98.054510, 1805.02960.
- [84] A. Bazavov, et al. (HotQCD), Chiral crossover in QCD at zero and non-zero chemical potentials, *Phys. Lett. B* 795 (2019) 15–21, doi:10.1016/j.physletb.2019.05.013, 1812.08235.
- [85] D. Bollweg, J. Goswami, O. Kaczmarek, F. Karsch, Swagato Mukherjee, P. Petreczky, C. Schmidt, P. Scior (HotQCD), Taylor expansions and Padé approximants for cumulants of conserved charge fluctuations at nonvanishing chemical potentials, *Phys. Rev. D* 105 (7) (2022) 074511, doi:10.1103/PhysRevD.105.074511, 2202.09184.
- [86] Massimo D'Elia, Maria-Paola Lombardo, Finite density QCD via imaginary chemical potential, *Phys. Rev. D* 67 (2003) 014505, doi:10.1103/PhysRevD.67.014505, hep-lat/0209146.
- [87] P. de Forcrand, O. Philipsen, QCD phase diagram at small densities from simulations with imaginary  $\mu$ , in: 5th International Conference on Strong and Electroweak Matter 2003, pp. 271–275, doi:10.1142/9789812704498\_0027, hep-ph/0301209.
- [88] Massimo D'Elia, Francesco Di Renzo, Maria Paola Lombardo, The Strongly interacting quark gluon plasma, and the critical behaviour of QCD at imaginary  $\mu$ , *Phys. Rev. D* 76 (2007) 114509, doi:10.1103/PhysRevD.76.114509, 0705.3814.
- [89] Paolo Cea, Leonardo Cosmai, Massimo D'Elia, Chiara Manneschi, Alessandro Papa, Analytic continuation of the critical line: Suggestions for QCD, *Phys. Rev. D* 80 (2009) 034501, doi:10.1103/PhysRevD.80.034501, 0905.1292.
- [90] Paolo Cea, Leonardo Cosmai, Alessandro Papa, Critical line of 2+1 flavor QCD: Toward the continuum limit, *Phys. Rev. D* 93 (1) (2016) 014507, doi:10.1103/PhysRevD.93.014507, 1508.07599.
- [91] Volodymyr Vovchenko, Attila Pasztor, Zoltan Fodor, Sándor D. Katz, Horst Stoecker, Repulsive baryonic interactions and lattice QCD observables at imaginary chemical potential, *Phys. Lett. B* 775 (2017) 71–78, doi:10.1016/j.physletb.2017.10.042, 1708.02852.
- [92] Volodymyr Vovchenko, Jan Steinheimer, Owe Philipsen, Horst Stoecker, Cluster Expansion Model for QCD Baryon Number Fluctuations: No Phase Transition at  $\mu_B/T < \pi$ , *Phys. Rev. D* 97 (11) (2018) 114030, doi:10.1103/PhysRevD.97.114030, 1711.01261.
- [93] S. Borsanyi, Z. Fodor, J. N. Guenther, R. Kara, S. D. Katz, P. Parotto, A. Pásztor, C. Ratti, K. K. Szabó, Lattice QCD equation of state at finite chemical potential from an alternative expansion scheme, *Phys. Rev. Lett.* 126 (23) (2021) 232001, doi:10.1103/PhysRevLett.126.232001, 2102.06660.

- [94] Szabolcs Borsanyi, Zoltan Fodor, Jana N. Guenther, Ruben Kara, Paolo Parotto, Attila Pasztor, Claudia Ratti, Kalman K. Szabo, Resummed lattice QCD equation of state at finite baryon density: Strangeness neutrality and beyond, *Phys. Rev. D* 105 (11) (2022) 114504, doi:10.1103/PhysRevD.105.114504, 2202.05574.
- [95] Ian M. Barbour, Susan E. Morrison, Elyakum G. Klepfish, John B. Kogut, Maria-Paola Lombardo, Results on finite density QCD, *Nucl. Phys. Proc. Suppl.* 60A (1998) 220–234, doi:10.1016/S0920-5632(97)00484-2, [,220(1997)], hep-lat/9705042.
- [96] Z. Fodor, S.D. Katz, A New method to study lattice QCD at finite temperature and chemical potential, *Phys.Lett.* B534 (2002) 87–92, doi:10.1016/S0370-2693(02)01583-6, hep-lat/0104001.
- [97] Z. Fodor, S.D. Katz, Lattice determination of the critical point of QCD at finite T and  $\mu$ , *JHEP* 0203 (2002) 014, doi:10.1088/1126-6708/2002/03/014, hep-lat/0106002.
- [98] Z. Fodor, S.D. Katz, Critical point of QCD at finite T and  $\mu$ , lattice results for physical quark masses, *JHEP* 0404 (2004) 050, doi:10.1088/1126-6708/2004/04/050, hep-lat/0402006.
- [99] P. de Forcrand, S. Kim, T. Takaishi, QCD simulations at small chemical potential, *Nucl. Phys. B Proc. Suppl.* 119 (2003) 541–543, doi:10.1016/S0920-5632(03)80451-6, hep-lat/0209126.
- [100] Andrei Alexandru, Manfred Faber, Ivan Horvath, Keh-Fei Liu, Lattice QCD at finite density via a new canonical approach, *Phys. Rev. D* 72 (2005) 114513, doi:10.1103/PhysRevD.72.114513, hep-lat/0507020.
- [101] Zoltan Fodor, Sandor D. Katz, Christian Schmidt, The Density of states method at non-zero chemical potential, *JHEP* 0703 (2007) 121, doi:10.1088/1126-6708/2007/03/121, hep-lat/0701022.
- [102] G. Endrodi, Z. Fodor, S. D. Katz, D. Sexty, K. K. Szabo, Cs. Torok, Applying constrained simulations for low temperature lattice QCD at finite baryon chemical potential, *Phys. Rev. D* 98 (7) (2018) 074508, doi:10.1103/PhysRevD.98.074508, 1807.08326.
- [103] Matteo Giordano, Kornel Kapas, Sandor D. Katz, Daniel Negradi, Attila Pasztor, Effect of stout smearing on the phase diagram from multiparameter reweighting in lattice QCD, *Phys. Rev. D* 102 (3) (2020) 034503, doi:10.1103/PhysRevD.102.034503, 2003.04355.
- [104] Matteo Giordano, Kornel Kapas, Sandor D. Katz, Daniel Negradi, Attila Pasztor, New approach to lattice QCD at finite density; results for the critical end point on coarse lattices, *JHEP* 05 (2020) 088, doi:10.1007/JHEP05(2020)088, 2004.10800.
- [105] Szabolcs Borsanyi, Zoltan Fodor, Matteo Giordano, Sandor D. Katz, Daniel Negradi, Attila Pasztor, Chik Him Wong, Lattice simulations of the QCD chiral transition at real baryon density, *Phys. Rev. D* 105 (5) (2022) L051506, doi:10.1103/PhysRevD.105.L051506, 2108.09213.
- [106] Szabolcs Borsanyi, Zoltan Fodor, Matteo Giordano, Jana N. Guenther, Sandor D. Katz, Attila Pasztor, Chik Him Wong, Equation of state of a hot-and-dense quark gluon plasma: Lattice simulations at real  $\mu B$  vs extrapolations, *Phys. Rev. D* 107 (9) (2023) L091503, doi:10.1103/PhysRevD.107.L091503, 2208.05398.
- [107] R. Hagedorn, Statistical thermodynamics of strong interactions at high-energies, *Nuovo Cim.Suppl.* 3 (1965) 147–186.
- [108] N. Cabibbo, G. Parisi, Exponential Hadronic Spectrum and Quark Liberation, *Phys.Lett.* B59 (1975) 67–69, doi:10.1016/0370-2693(75)90158-6.
- [109] F. R. Brown, N. H. Christ, Y. F. Deng, M. S. Gao, T. J. Woch, Nature of the Deconfining Phase Transition in SU(3) Lattice Gauge Theory, *Phys. Rev. Lett.* 61 (1988) 2058, doi:10.1103/PhysRevLett.61.2058.
- [110] M. Fukugita, M. Okawa, A. Ukawa, Order of the Deconfining Phase Transition in SU(3) Lattice Gauge Theory, *Phys.Rev.Lett.* 63 (1989) 1768, doi:10.1103/PhysRevLett.63.1768.
- [111] Y. Aoki, Z. Fodor, S.D. Katz, K.K. Szabo, The QCD transition temperature: Results with physical masses in the continuum limit, *Phys.Lett. B* 643 (2006) 46–54, doi:10.1016/j.physletb.2006.10.021, hep-lat/0609068.
- [112] Y. Aoki, Szabolcs Borsanyi, Stephan Durr, Zoltan Fodor, Sandor D. Katz, et al., The QCD transition temperature: results with physical masses in the continuum limit II., *JHEP* 0906 (2009) 088, doi:10.1088/1126-6708/2009/06/088, 0903.4155.
- [113] H. T. Ding, O. Kaczmarek, F. Karsch, P. Petreczky, Mugdha Sarkar, C. Schmidt, Sipaz Sharma, Curvature of the chiral phase transition line from the magnetic equation of state of (2+1)-flavor QCD, *Phys. Rev. D* 109 (11) (2024) 114516, doi:10.1103/PhysRevD.109.114516, 2403.09390.
- [114] Szabolcs Borsanyi, Zoltan Fodor, Jana N. Guenther, Paolo Parotto, Attila Pasztor, Ludovica Pirelli, Kalman K. Szabo, Chik Him Wong, QCD deconfinement transition line up to  $\mu B=400$  MeV from finite volume lattice simulations, *Phys. Rev. D* 110 (11) (2024) 114507, doi:10.1103/PhysRevD.110.114507, 2410.06216.
- [115] A. Bazavov, N. Brambilla, H. T. Ding, P. Petreczky, H. P. Schadler, A. Vairo, J. H. Weber, Polyakov loop in 2+1 flavor QCD from low to high temperatures, *Phys. Rev. D* 93 (11) (2016) 114502, doi:10.1103/PhysRevD.93.114502, 1603.06637.
- [116] Szabolcs Borsanyi, Zoltan Fodor, Jana N. Guenther, Ruben Kara, Paolo Parotto, Attila Pasztor, Ludovica Pirelli, Chik Him Wong, Chiral versus deconfinement properties of the QCD crossover: Differences in the volume and chemical potential dependence from the lattice, *Phys. Rev. D* 111 (1) (2025) 014506, doi:10.1103/PhysRevD.111.014506.
- [117] A. Bazavov, et al. (HotQCD Collaboration), Equation of state in (2+1)-flavor QCD, *Phys.Rev. D* 90 (9) (2014) 094503, doi:10.1103/PhysRevD.90.094503, 1407.6387.
- [118] D. Bollweg, D. A. Clarke, J. Goswami, O. Kaczmarek, F. Karsch, Swagato Mukherjee, P. Petreczky, C. Schmidt, Sipaz Sharma (HotQCD), Equation of state and speed of sound of (2+1)-flavor QCD in strangeness-neutral matter at nonvanishing net baryon-number density, *Phys. Rev. D* 108 (1) (2023) 014510, doi:10.1103/PhysRevD.108.014510, 2212.09043.
- [119] J. Engels, J. Fingberg, F. Karsch, D. Miller, M. Weber, Nonperturbative thermodynamics of SU(N) gauge theories, *Phys.Lett.* B252 (1990) 625–630, doi:10.1016/0370-2693(90)90496-S.
- [120] Szabolcs Borsanyi, Zoltan Fodor, Christian Hoelbling, Sandor D. Katz, Stefan Krieg, et al., Full result for the QCD equation of state with 2+1 flavors, *Phys.Lett. B* 730 (2014) 99–104, doi:10.1016/j.physletb.2014.01.007, 1309.5258.
- [121] C.R. Allton, S. Ejiri, S.J. Hands, O. Kaczmarek, F. Karsch, et al., The QCD thermal phase transition in the presence of a small chemical potential, *Phys.Rev. D* 66 (2002) 074507, doi:10.1103/PhysRevD.66.074507, hep-lat/0204010.
- [122] Szabolcs Borsanyi, Zoltan Fodor, Jana N. Guenther, Sandor D. Katz, Paolo Parotto, Attila Pasztor, David Pesznyak, Kalman K. Szabo, Chik Him Wong, Continuum-extrapolated high-order baryon fluctuations, *Phys. Rev. D* 110 (1) (2024) L011501, doi:10.1103/PhysRevD.110.L011501, 2312.07528.
- [123] Akihiko Monnai, Björn Schenke, Chun Shen, Equation of state at finite densities for QCD matter in nuclear collisions, *Phys. Rev. C* 100 (2) (2019) 024907, doi:10.1103/PhysRevC.100.024907, 1902.05095.
- [124] J. Noronha-Hostler, P. Parotto, C. Ratti, J. M. Stafford, Lattice-based equation of state at finite baryon number, electric charge and strangeness chemical potentials, *Phys. Rev. C* 100 (6) (2019) 064910, doi:10.1103/PhysRevC.100.064910, 1902.06723.
- [125] Massimo D'Elia, Giuseppe Gagliardi, Francesco Sanfilippo, Higher order quark number fluctuations via imaginary chemical potentials in  $N_f = 2 + 1$  QCD, *Phys. Rev. D* 95 (9) (2017) 094503, doi:10.1103/PhysRevD.95.094503, 1611.08285.
- [126] Szabolcs Borsanyi, Zoltan Fodor, Jana N. Guenther, Sandor K. Katz, Kalman K. Szabo, Attila Pasztor, Israel Portillo, Claudia Ratti, Higher order fluctuations and correlations of conserved charges from lattice QCD, *JHEP* 10 (2018) 205, doi:10.1007/JHEP10(2018)205, 1805.04445.

- [127] Ahmed Abuali, Szabolcs Borsányi, Zoltán Fodor, Johannes Jahan, Micheal Kahangirwe, Paolo Parotto, Attila Pásztor, Claudia Ratti, Hitansh Shah, Seth A. Trubulsi, New 4D lattice QCD equation of state: Extended density coverage from a generalized  $T^*$  expansion, *Phys. Rev. D* 112 (5) (2025) 054502, doi:10.1103/2dmh-26yh, 2504.01881.
- [128] K. Kajantie, M. Laine, K. Rummukainen, Y. Schroder, The Pressure of hot QCD up to  $g_6 \ln(1/g)$ , *Phys. Rev. D* 67 (2003) 105008, doi:10.1103/PhysRevD.67.105008, hep-ph/0211321.
- [129] Andrei D. Linde, Infrared Problem in Thermodynamics of the Yang-Mills Gas, *Phys. Lett. B* 96 (1980) 289–292, doi:10.1016/0370-2693(80)90769-8.
- [130] David J. Gross, Robert D. Pisarski, Laurence G. Yaffe, QCD and Instantons at Finite Temperature, *Rev. Mod. Phys.* 53 (1981) 43, doi:10.1103/RevModPhys.53.43.
- [131] Eric Braaten, Robert D. Pisarski, Simple effective Lagrangian for hard thermal loops, *Phys. Rev. D* 45 (1992) R1827–R1830, doi:10.1103/PhysRevD.45.R1827.
- [132] Jens O. Andersen, Eric Braaten, Emmanuel Petitgirard, Michael Strickland, HTL perturbation theory to two loops, *Phys. Rev. D* 66 (2002) 085016, doi:10.1103/PhysRevD.66.085016, hep-ph/0205085.
- [133] Jens O. Andersen, Lars E. Leganger, Michael Strickland, Nan Su, Three-loop HTL QCD thermodynamics, *JHEP* 1108 (2011) 053, doi:10.1007/JHEP08(2011)053, 1103.2528.
- [134] Eric Braaten, Agustín Nieto, Effective field theory approach to high temperature thermodynamics, *Phys. Rev. D* 51 (1995) 6990–7006, doi:10.1103/PhysRevD.51.6990, hep-ph/9501375.
- [135] Sz. Borsányi, et al., Calculation of the axion mass based on high-temperature lattice quantum chromodynamics, *Nature* 539 (7627) (2016) 69–71, doi:10.1038/nature20115, 1606.07494.
- [136] Jacopo Ghiglieri, Aleksí Kurkela, Michael Strickland, Aleksí Vuorinen, Perturbative Thermal QCD: Formalism and Applications, *Phys. Rept.* 880 (2020) 1–73, doi:10.1016/j.physrep.2020.07.004, 2002.10188.
- [137] J.P. Blaizot, Edmond Iancu, A. Rebhan, Quark number susceptibilities from HTL resummed thermodynamics, *Phys. Lett. B* 523 (2001) 143–150, doi:10.1016/S0370-2693(01)01316-8, hep-ph/0110369.
- [138] Najmul Haque, Jens O. Andersen, Munshi G. Mustafa, Michael Strickland, Nan Su, Three-loop HTLpt Pressure and Susceptibilities at Finite Temperature and Density, *Phys. Rev. D* 89 (2014) 061701, doi:10.1103/PhysRevD.89.061701, 1309.3968.
- [139] Jens O. Andersen, Sylvain Moggiacci, Nan Su, Aleksí Vuorinen, Quark number susceptibilities from resummed perturbation theory, *Phys. Rev. D* 87 (2013) 074003, doi:10.1103/PhysRevD.87.074003, 1210.0912.
- [140] Najmul Haque, Munshi G. Mustafa, Michael Strickland, Quark Number Susceptibilities from Two-Loop Hard Thermal Loop Perturbation Theory, *JHEP* 1307 (2013) 184, doi:10.1007/JHEP07(2013)184, 1302.3228.
- [141] Jens O. Andersen, Najmul Haque, Munshi G. Mustafa, Michael Strickland, Three-loop HTLpt thermodynamics at finite temperature and isospin chemical potential, *Phys. Rev. D* 93 (2016) 054045, doi:10.1103/PhysRevD.93.054045, 1511.04660.
- [142] R. Bellwied, S. Borsányi, Z. Fodor, S. D. Katz, A. Pásztor, C. Ratti, K. K. Szabo, Fluctuations and correlations in high temperature QCD, *Phys. Rev. D* 92 (11) (2015) 114505, doi:10.1103/PhysRevD.92.114505, 1507.04627.
- [143] H. T. Ding, Swagato Mukherjee, H. Ohno, P. Petreczky, H. P. Schadler, Diagonal and off-diagonal quark number susceptibilities at high temperatures, *Phys. Rev. D* 92 (7) (2015) 074043, doi:10.1103/PhysRevD.92.074043, 1507.06637.
- [144] Najmul Haque, Aritra Bandyopadhyay, Jens O. Andersen, Munshi G. Mustafa, Michael Strickland, et al., Three-loop HTLpt thermodynamics at finite temperature and chemical potential, *JHEP* 1405 (2014) 027, doi:10.1007/JHEP05(2014)027, 1402.6907.
- [145] Sylvain Moggiacci, Jens O. Andersen, Michael Strickland, Nan Su, Aleksí Vuorinen, Equation of State of hot and dense QCD: Resummed perturbation theory confronts lattice data, *JHEP* 1312 (2013) 055, doi:10.1007/JHEP12(2013)055, 1307.8098.
- [146] A. Bazavov, H.-T. Ding, P. Hegde, F. Karsch, C. Miao, et al., Quark number susceptibilities at high temperatures, *Phys. Rev. D* 88 (9) (2013) 094021, doi:10.1103/PhysRevD.88.094021, 1309.2317.
- [147] Thomas Appelquist, Robert D. Pisarski, High-Temperature Yang-Mills Theories and Three-Dimensional Quantum Chromodynamics, *Phys. Rev. D* 23 (1981) 2305, doi:10.1103/PhysRevD.23.2305.
- [148] K. Kajantie, M. Laine, K. Rummukainen, Mikhail E. Shaposhnikov, Generic rules for high temperature dimensional reduction and their application to the standard model, *Nucl. Phys. B* 458 (1996) 90–136, doi:10.1016/0550-3213(95)00549-8, hep-ph/9508379.
- [149] Eric Braaten, Agustín Nieto, Free energy of QCD at high temperature, *Phys. Rev. D* 53 (1996) 3421–3437, doi:10.1103/PhysRevD.53.3421, hep-ph/9510408.
- [150] A. Hietanen, K. Kajantie, M. Laine, K. Rummukainen, Y. Schroder, Three-dimensional physics and the pressure of hot QCD, *Phys. Rev. D* 79 (2009) 045018, doi:10.1103/PhysRevD.79.045018, 0811.4664.
- [151] Ari Hietanen, Kari Rummukainen, The Diagonal and off-diagonal quark number susceptibility of high temperature and finite density QCD, *JHEP* 04 (2008) 078, doi:10.1088/1126-6708/2008/04/078, 0802.3979.
- [152] Kari Rummukainen, Niels Schlusser, High order quark number susceptibilities in hot QCD from lattice electrostatic QCD, *Phys. Rev. D* 106 (5) (2022) 054507, doi:10.1103/PhysRevD.106.054507, 2108.13236.
- [153] Mikko Laine, York Schroder, Quark mass thresholds in QCD thermodynamics, *Phys. Rev. D* 73 (2006) 085009, doi:10.1103/PhysRevD.73.085009, hep-ph/0603048.
- [154] Christof Wetterich, Exact evolution equation for the effective potential, *Phys. Lett. B* 301 (1993) 90–94, doi:10.1016/0370-2693(93)90726-X, 1710.05815.
- [155] Ulrich Ellwanger, FLOW equations for N point functions and bound states, *Z. Phys. C* 62 (1994) 503–510, doi:10.1007/BF0155911, hep-ph/9308260.
- [156] Tim R. Morris, The Exact renormalization group and approximate solutions, *Int. J. Mod. Phys. A* 9 (1994) 2411–2450, doi:10.1142/S0217751X94000972, hep-ph/9308265.
- [157] N. Dupuis, L. Canet, A. Eichhorn, W. Metzner, J. M. Pawłowski, M. Tissier, N. Wschebor, The nonperturbative functional renormalization group and its applications, *Phys. Rept.* 910 (2021) 1–114, doi:10.1016/j.physrep.2021.01.001, 2006.04853.
- [158] Friederike Ihssen, Jan M. Pawłowski, Franz R. Sattler, Nicolas Wink, Towards quantitative precision in functional QCD I (2024), 2408.08413.
- [159] Christian S. Fischer, Axel Maas, Jan M. Pawłowski, On the infrared behavior of Landau gauge Yang-Mills theory, *Annals Phys.* 324 (2009) 2408–2437, doi:10.1016/j.aop.2009.07.009, 0810.1987.
- [160] Anton K. Cyrol, Leonard Fister, Mario Mitter, Jan M. Pawłowski, Nils Strodthoff, Landau gauge Yang-Mills correlation functions, *Phys. Rev. D* 94 (5) (2016) 054005, doi:10.1103/PhysRevD.94.054005, 1605.01856.
- [161] Markus Q. Huber, Correlation functions of Landau gauge Yang-Mills theory, *Phys. Rev. D* 101 (2020) 114009, doi:10.1103/PhysRevD.101.114009, 2003.13703.
- [162] Jens Braun, Holger Gies, Jan M. Pawłowski, Quark Confinement from Color Confinement, *Phys. Lett. B* 684 (2010) 262–267, doi:10.1016/j.physletb.2010.01.009, 0708.2413.

- [163] Holger Gies, Christof Wetterich, Renormalization flow of bound states, *Phys. Rev. D* 65 (2002) 065001, doi:10.1103/PhysRevD.65.065001, hep-th/0107221.
- [164] Holger Gies, Christof Wetterich, Universality of spontaneous chiral symmetry breaking in gauge theories, *Phys. Rev. D* 69 (2004) 025001, doi:10.1103/PhysRevD.69.025001, hep-th/0209183.
- [165] Jan M. Pawłowski, Aspects of the functional renormalisation group, *Annals Phys.* 322 (2007) 2831–2915, doi:10.1016/j.aop.2007.01.007, hep-th/0512261.
- [166] Kenji Fukushima, Jan M. Pawłowski, Nils Strodthoff, Emergent hadrons and diquarks, *Annals Phys.* 446 (2022) 169106, doi:10.1016/j.aop.2022.169106, 2103.01129.
- [167] Jens Braun, Leonard Fister, Jan M. Pawłowski, Fabian Rennecke, From Quarks and Gluons to Hadrons: Chiral Symmetry Breaking in Dynamical QCD, *Phys. Rev. D* 94 (3) (2016) 034016, doi:10.1103/PhysRevD.94.034016, 1412.1045.
- [168] Wei-jie Fu, Jan M. Pawłowski, Fabian Rennecke, QCD phase structure at finite temperature and density, *Phys. Rev. D* 101 (5) (2020) 054032, doi:10.1103/PhysRevD.101.054032, 1909.02991.
- [169] Jens Braun, Holger Gies, Chiral phase boundary of QCD at finite temperature, *JHEP* 06 (2006) 024, doi:10.1088/1126-6708/2006/06/024, hep-ph/0602226.
- [170] Mario Mitter, Jan M. Pawłowski, Nils Strodthoff, Chiral symmetry breaking in continuum QCD, *Phys. Rev. D* 91 (2015) 054035, doi:10.1103/PhysRevD.91.054035, 1411.7978.
- [171] Jens Braun, Lisa M. Haas, Florian Marhauser, Jan M. Pawłowski, Phase Structure of Two-Flavor QCD at Finite Chemical Potential, *Phys. Rev. Lett.* 106 (2011) 022002, doi:10.1103/PhysRevLett.106.022002, 0908.0008.
- [172] Christian S. Fischer, QCD at finite temperature and chemical potential from Dyson-Schwinger equations, *Prog. Part. Nucl. Phys.* 105 (2019) 1–60, doi:10.1016/j.ppnp.2019.01.002, 1810.12938.
- [173] Gernot Eichmann, Helios Sanchis-Alepuz, Richard Williams, Reinhard Alkofer, Christian S. Fischer, Baryons as relativistic three-quark bound states, *Prog. Part. Nucl. Phys.* 91 (2016) 1–100, doi:10.1016/j.ppnp.2016.07.001, 1606.09602.
- [174] Christian S. Fischer, Axel Maas, Jens A. Müller, Chiral and deconfinement transition from correlation functions: SU(2) vs. SU(3), *Eur. Phys. J. C* 68 (2010) 165–181, doi:10.1140/epjc/s10052-010-1343-1, 1003.1960.
- [175] Christian S. Fischer, Jan Luecker, Jan M. Pawłowski, Phase structure of QCD for heavy quarks, *Phys. Rev. D* 91 (1) (2015) 014024, doi:10.1103/PhysRevD.91.014024, 1409.8462.
- [176] Craig D. Roberts, Sebastian M. Schmidt, Dyson-Schwinger equations: Density, temperature and continuum strong QCD, *Prog. Part. Nucl. Phys.* 45 (2000) S1–S103, doi:10.1016/S0146-6410(00)90011-5, nucl-th/0005064.
- [177] Christian S. Fischer, Jens A. Müller, On critical scaling at the QCD  $N_f = 2$  chiral phase transition, *Phys. Rev. D* 84 (2011) 054013, doi:10.1103/PhysRevD.84.054013, 1106.2700.
- [178] Christian S. Fischer, Jan Luecker, Propagators and phase structure of  $N_f=2$  and  $N_f=2+1$  QCD, *Phys. Lett. B* 718 (2013) 1036–1043, doi:10.1016/j.physletb.2012.11.054, 1206.5191.
- [179] Christian S. Fischer, Leonard Fister, Jan Luecker, Jan M. Pawłowski, Polyakov loop potential at finite density, *Phys. Lett. B* 732 (2014) 273–277, doi:10.1016/j.physletb.2014.03.057, 1306.6022.
- [180] Christian S. Fischer, Jan Luecker, Christian A. Welzbacher, Phase structure of three and four flavor QCD, *Phys. Rev. D* 90 (3) (2014) 034022, doi:10.1103/PhysRevD.90.034022, 1405.4762.
- [181] Gernot Eichmann, Christian S. Fischer, Christian A. Welzbacher, Baryon effects on the location of QCD's critical end point, *Phys. Rev. D* 93 (3) (2016) 034013, doi:10.1103/PhysRevD.93.034013, 1509.02082.
- [182] Pascal J. Gunkel, Christian S. Fischer, Locating the critical endpoint of QCD: Mesonic backcoupling effects, *Phys. Rev. D* 104 (5) (2021) 054022, doi:10.1103/PhysRevD.104.054022, 2106.08356.
- [183] Fei Gao, Jing Chen, Yu-Xin Liu, Si-Xue Qin, Craig D. Roberts, Sebastian M. Schmidt, Phase diagram and thermal properties of strong-interaction matter, *Phys. Rev. D* 93 (9) (2016) 094019, doi:10.1103/PhysRevD.93.094019, 1507.00875.
- [184] Philipp Isserstedt, Michael Buballa, Christian S. Fischer, Pascal J. Gunkel, Baryon number fluctuations in the QCD phase diagram from Dyson-Schwinger equations, *Phys. Rev. D* 100 (7) (2019) 074011, doi:10.1103/PhysRevD.100.074011, 1906.11644.
- [185] Anton K. Cyrol, Mario Mitter, Jan M. Pawłowski, Nils Strodthoff, Nonperturbative quark, gluon, and meson correlators of unquenched QCD, *Phys. Rev. D* 97 (5) (2018) 054006, doi:10.1103/PhysRevD.97.054006, 1706.06326.
- [186] S. Zafeiropoulos, P. Boucaud, F. De Soto, J. Rodríguez-Quintero, J. Segovia, Strong Running Coupling from the Gauge Sector of Domain Wall Lattice QCD with Physical Quark Masses, *Phys. Rev. Lett.* 122 (16) (2019) 162002, doi:10.1103/PhysRevLett.122.162002, 1902.08148.
- [187] Fei Gao, Ioannis Papavassiliou, Jan M. Pawłowski, Fully coupled functional equations for the quark sector of QCD, *Phys. Rev. D* 103 (9) (2021) 094013, doi:10.1103/PhysRevD.103.094013, 2102.13053.
- [188] Yi Lu, Fei Gao, Yu-Xin Liu, Jan M. Pawłowski, QCD equation of state and thermodynamic observables from computationally minimal Dyson-Schwinger equations, *Phys. Rev. D* 110 (1) (2024) 014036, doi:10.1103/PhysRevD.110.014036, 2310.18383.
- [189] Yi Lu, Fei Gao, Yu-xin Liu, Jan M. Pawłowski, Finite density signatures of confining and chiral dynamics in QCD thermodynamics and fluctuations of conserved charges (2025), 2504.05099.
- [190] Fei Gao, Jan M. Pawłowski, Chiral phase structure and critical end point in QCD, *Phys. Lett. B* 820 (2021) 136584, doi:10.1016/j.physletb.2021.136584, 2010.13705.
- [191] Wei-jie Fu, Xiaofeng Luo, Jan M. Pawłowski, Fabian Rennecke, Rui Wen, Shi Yin, Hyper-order baryon number fluctuations at finite temperature and density, *Phys. Rev. D* 104 (9) (2021) 094047, doi:10.1103/PhysRevD.104.094047, 2101.06035.
- [192] Wei-jie Fu, Xiaofeng Luo, Jan M. Pawłowski, Fabian Rennecke, Shi Yin, Ripples of the QCD critical point, *Phys. Rev. D* 111 (3) (2025) L031502, doi:10.1103/PhysRevD.111.L031502, 2308.15508.
- [193] F. C. Hansen, H. Leutwyler, Charge correlations and topological susceptibility in QCD, *Nucl. Phys. B* 350 (1991) 201–227, doi:10.1016/0550-3213(91)90259-Z.
- [194] F. Beutler, A. Andronic, P. Braun-Munzinger, K. Redlich, J. Stachel, The Canonical partition function for relativistic hadron gases, *Eur. Phys. J. C* 67 (2010) 439–444, doi:10.1140/epjc/s10052-010-1309-3, 0910.1697.
- [195] Volodymyr Vovchenko, Benjamin Dönigus, Horst Stoecker, Canonical statistical model analysis of p-p, p-Pb, and Pb-Pb collisions at energies available at the CERN Large Hadron Collider, *Phys. Rev. C* 100 (5) (2019) 054906, doi:10.1103/PhysRevC.100.054906, 1906.03145.
- [196] Szabolcs Borsanyi, Zoltan Fodor, Sandor D. Katz, Stefan Krieg, Claudia Ratti, et al., Fluctuations of conserved charges at finite temperature from lattice QCD, *JHEP* 1201 (2012) 138, doi:10.1007/JHEP01(2012)138, 1112.4416.
- [197] A. Bazavov, et al. (HotQCD Collaboration), Fluctuations and Correlations of net baryon number, electric charge, and strangeness: A comparison of lattice QCD results with the hadron resonance gas model, *Phys. Rev. D* 86 (2012) 034509, doi:10.1103/PhysRevD.86.034509, 1203.0784.

- [198] A. Bazavov, et al. (HotQCD), Equation of state in (2+1)-flavor QCD, Phys. Rev. D 90 (2014) 094503, doi:10.1103/PhysRevD.90.094503, 1407.6387.
- [199] Volodymyr Vovchenko, Hadron resonance gas with van der Waals interactions, Int. J. Mod. Phys. E 29 (05) (2020) 2040002, doi:10.1142/S0218301320400029, 2004.06331.
- [200] Pasi Huovinen, Peter Petreczky, Hadron Resonance Gas with Repulsive Interactions and Fluctuations of Conserved Charges, Phys. Lett. B 777 (2018) 125–130, doi:10.1016/j.physletb.2017.12.001, 1708.00879.
- [201] Roger Dashen, Shang-Keng Ma, Herbert J. Bernstein, S Matrix formulation of statistical mechanics, Phys. Rev. 187 (1969) 345–370, doi:10.1103/PhysRev.187.345.
- [202] R. Venugopalan, M. Prakash, Thermal properties of interacting hadrons, Nucl. Phys. A 546 (1992) 718–760, doi:10.1016/0375-9474(92)90005-5.
- [203] César Fernández-Ramírez, Pok Man Lo, Peter Petreczky, Thermodynamics of the strange baryon system from a coupled-channels analysis and missing states, Phys. Rev. C 98 (4) (2018) 044910, doi:10.1103/PhysRevC.98.044910, 1806.02177.
- [204] Anton Andronic, Peter Braun-Munzinger, Bengt Friman, Pok Man Lo, Krzysztof Redlich, Johanna Stachel, The thermal proton yield anomaly in Pb-Pb collisions at the LHC and its resolution, Phys. Lett. B 792 (2019) 304–309, doi:10.1016/j.physletb.2019.03.052, 1808.03102.
- [205] A. Bazavov, H. T. Ding, P. Hegde, O. Kaczmarek, F. Karsch, et al., Additional Strange Hadrons from QCD Thermodynamics and Strangeness Freeze-out in Heavy Ion Collisions, Phys. Rev. Lett. 113 (2014) 072001, doi:10.1103/PhysRevLett.113.072001, 1404.6511.
- [206] Paolo Alba, et al., Constraining the hadronic spectrum through QCD thermodynamics on the lattice, Phys. Rev. D 96 (3) (2017) 034517, doi:10.1103/PhysRevD.96.034517, 1702.01113.
- [207] P. Alba, V. Mantovani Sarti, J. Noronha-Hostler, P. Parotto, I. Portillo-Vazquez, C. Ratti, J. M. Stafford, Influence of hadronic resonances on the chemical freeze-out in heavy-ion collisions, Phys. Rev. C 101 (5) (2020) 054905, doi:10.1103/PhysRevC.101.054905, 2002.12395.
- [208] D. Bollweg, J. Goswami, O. Kaczmarek, F. Karsch, Swagato Mukherjee, P. Petreczky, C. Schmidt, P. Scior (HotQCD), Second order cumulants of conserved charge fluctuations revisited: Vanishing chemical potentials, Phys. Rev. D 104 (7) (2021), doi:10.1103/PhysRevD.104.074512, 2107.10011.
- [209] Simon Capstick, Nathan Isgur, Baryons in a Relativized Quark Model with Chromodynamics, Phys. Rev. D 34 (1986) 2809, doi:10.1103/PhysRevD.34.2809.
- [210] D. Ebert, R. N. Faustov, V. O. Galkin, Mass spectra and Regge trajectories of light mesons in the relativistic quark model, Phys. Rev. D 79 (2009) 114029, doi:10.1103/PhysRevD.79.114029, 0903.5183.
- [211] M. Ferraris, M. M. Giannini, M. Pizzo, E. Santopinto, L. Tiator, A Three body force model for the baryon spectrum, Phys. Lett. B 364 (1995) 231–238, doi:10.1016/0370-2693(95)01091-2.
- [212] Somenath Pal, Guruprasad Kadam, Abhijit Bhattacharyya, Hadron resonance gas model with repulsive mean-field interactions: Specific heat, isothermal compressibility and speed of sound, Nucl. Phys. A 1023 (2022) 122464, doi:10.1016/j.nuclphysa.2022.122464, 2104.08531.
- [213] Deeptak Biswas, Peter Petreczky, Sayantan Sharma, Chiral condensate and the equation of state at nonzero baryon density from the hadron resonance gas model with a repulsive mean field, Phys. Rev. C 109 (5) (2024) 055206, doi:10.1103/PhysRevC.109.055206, 2401.02874.
- [214] Murray Gell-Mann, M. Levy, The axial vector current in beta decay, Nuovo Cim. 16 (1960) 705, doi:10.1007/BF02859738.
- [215] Ulf-G. Meißner, Chiral perturbation theory (2024), 2410.21912.
- [216] J. Gasser, H. Leutwyler, Chiral Perturbation Theory to One Loop, Annals Phys. 158 (1984) 142, doi:10.1016/0003-4916(84)90242-2.
- [217] P. Gerber, H. Leutwyler, Hadrons Below the Chiral Phase Transition, Nucl. Phys. B 321 (1989) 387, doi:10.1016/0550-3213(89)90349-0.
- [218] Yoichiro Nambu, G. Jona-Lasinio, Dynamical Model of Elementary Particles Based on an Analogy with Superconductivity. I., Phys. Rev. 122 (1961) 345–358, doi:10.1103/PhysRev.122.345.
- [219] Yoichiro Nambu, G. Jona-Lasinio, Dynamical model of elementary particles based on an analogy with superconductivity. II., Phys. Rev. 124 (1961) 246–254, doi:10.1103/PhysRev.124.246.
- [220] S. P. Klevansky, The Nambu-Jona-Lasinio model of quantum chromodynamics, Rev. Mod. Phys. 64 (1992) 649–708, doi:10.1103/RevModPhys.64.649.
- [221] M. Asakawa, K. Yazaki, Chiral Restoration at Finite Density and Temperature, Nucl. Phys. A 504 (1989) 668–684, doi:10.1016/0375-9474(89)90002-X.
- [222] Michael Buballa, NJL model analysis of quark matter at large density, Phys. Rept. 407 (2005) 205–376, doi:10.1016/j.physrep.2004.11.004, hep-ph/0402234.
- [223] Bernd-Jochen Schaefer, Jochen Wambach, The Phase diagram of the quark meson model, Nucl. Phys. A 757 (2005) 479–492, doi:10.1016/j.nuclphysa.2005.04.012, nucl-th/0403039.
- [224] Kenji Fukushima, Phase diagrams in the three-flavor Nambu-Jona-Lasinio model with the Polyakov loop, Phys. Rev. D 77 (2008) 114028, doi:10.1103/PhysRevD.77.114028, [Erratum: Phys. Rev. D 78, 039902 (2008)], 0803.3318.
- [225] C. Ratti, Simon Roessner, M. A. Thaler, W. Weise, Thermodynamics of the PNJL model, Eur. Phys. J. C 49 (2007) 213–217, doi:10.1140/epjc/s10052-006-0065-x, hep-ph/0609218.
- [226] Claudia Ratti, Michael A. Thaler, Wolfram Weise, Phase diagram and thermodynamics of the PNJL model (2006), nucl-th/0604025.
- [227] Bernd-Jochen Schaefer, Jan M. Pawłowski, Jochen Wambach, The Phase Structure of the Polyakov–Quark–Meson Model, Phys. Rev. D 76 (2007) 074023, doi:10.1103/PhysRevD.76.074023, 0704.3234.
- [228] Lisa M. Haas, Rainer Stiele, Jens Braun, Jan M. Pawłowski, Jürgen Schaffner-Bielich, Improved Polyakov-loop potential for effective models from functional calculations, Phys. Rev. D 87 (7) (2013) 076004, doi:10.1103/PhysRevD.87.076004, 1302.1993.
- [229] V. Skokov, Fluctuations of conserved charges in the Polyakov loop extended quark-meson model at finite baryon density, Acta Phys. Polon. Supp. 5 (2012) 877–886, doi:10.5506/APhysPolBSupp.5.877.
- [230] Mark G. Alford, Juergen Berges, Krishna Rajagopal, Magnetic fields within color superconducting neutron star cores, Nucl. Phys. B 571 (2000) 269–284, doi:10.1016/S0550-3213(99)00830-5, hep-ph/9910254.
- [231] Mark G. Alford, Andreas Schmitt, Krishna Rajagopal, Thomas Schäfer, Color superconductivity in dense quark matter, Rev. Mod. Phys. 80 (2008) 1455–1515, doi:10.1103/RevModPhys.80.1455, 0709.4635.
- [232] Tina K. Herbst, Jan M. Pawłowski, Bernd-Jochen Schaefer, Phase structure and thermodynamics of QCD, Phys. Rev. D 88 (1) (2013) 014007, doi:10.1103/PhysRevD.88.014007, 1302.1426.
- [233] Tina Katharina Herbst, Mario Mitter, Jan M. Pawłowski, Bernd-Jochen Schaefer, Rainer Stiele, Thermodynamics of QCD at vanishing density, Phys. Lett. B 731 (2014) 248–256, doi:10.1016/j.physletb.2014.02.045, 1308.3621.
- [234] Steven S. Gubser, Abhinav Nellore, Silviu S. Pufu, Fabio D. Rocha, Thermodynamics and bulk viscosity of approximate black hole duals to finite temperature quantum chromodynamics, Phys. Rev. Lett. 101 (2008) 131601, doi:10.1103/PhysRevLett.101.131601, 0804.1950.
- [235] Steven S. Gubser, Abhinav Nellore, Mimicking the QCD equation of state with a dual black hole, Phys. Rev. D 78 (2008) 086007, doi:10.1103/PhysRevD.78.086007, 0804.0434.

- [236] Romulo Rougemont, Joaquin Grefa, Mauricio Hippert, Jorge Noronha, Jacquelyn Noronha-Hostler, Israel Portillo, Claudia Ratti, Hot QCD phase diagram from holographic Einstein–Maxwell–Dilaton models, *Prog. Part. Nucl. Phys.* 135 (2024) 104093, doi:10.1016/j.pnpnp.2023.104093, 2307.03885.
- [237] Oliver DeWolfe, Steven S. Gubser, Christopher Rosen, A holographic critical point, *Phys. Rev. D* 83 (2011) 086005, doi:10.1103/PhysRevD.83.086005, 1012.1864.
- [238] Oliver DeWolfe, Steven S. Gubser, Christopher Rosen, Dynamic critical phenomena at a holographic critical point, *Phys. Rev. D* 84 (2011) 126014, doi:10.1103/PhysRevD.84.126014, 1108.2029.
- [239] Steven S. Gubser, Silviu S. Pufu, Fabio D. Rocha, Bulk viscosity of strongly coupled plasmas with holographic duals, *JHEP* 08 (2008) 085, doi:10.1088/1126-6708/2008/08/085, 0806.0407.
- [240] Stefano I. Finazzo, Romulo Rougemont, Hugo Marrochio, Jorge Noronha, Hydrodynamic transport coefficients for the non-conformal quark-gluon plasma from holography, *JHEP* 02 (2015) 051, doi:10.1007/JHEP02(2015)051, 1412.2968.
- [241] Romulo Rougemont, Jorge Noronha, Jacquelyn Noronha-Hostler, Suppression of baryon diffusion and transport in a baryon rich strongly coupled quark-gluon plasma, *Phys. Rev. Lett.* 115 (20) (2015) 202301, doi:10.1103/PhysRevLett.115.202301, 1507.06972.
- [242] Joaquin Grefa, Mauricio Hippert, Jorge Noronha, Jacquelyn Noronha-Hostler, Israel Portillo, Claudia Ratti, Romulo Rougemont, Transport coefficients of the quark-gluon plasma at the critical point and across the first-order line, *Phys. Rev. D* 106 (3) (2022) 034024, doi:10.1103/PhysRevD.106.034024, 2203.00139.
- [243] Renato Critelli, Jorge Noronha, Jacquelyn Noronha-Hostler, Israel Portillo, Claudia Ratti, Romulo Rougemont, Critical point in the phase diagram of primordial quark-gluon matter from black hole physics, *Phys. Rev. D* 96 (9) (2017) 096026, doi:10.1103/PhysRevD.96.096026, 1706.00455.
- [244] Mauricio Hippert, Joaquin Grefa, T. Andrew Manning, Jorge Noronha, Jacquelyn Noronha-Hostler, Israel Portillo Vazquez, Claudia Ratti, Romulo Rougemont, Michael Trujillo, Bayesian location of the QCD critical point from a holographic perspective, *Phys. Rev. D* 110 (9) (2024) 094006, doi:10.1103/PhysRevD.110.094006, 2309.00579.
- [245] Joaquin Grefa, Jorge Noronha, Jacquelyn Noronha-Hostler, Israel Portillo, Claudia Ratti, Romulo Rougemont, Hot and dense quark-gluon plasma thermodynamics from holographic black holes, *Phys. Rev. D* 104 (3) (2021) 034002, doi:10.1103/PhysRevD.104.034002, 2102.12042.
- [246] Mikhail A. Stephanov, QCD phase diagram and the critical point, *Prog. Theor. Phys. Suppl.* 153 (2004) 139–156, doi:10.1142/S0217751X05027965, [Int. J. Mod. Phys. A20,4387(2005)], hep-ph/0402115.
- [247] Frank R. Brown, Frank P. Butler, Hong Chen, Norman H. Christ, Zhi-hua Dong, et al., On the existence of a phase transition for QCD with three light quarks, *Phys. Rev. Lett.* 65 (1990) 2491–2494, doi:10.1103/PhysRevLett.65.2491.
- [248] Robert D. Pisarski, Frank Wilczek, Remarks on the Chiral Phase Transition in Chromodynamics, *Phys. Rev. D* 29 (1984) 338–341, doi:10.1103/PhysRevD.29.338.
- [249] Krishna Rajagopal, The Chiral phase transition in QCD: Critical phenomena and long wavelength pion oscillations (1995) 484–554, doi:10.1142/9789812830661\_0009, hep-ph/9504310.
- [250] Francesca Cuteri, Owe Philipsen, Alessandro Sciarra, On the order of the QCD chiral phase transition for different numbers of quark flavours, *JHEP* 11 (2021) 141, doi:10.1007/JHEP11(2021)141, 2107.12739.
- [251] Francesco Giacosa, Győző Kovács, Péter Kovács, Robert D. Pisarski, Fabian Rennecke, Anomalous U(1)A couplings and the Columbia plot, *Phys. Rev. D* 111 (1) (2025) 016014, doi:10.1103/PhysRevD.111.016014, 2410.08185.
- [252] Larry D. McLerran, Benjamin Svetitsky, Quark Liberation at High Temperature: A Monte Carlo Study of SU(2) Gauge Theory, *Phys. Rev. D* 24 (1981) 450, doi:10.1103/PhysRevD.24.450.
- [253] Larry D. McLerran, Benjamin Svetitsky, A Monte Carlo Study of SU(2) Yang-Mills Theory at Finite Temperature, *Phys. Lett. B* 98 (1981) 195, doi:10.1016/0370-2693(81)90986-2.
- [254] J. Kuti, J. Polonyi, K. Szlachanyi, Monte Carlo Study of SU(2) Gauge Theory at Finite Temperature, *Phys. Lett. B* 98 (1981) 199, doi:10.1016/0370-2693(81)90987-4.
- [255] J. Engels, J. Fingberg, M. Weber, Finite Size Scaling Analysis of SU(2) Lattice Gauge Theory in (3+1)-dimensions, *Nucl. Phys. B* 332 (1990) 737, doi:10.1016/0550-3213(90)90010-B.
- [256] Biagio Lucini, Michael Teper, Urs Wenger, The Deconfinement transition in SU(N) gauge theories, *Phys. Lett. B* 545 (2002) 197–206, doi:10.1016/S0370-2693(02)02556-X, hep-lat/0206029.
- [257] L.G. Yaffe, B. Svetitsky, First Order Phase Transition in the SU(3) Gauge Theory at Finite Temperature, *Phys. Rev. D* 26 (1982) 963, doi:10.1103/PhysRevD.26.963.
- [258] Biagio Lucini, Michael Teper, Urs Wenger, Properties of the deconfining phase transition in SU(N) gauge theories, *JHEP* 0502 (2005) 033, doi:10.1088/1126-6708/2005/02/033, hep-lat/0502003.
- [259] S. Borsanyi, Kara R., Z. Fodor, D. A. Godzieba, P. Parotto, D. Sexty, Precision study of the continuum SU(3) Yang-Mills theory: How to use parallel tempering to improve on supercritical slowing down for first order phase transitions, *Phys. Rev. D* 105 (7) (2022) 074513, doi:10.1103/PhysRevD.105.074513, 2202.05234.
- [260] Mizuki Shirogane, Shinji Ejiri, Ryo Iwami, Kazuyuki Kanaya, Masakiyo Kitazawa, Hiroshi Suzuki, Yusuke Taniguchi, Takashi Umeda (WHOT-QCD), Latent heat and pressure gap at the first-order deconfining phase transition of SU(3) Yang-Mills theory using the small flow-time expansion method, *PTEP* 2021 (1) (2021) 013B08, doi:10.1093/ptep/ptaa184, 2011.10292.
- [261] Leonardo Giusti, Mitsuaki Hirasawa, Michele Pepe, Luca Virzi, A precise study of the thermodynamic properties of the SU(3) Yang-Mills theory across the deconfinement transition, *Phys. Lett. B* 868 (2025) 139775, doi:10.1016/j.physletb.2025.139775, 2501.10284.
- [262] G. Boyd, J. Engels, F. Karsch, E. Laermann, C. Legeland, et al., Thermodynamics of SU(3) lattice gauge theory, *Nucl. Phys. B* 469 (1996) 419–444, doi:10.1016/0550-3213(96)00170-8, hep-lat/9602007.
- [263] Sz. Borsanyi, G. Endrodi, Z. Fodor, S.D. Katz, K.K. Szabo, Precision SU(3) lattice thermodynamics for a large temperature range, *JHEP* 1207 (2012) 056, doi:10.1007/JHEP07(2012)056, 1204.6184.
- [264] Michele Caselle, Alessandro Nada, Marco Panero, QCD thermodynamics from lattice calculations with nonequilibrium methods: The SU(3) equation of state, *Phys. Rev. D* 98 (5) (2018) 054513, doi:10.1103/PhysRevD.98.054513, 1801.03110.
- [265] Atsushi Kiyohara, Masakiyo Kitazawa, Shinji Ejiri, Kazuyuki Kanaya, Finite-size scaling around the critical point in the heavy quark region of QCD, *Phys. Rev. D* 104 (11) (2021) 114509, doi:10.1103/PhysRevD.104.114509, 2108.00118.
- [266] F. Karsch, C. Schmidt, S. Stickan, Common features of deconfining and chiral critical points in QCD and the three state Potts model in an external field, *Comput. Phys. Commun.* 147 (2002) 451–454, doi:10.1016/S0010-4655(02)00327-2, hep-lat/0111059.
- [267] H. Saito, et al. (WHOT-QCD Collaboration), Phase structure of finite temperature QCD in the heavy quark region, *Phys. Rev. D* 84 (2011) 054502, doi:10.1103/PhysRevD.84.054502, 1106.0974.
- [268] Francesca Cuteri, Owe Philipsen, Alena Schön, Alessandro Sciarra, Deconfinement critical point of lattice QCD with  $N_f=2$  Wilson fermions, *Phys. Rev. D* 103 (1) (2021) 014513, doi:10.1103/PhysRevD.103.014513, 2009.14033.

- [269] Kouji Kashiwa, Robert D. Pisarski, Vladimir V. Skokov, Critical endpoint for deconfinement in matrix and other effective models, *Phys. Rev. D* 85 (2012) 114029, doi:10.1103/PhysRevD.85.114029, 1205.0545.
- [270] David Anthony Clarke, Olaf Kaczmarek, Frithjof Karsch, Anirban Lahiri, Mugdha Sarkar, Sensitivity of the Polyakov loop and related observables to chiral symmetry restoration, *Phys. Rev. D* 103 (1) (2021) L011501, doi:10.1103/PhysRevD.103.L011501, 2008.11678.
- [271] C. Vafa, Edward Witten, Restrictions on Symmetry Breaking in Vector-Like Gauge Theories, *Nucl. Phys. B* 234 (1984) 173–188, doi:10.1016/0550-3213(84)90230-X.
- [272] Don Weingarten, Mass Inequalities for QCD, *Phys. Rev. Lett.* 51 (1983) 1830, doi:10.1103/PhysRevLett.51.1830.
- [273] Edward Shuryak, Nonperturbative Topological Phenomena in QCD and Related Theories, *Lecture Notes in Physics*, vol. 977 2021, ISBN 978-3-030-62989-2, 978-3-030-62990-8, doi:10.1007/978-3-030-62990-8.
- [274] Andrea Pelissetto, Ettore Vicari, Relevance of the axial anomaly at the finite-temperature chiral transition in QCD, *Phys. Rev. D* 88 (10) (2013) 105018, doi:10.1103/PhysRevD.88.105018, 1309.5446.
- [275] Vicente Azcoiti, Axial  $U_A(1)$  Anomaly: A New Mechanism to Generate Massless Bosons, *Symmetry* 13 (2) (2021) 209, doi:10.3390/sym13020209, 2101.06439.
- [276] H. T. Ding, et al. (HotQCD), Chiral Phase Transition Temperature in  $(2+1)$ -Flavor QCD, *Phys. Rev. Lett.* 123 (6) (2019) 062002, doi:10.1103/PhysRevLett.123.062002, 1903.04801.
- [277] Andrey Yu. Kotov, Maria Paola Lombardo, Anton Trunin, QCD transition at the physical point, and its scaling window from twisted mass Wilson fermions, *Phys. Lett. B* 823 (2021) 136749, doi:10.1016/j.physletb.2021.136749, 2105.09842.
- [278] Jens Braun, Wei-jie Fu, Jan M. Pawłowski, Fabian Rennecke, Daniel Rosenblüh, Shi Yin, Chiral susceptibility in  $(2+1)$ -flavor QCD, *Phys. Rev. D* 102 (5) (2020) 056010, doi:10.1103/PhysRevD.102.056010, 2003.13112.
- [279] Fei Gao, Jan M. Pawłowski, Phase structure of  $(2+1)$ -flavor QCD and the magnetic equation of state, *Phys. Rev. D* 105 (9) (2022) 094020, doi:10.1103/PhysRevD.105.094020, 2112.01395.
- [280] Julian Bernhardt, Christian S. Fischer, QCD phase transitions in the light quark chiral limit, *Phys. Rev. D* 108 (11) (2023) 114018, doi:10.1103/PhysRevD.108.114018, 2309.06737.
- [281] Jens Braun, et al., Soft modes in hot QCD matter, *Phys. Rev. D* 111 (9) (2025) 094010, doi:10.1103/PhysRevD.111.094010, 2310.19853.
- [282] Peter Petreczky, Hans-Peter Schadler, Sayantan Sharma, The topological susceptibility in finite temperature QCD and axion cosmology, *Phys. Lett. B* 762 (2016) 498–505, doi:10.1016/j.physletb.2016.09.063, 1606.03145.
- [283] Edward V. Shuryak, Which chiral symmetry is restored in hot QCD?, *Comments Nucl. Part. Phys.* 21 (4) (1994) 235–248, hep-ph/9310253.
- [284] Ting Wai Chiu, Tung Han Hsieh, Yao Yuan Mao (TWQCD), Topological Susceptibility in Two Flavors Lattice QCD with the Optimal Domain-Wall Fermion, *Phys. Lett. B* 702 (2011) 131–134, doi:10.1016/j.physletb.2011.06.070, 1105.4414.
- [285] Guido Cossu, Sinya Aoki, Hidenori Fukaya, Shoji Hashimoto, Takashi Kaneko, Hideo Matsufuru, Jun-Ichi Noaki, Finite temperature study of the axial  $U(1)$  symmetry on the lattice with overlap fermion formulation, *Phys. Rev. D* 87 (11) (2013) 114514, doi:10.1103/PhysRevD.87.114514, [Erratum: *Phys. Rev. D* 88, 019901 (2013)], 1304.6145.
- [286] Bastian B. Brandt, Anthony Francis, Harvey B. Meyer, Owe Philipsen, Daniel Robaina, Hartmut Wittig, On the strength of the  $U_A(1)$  anomaly at the chiral phase transition in  $N_f = 2$  QCD, *JHEP* 12 (2016) 158, doi:10.1007/JHEP12(2016)158, 1608.06882.
- [287] A. Tomiya, G. Cossu, S. Aoki, H. Fukaya, S. Hashimoto, T. Kaneko, J. Noaki, Evidence of effective axial  $U(1)$  symmetry restoration at high temperature QCD, *Phys. Rev. D* 96 (3) (2017) 034509, doi:10.1103/PhysRevD.96.034509, [Addendum: *Phys. Rev. D* 96, 079902 (2017)], 1612.01908.
- [288] S. Aoki, Y. Aoki, G. Cossu, H. Fukaya, S. Hashimoto, T. Kaneko, C. Rohrer, K. Suzuki (JLQCD), Study of the axial  $U(1)$  anomaly at high temperature with lattice chiral fermions, *Phys. Rev. D* 103 (7) (2021) 074506, doi:10.1103/PhysRevD.103.074506, 2011.01499.
- [289] H. T. Ding, S. T. Li, Swagato Mukherjee, A. Tomiya, X. D. Wang, Y. Zhang, Correlated Dirac Eigenvalues and Axial Anomaly in Chiral Symmetric QCD, *Phys. Rev. Lett.* 126 (8) (2021) 082001, doi:10.1103/PhysRevLett.126.082001, 2010.14836.
- [290] Rajiv V. Gavai, Mischa E. Jaensch, Olaf Kaczmarek, Frithjof Karsch, Mugdha Sarkar, Ravi Shanker, Sayantan Sharma, Sipaz Sharma, Tristan Ueding, Aspects of the chiral crossover transition in  $(2+1)$ -flavor QCD with Möbius domain-wall fermions, *Phys. Rev. D* 111 (3) (2025) 034507, doi:10.1103/PhysRevD.111.034507, 2411.10217.
- [291] Takuya Kanazawa, Naoki Yamamoto, Quasi-instantons in QCD with chiral symmetry restoration, *Phys. Rev. D* 91 (2015) 105015, doi:10.1103/PhysRevD.91.105015, 1410.3614.
- [292] Reka A. Vig, Tamas G. Kovacs, Ideal topological gas in the high temperature phase of  $SU(3)$  gauge theory, *Phys. Rev. D* 103 (11) (2021) 114510, doi:10.1103/PhysRevD.103.114510, 2101.01498.
- [293] M. F. Atiyah, I. M. Singer, The Index of elliptic operators. 1, *Annals Math.* 87 (1968) 484–530, doi:10.2307/1970715.
- [294] Robert G. Edwards, Urs M. Heller, Joe E. Kiskis, Rajamani Narayanan, Chiral condensate in the deconfined phase of quenched gauge theories, *Phys. Rev. D* 61 (2000) 074504, doi:10.1103/PhysRevD.61.074504, hep-lat/9910041.
- [295] Viktor Dick, Frithjof Karsch, Edwin Laermann, Swagato Mukherjee, Sayantan Sharma, Microscopic origin of  $U_A(1)$  symmetry violation in the high temperature phase of QCD, *Phys. Rev. D* 91 (9) (2015) 094504, doi:10.1103/PhysRevD.91.094504, 1502.06190.
- [296] Vicente Azcoiti, Spectral density of the Dirac-Ginsparg-Wilson operator, chiral  $U(1)$  anomaly, and analyticity in the high temperature phase of QCD, *Phys. Rev. D* 107 (11) (2023) 114516, doi:10.1103/PhysRevD.107.114516, 2304.14725.
- [297] Tamas G. Kovacs, Fate of Chiral Symmetries in the Quark-Gluon Plasma from an Instanton-Based Random Matrix Model of QCD, *Phys. Rev. Lett.* 132 (13) (2024) 131902, doi:10.1103/PhysRevLett.132.131902, 2311.04208.
- [298] Tom Banks, A. Casher, Chiral Symmetry Breaking in Confining Theories, *Nucl. Phys. B* 169 (1980) 103–125, doi:10.1016/0550-3213(80)90255-2.
- [299] Andrei Alexandru, Ivan Horváth, Possible New Phase of Thermal QCD, *Phys. Rev. D* 100 (9) (2019) 094507, doi:10.1103/PhysRevD.100.094507, 1906.08047.
- [300] H.-T. Ding, A. Bazavov, P. Hegde, F. Karsch, S. Mukherjee, et al., Exploring phase diagram of  $N_f = 3$  QCD at  $\mu = 0$  with HISQ fermions, *PoS LATTICE2011* (2011) 191, 1111.0185.
- [301] Lukas Varnhorst, The  $N_f=3$  critical endpoint with smeared staggered quarks, *PoS LATTICE2014* (2015) 193.
- [302] G. Fejos, Second-order chiral phase transition in three-flavor quantum chromodynamics?, *Phys. Rev. D* 105 (7) (2022) L071506, doi:10.1103/PhysRevD.105.L071506, 2201.07909.
- [303] G. Fejos, T. Hatsuda, Order of the  $SU(N_f) \times SU(N_f)$  chiral transition via the functional renormalization group, *Phys. Rev. D* 110 (1) (2024) 016021, doi:10.1103/PhysRevD.110.016021, 2404.00554.
- [304] Simon Resch, Fabian Rennecke, Bernd-Jochen Schaefer, Mass sensitivity of the three-flavor chiral phase transition, *Phys. Rev. D* 99 (7) (2019) 076005, doi:10.1103/PhysRevD.99.076005, 1712.07961.
- [305] Andre Roberge, Nathan Weiss, Gauge Theories With Imaginary Chemical Potential and the Phases of QCD, *Nucl. Phys. B* 275 (1986) 734, doi:10.1016/0550-3213(86)90582-1.

- [306] Claudio Bonati, Massimo D'Elia, Marco Mariti, Michele Mesiti, Francesco Negro, Francesco Sanfilippo, Roberge-Weiss endpoint at the physical point of  $N_f = 2 + 1$  QCD, *Phys. Rev. D* 93 (7) (2016) 074504, doi:10.1103/PhysRevD.93.074504, 1602.01426.
- [307] Joseph I. Kapusta, Charles Gale, *Finite-Temperature Field Theory*, second ed., Cambridge University Press 2006, ISBN 9780511535130, cambridge Books Online, URL <http://dx.doi.org/10.1017/CB09780511535130>.
- [308] Owe Philipsen, Christopher Pinke, The nature of the Roberge-Weiss transition in  $N_f = 2$  QCD with Wilson fermions, *Phys. Rev. D* 89 (9) (2014) 094504, 1402.0838.
- [309] F. Cuteri, J. Goswami, F. Karsch, Anirban Lahiri, M. Neumann, O. Philipsen, Christian Schmidt, A. Sciarra, Toward the chiral phase transition in the Roberge-Weiss plane, *Phys. Rev. D* 106 (1) (2022) 014510, doi:10.1103/PhysRevD.106.014510, 2205.12707.
- [310] Claudio Bonati, Enrico Calore, Massimo D'Elia, Michele Mesiti, Francesco Negro, Francesco Sanfilippo, Sebastiano Fabio Schifano, Giorgio Silvi, Raffaele Tripiccone, Roberge-Weiss endpoint and chiral symmetry restoration in  $N_f = 2 + 1$  QCD, *Phys. Rev. D* 99 (2019) 014502, 1807.02106.
- [311] Chen-Ning Yang, T. D. Lee, Statistical theory of equations of state and phase transitions. 1. Theory of condensation, *Phys. Rev.* 87 (1952) 404–409, doi:10.1103/PhysRev.87.404.
- [312] T. D. Lee, Chen-Ning Yang, Statistical theory of equations of state and phase transitions. 2. Lattice gas and Ising model, *Phys. Rev.* 87 (1952) 410–419, doi:10.1103/PhysRev.87.410.
- [313] Andrew Connolly, Gregory Johnson, Fabian Rennecke, Vladimir Skokov, Universal Location of the Yang-Lee Edge Singularity in  $O(N)$  Theories, *Phys. Rev. Lett.* 125 (19) (2020) 191602, doi:10.1103/PhysRevLett.125.191602, 2006.12541.
- [314] Gregory Johnson, Fabian Rennecke, Vladimir V. Skokov, Universal location of Yang-Lee edge singularity in classic  $O(N)$  universality classes, *Phys. Rev. D* 107 (11) (2023) 116013, doi:10.1103/PhysRevD.107.116013, 2211.00710.
- [315] Fabian Rennecke, Vladimir V. Skokov, Universal location of Yang-Lee edge singularity for a one-component field theory in  $1 \leq d \leq 4$ , *Annals Phys.* 444 (2022) 169010, doi:10.1016/j.aop.2022.169010, 2203.16651.
- [316] Frithjof Karsch, Christian Schmidt, Simran Singh, Lee-Yang and Langer edge singularities from analytic continuation of scaling functions, *Phys. Rev. D* 109 (1) (2024) 014508, doi:10.1103/PhysRevD.109.014508, 2311.13530.
- [317] Tatsuya Wada, Masakiyo Kitazawa, Kazuyuki Kanaya, Locating Critical Points Using Ratios of Lee-Yang Zeros, *Phys. Rev. Lett.* 134 (16) (2025) 162302, doi:10.1103/PhysRevLett.134.162302, 2410.19345.
- [318] Vladimir V. Skokov, Two lectures on Yang-Lee edge singularity and analytic structure of QCD equation of state, *SciPost Phys. Lect. Notes* 91 (2025) 1, doi:10.21468/SciPostPhysLectNotes.91, 2411.02663.
- [319] P. Dimopoulos, L. Dini, F. Di Renzo, J. Goswami, G. Nicotra, C. Schmidt, S. Singh, K. Zambello, F. Ziesché, Contribution to understanding the phase structure of strong interaction matter: Lee-Yang edge singularities from lattice QCD, *Phys. Rev. D* 105 (3) (2022) 034513, doi:10.1103/PhysRevD.105.034513, 2110.15933.
- [320] David A. Clarke, Petros Dimopoulos, Francesco Di Renzo, Jishnu Goswami, Christian Schmidt, Simran Singh, Kevin Zambello, Searching for the QCD critical end point using multipoint Padé approximations, *Phys. Rev. D* 112 (9) (2025) L091504, doi:10.1103/PhysRevD.112.091504, 2405.10196.
- [321] Alexander Adam, Szabolcs Borsányi, Zoltan Fodor, Jana N. Guenther, Piyush Kumar, Paolo Parotto, Attila Pásztor, Chik Him Wong, High-precision baryon number cumulants from lattice QCD in a finite box: cumulant ratios, Lee-Yang zeros and critical endpoint predictions (2025), 2507.13254.
- [322] Gokce Basar, QCD critical point, Lee-Yang edge singularities, and Padé resummations, *Phys. Rev. C* 110 (1) (2024) 015203, doi:10.1103/PhysRevC.110.015203, 2312.06952.
- [323] Alexander Adam, Szabolcs Borsányi, Zoltán Fodor, Jana N. Guenther, Paolo Parotto, Attila Pásztor, Dávid Pesznyák, Ludovica Pirelli, Chik Him Wong, Search for a Lee-Yang edge singularity in high-statistics Wuppertal-Budapest data, *PoS LATTICE2024* (2025) 178, doi:10.22323/1.466.0178, 2502.03211.
- [324] Dmitri E. Kharzeev, Larry D. McLerran, Harmen J. Warringa, The Effects of topological charge change in heavy ion collisions: 'Event by event P and CP violation', *Nucl. Phys. A* 803 (2008) 227–253, doi:10.1016/j.nuclphysa.2008.02.298, 0711.0950.
- [325] Jens O. Andersen, William R. Naylor, Anders Tranberg, Phase diagram of QCD in a magnetic field: A review, *Rev. Mod. Phys.* 88 (2016) 025001, doi:10.1103/RevModPhys.88.025001, 1411.7176.
- [326] Gergely Endrodi, QCD with background electromagnetic fields on the lattice: A review, *Prog. Part. Nucl. Phys.* 141 (2025) 104153, doi:10.1016/j.pnpnp.2024.104153, 2406.19780.
- [327] Igor A. Shovkovy, Magnetic Catalysis: A Review, *Lect. Notes Phys.* 871 (2013) 13–49, doi:10.1007/978-3-642-37305-3, 1207.5081.
- [328] Massimo D'Elia, Francesco Negro, Chiral Properties of Strong Interactions in a Magnetic Background, *Phys. Rev. D* 83 (2011) 114028, doi:10.1103/PhysRevD.83.114028, 1103.2080.
- [329] G.S. Bali, F. Bruckmann, G. Endrodi, Z. Fodor, S.D. Katz, et al., QCD quark condensate in external magnetic fields, *Phys. Rev. D* 86 (2012) 071502, doi:10.1103/PhysRevD.86.071502, 1206.4205.
- [330] B. B. Brandt, F. Cuteri, G. Endrődi, G. Markó, L. Sandbote, A. D. M. Valois, Thermal QCD in a non-uniform magnetic background, *JHEP* 11 (2023) 229, doi:10.1007/JHEP11(2023)229, 2305.19029.
- [331] Falk Bruckmann, Gergely Endrodi, Tamas G. Kovacs, Inverse magnetic catalysis and the Polyakov loop, *JHEP* 1304 (2013) 112, doi:10.1007/JHEP04(2013)112, 1303.3972.
- [332] G.S. Bali, F. Bruckmann, G. Endrodi, Z. Fodor, S.D. Katz, et al., The QCD phase diagram for external magnetic fields, *JHEP* 1202 (2012) 044, doi:10.1007/JHEP02(2012)044, 1111.4956.
- [333] Gergely Endrodi, Critical point in the QCD phase diagram for extremely strong background magnetic fields, *JHEP* 07 (2015) 173, doi:10.1007/JHEP07(2015)173, 1504.08280.
- [334] Gergely Endrődi, QCD in magnetic fields: from Hofstadter's butterfly to the phase diagram, *PoS LATTICE2014* (2014) 018, 1410.8028.
- [335] Thomas D. Cohen, Naoki Yamamoto, New critical point for QCD in a magnetic field, *Phys. Rev. D* 89 (5) (2014) 054029, doi:10.1103/PhysRevD.89.054029, 1310.2234.
- [336] Massimo D'Elia, Lorenzo Maio, Francesco Sanfilippo, Alfredo Stanzione, Phase diagram of QCD in a magnetic background, *Phys. Rev. D* 105 (3) (2022) 034511, doi:10.1103/PhysRevD.105.034511, 2111.11237.
- [337] Massimo D'Elia, Lorenzo Maio, Kevin Zambello, Giuseppe Zanichelli, Roberge-Weiss transition for QCD in a magnetic background, *Phys. Rev. D* 111 (9) (2025) 094509, doi:10.1103/PhysRevD.111.094509, 2502.19294.
- [338] Ryan Abbott, William Detmold, Fernando Romero-López, Zohreh Davoudi, Marc Illa, Assumpta Parreño, Robert J. Perry, Phiala E. Shanahan, Michael L. Wagman (NPLQCD), Lattice quantum chromodynamics at large isospin density, *Phys. Rev. D* 108 (11) (2023) 114506, doi:10.1103/PhysRevD.108.114506, 2307.15014.
- [339] Ryan Abbott, William Detmold, Marc Illa, Assumpta Parreño, Robert J. Perry, Fernando Romero-López, Phiala E. Shanahan, Michael L. Wagman (NPLQCD), QCD Constraints on Isospin-Dense Matter and the Nuclear Equation of State, *Phys. Rev. Lett.* 134 (1) (2025) 011903, doi:10.1103/PhysRevLett.134.011903, 2406.09273.

- [340] D. T. Son, Misha A. Stephanov, QCD at finite isospin density, *Phys. Rev. Lett.* 86 (2001) 592–595, doi:10.1103/PhysRevLett.86.592, hep-ph/0005225.
- [341] Bastian B. Brandt, Gergely Endrodi, Reliability of Taylor expansions in QCD, *Phys. Rev. D* 99 (1) (2019) 014518, doi:10.1103/PhysRevD.99.014518, 1810.11045.
- [342] Szabolcs Borsanyi, Zoltan Fodor, Matteo Giordano, Jana N. Guenther, Sandor D. Katz, Attila Pasztor, Chik Him Wong, Can rooted staggered fermions describe nonzero baryon density at low temperatures?, *Phys. Rev. D* 109 (5) (2024) 054509, doi:10.1103/PhysRevD.109.054509, 2308.06105.
- [343] B. B. Brandt, G. Endrodi, S. Schmalzbauer, QCD phase diagram for nonzero isospin-asymmetry, *Phys. Rev. D* 97 (5) (2018) 054514, doi:10.1103/PhysRevD.97.054514, 1712.08190.
- [344] Hauke Koehn, et al., From existing and new nuclear and astrophysical constraints to stringent limits on the equation of state of neutron-rich dense matter, *Phys. Rev. X* 15 (2) (2025) 021014, doi:10.1103/PhysRevX.15.021014, 2402.04172.
- [345] Brynmor Haskell, Armen Sedrakian, Superfluidity and Superconductivity in Neutron Stars, *Astrophys. Space Sci. Libr.* 457 (2018) 401–454, doi:10.1007/978-3-319-97616-7\_8, 1709.10340.
- [346] Gentaro Watanabe, Kei Iida, Katsuhiko Sato, Thermodynamic properties of nuclear 'pasta' in neutron star crusts, *Nucl. Phys. A* 676 (2000) 455–473, doi:10.1016/S0375-9474(00)00197-4, [Erratum: *Nucl. Phys. A* 726, 357–365 (2003)], astro-ph/0001273.
- [347] David Blaschke, Hovik Grigorian, Gerd Röpke, Chirally improved quark Pauli blocking in nuclear matter and applications to quark deconfinement in neutron stars, *Particles* 3 (2) (2020) 477–499, doi:10.3390/particles3020033, 2005.10218.
- [348] Larry McLerran, Robert D. Pisarski, Phases of cold, dense quarks at large  $N(c)$ , *Nucl. Phys. A* 796 (2007) 83–100, doi:10.1016/j.nuclphysa.2007.08.013, 0706.2191.
- [349] Larry McLerran, Sanjay Reddy, Quarkyonic Matter and Neutron Stars, *Phys. Rev. Lett.* 122 (12) (2019) 122701, doi:10.1103/PhysRevLett.122.122701, 1811.12503.
- [350] J. M. Lattimer, M. Prakash, The physics of neutron stars, *Science* 304 (2004) 536–542, doi:10.1126/science.1090720, astro-ph/0405262.
- [351] John Antoniadis, et al., A Massive Pulsar in a Compact Relativistic Binary, *Science* 340 (2013) 6131, doi:10.1126/science.1233232, 1304.6875.
- [352] H. T. Cromartie, et al. (NANOGrav), Relativistic Shapiro delay measurements of an extremely massive millisecond pulsar, *Nature Astron.* 4 (1) (2019) 72–76, doi:10.1038/s41550-019-0880-2, 1904.06759.
- [353] Roger W. Romani, D. Kandel, Alexei V. Filippenko, Thomas G. Brink, Weikang Zheng, PSR J1810+1744: Companion Darkening and a Precise High Neutron Star Mass, *Astrophys. J. Lett.* 908 (2) (2021) L46, doi:10.3847/2041-8213/abe2b4, 2101.09822.
- [354] Roger W. Romani, D. Kandel, Alexei V. Filippenko, Thomas G. Brink, Weikang Zheng, PSR J0952–0607: The Fastest and Heaviest Known Galactic Neutron Star, *Astrophys. J. Lett.* 934 (2) (2022) L17, doi:10.3847/2041-8213/ac8007, 2207.05124.
- [355] Richard C. Tolman, Static solutions of Einstein's field equations for spheres of fluid, *Phys. Rev.* 55 (1939) 364–373, doi:10.1103/PhysRev.55.364.
- [356] J. R. Oppenheimer, G. M. Volkoff, On massive neutron cores, *Phys. Rev.* 55 (1939) 374–381, doi:10.1103/PhysRev.55.374.
- [357] Lee Lindblom, Determining the Nuclear Equation of State from Neutron-Star Masses and Radii, *ApJ* 398 (1992) 569, doi:10.1086/171882.
- [358] Tanja Hinderer, Benjamin D. Lackey, Ryan N. Lang, Jocelyn S. Read, Tidal deformability of neutron stars with realistic equations of state and their gravitational wave signatures in binary inspiral, *Phys. Rev. D* 81 (2010) 123016, doi:10.1103/PhysRevD.81.123016, 0911.3535.
- [359] Yuichiro Sekiguchi, Kenta Kiuchi, Koutarou Kyutoku, Masaru Shibata, Effects of hyperons in binary neutron star mergers, *Phys. Rev. Lett.* 107 (2011) 211101, doi:10.1103/PhysRevLett.107.211101, 1110.4442.
- [360] Sebastiano Bernuzzi, David Radice, Christian D. Ott, Luke F. Roberts, Philipp Moesta, Filippo Galeazzi, How loud are neutron star mergers?, *Phys. Rev. D* 94 (2) (2016) 024023, doi:10.1103/PhysRevD.94.024023, 1512.06397.
- [361] Albino Perego, Sebastiano Bernuzzi, David Radice, Thermodynamics conditions of matter in neutron star mergers, *Eur. Phys. J. A* 55 (8) (2019) 124, doi:10.1140/epja/i2019-12810-7, 1903.07898.
- [362] Katerina Chatziioannou, H. Thankful Cromartie, Stefano Gandolfi, Ingo Tews, David Radice, Andrew W. Steiner, Anna L. Watts, Neutron stars and the dense matter equation of state: from microscopic theory to macroscopic observations (2024), 2407.11153.
- [363] Eemeli Annala, Tyler Gorda, Aleks Kurkela, Aleks Vuorinen, Gravitational-wave constraints on the neutron-star-matter Equation of State, *Phys. Rev. Lett.* 120 (17) (2018) 172703, doi:10.1103/PhysRevLett.120.172703, 1711.02644.
- [364] Eemeli Annala, Tyler Gorda, Aleks Kurkela, Joonas Nättilä, Aleks Vuorinen, Evidence for quark-matter cores in massive neutron stars, *Nature Phys.* 16 (9) (2020) 907–910, doi:10.1038/s41567-020-0914-9, 1903.09121.
- [365] Oleg Komoltsev, Aleks Kurkela, How Perturbative QCD Constrains the Equation of State at Neutron-Star Densities, *Phys. Rev. Lett.* 128 (20) (2022) 202701, doi:10.1103/PhysRevLett.128.202701, 2111.05350.
- [366] Debora Mroczek, M. Coleman Miller, Jacquelyn Noronha-Hostler, Nicolas Yunes, Nontrivial features in the speed of sound inside neutron stars, *Phys. Rev. D* 110 (12) (2024) 123009, doi:10.1103/PhysRevD.110.123009, 2309.02345.
- [367] Eliot Finch, Isaac Legred, Katerina Chatziioannou, Reed Essick, Sophia Han, Philippe Landry, Unified nonparametric equation-of-state inference from the neutron-star crust to perturbative-QCD densities, *Phys. Rev. D* 112 (10) (2025) 103023, doi:10.1103/krc7-kz2l, 2505.13691.
- [368] John C. Collins, M. J. Perry, Superdense Matter: Neutrons Or Asymptotically Free Quarks?, *Phys. Rev. Lett.* 34 (1975) 1353, doi:10.1103/PhysRevLett.34.1353.
- [369] Leon N. Cooper, Bound electron pairs in a degenerate Fermi gas, *Phys. Rev.* 104 (1956) 1189–1190, doi:10.1103/PhysRev.104.1189.
- [370] Bertrand C. Barrois, Superconducting Quark Matter, *Nucl. Phys. B* 129 (1977) 390–396, doi:10.1016/0550-3213(77)90123-7.
- [371] Robert D. Pisarski, Dirk H. Rischke, Color superconductivity in weak coupling, *Phys. Rev. D* 61 (2000) 074017, doi:10.1103/PhysRevD.61.074017, nucl-th/9910056.
- [372] Krishna Rajagopal, Frank Wilczek, The Condensed matter physics of QCD 2000 pp. 2061–2151, doi:10.1142/9789812810458.0043, hep-ph/0011333.
- [373] Mark G. Alford, Krishna Rajagopal, Frank Wilczek, Color flavor locking and chiral symmetry breaking in high density QCD, *Nucl. Phys. B* 537 (1999) 443–458, doi:10.1016/S0550-3213(98)00668-3, hep-ph/9804403.
- [374] Thomas Schäfer, Frank Wilczek, Continuity of quark and hadron matter, *Phys. Rev. Lett.* 82 (1999) 3956–3959, doi:10.1103/PhysRevLett.82.3956, hep-ph/9811473.
- [375] D. T. Son, Misha A. Stephanov, Inverse meson mass ordering in color flavor locking phase of high density QCD, *Phys. Rev. D* 61 (2000) 074012, doi:10.1103/PhysRevD.61.074012, hep-ph/9910491.
- [376] D. T. Son, Misha A. Stephanov, Inverse meson mass ordering in color flavor locking phase of high density QCD: Erratum, *Phys. Rev. D* 62 (2000) 059902, doi:10.1103/PhysRevD.62.059902, hep-ph/0004095.
- [377] R. Casalbuoni, Raoul Gatto, Effective theory for color flavor locking in high density QCD, *Phys. Lett. B* 464 (1999) 111–116, doi:10.1016/S0370-2693(99)01032-1, hep-ph/9908227.

- [378] F. Gastineau, R. Nebauer, J. Aichelin, Thermodynamics of the three flavor NJL model: Chiral symmetry breaking and color superconductivity, *Phys. Rev. C* 65 (2002) 045204, doi:10.1103/PhysRevC.65.045204, hep-ph/0101289.
- [379] Mark G. Alford, Krishna Rajagopal, Frank Wilczek, QCD at finite baryon density: Nucleon droplets and color superconductivity, *Phys. Lett. B* 422 (1998) 247–256, doi:10.1016/S0370-2693(98)00051-3, hep-ph/9711395.
- [380] R. Rapp, Thomas Schäfer, Edward V. Shuryak, M. Velkovsky, Diquark Bose condensates in high density matter and instantons, *Phys. Rev. Lett.* 81 (1998) 53–56, doi:10.1103/PhysRevLett.81.53, hep-ph/9711396.